

**The Compositions and Routes of the Fluids Generating
the Navan Giant Base-Metal Orebody.**

Robert James Blakeman

Thesis submitted for the degree of Doctor of Philosophy

**The Faculty of Science, Division of Earth Sciences,
Department of Geography and Topographic Sciences,
University of Glasgow.**

April 2002.

ProQuest Number: 13818743

All rights reserved

INFORMATION TO ALL USERS

The quality of this reproduction is dependent upon the quality of the copy submitted.

In the unlikely event that the author did not send a complete manuscript and there are missing pages, these will be noted. Also, if material had to be removed, a note will indicate the deletion.



ProQuest 13818743

Published by ProQuest LLC (2018). Copyright of the Dissertation is held by the Author.

All rights reserved.

This work is protected against unauthorized copying under Title 17, United States Code
Microform Edition © ProQuest LLC.

ProQuest LLC.
789 East Eisenhower Parkway
P.O. Box 1346
Ann Arbor, MI 48106 – 1346

GLASGOW
UNIVERSITY
LIBRARY:

12554

COPY 1

DECLARATION

The material presented in this thesis is the result of research carried out between October 1997 and November 2000 in the Division of Earth Sciences, Department of Geography and Topographic Sciences, University of Glasgow, under the supervision of Professor Michael Russell.

This thesis is based on my own independent research and any published or unpublished material used by me has been given full acknowledgment in the text.

Robert Blakeman

Professor M.J. Russell.

Abstract

Models of genesis for the Navan orebody are of two distinct types. An early hypothesis that mesothermal (though non-magmatic) deposition of ore began when a supernatant seawater brine still had access to the host sediments (during the early to mid-Lower Carboniferous), has been challenged by recent suggestions favouring a later (mid-Lower to Upper Carboniferous) mineralisation derived from cooler fluids traversing either the Carboniferous basin, or the underlying basement from the south. These models, characterized here as Irish Type and Mississippi Valley Type (MVT) respectively, are interrogated as to their particular predictions with regard to metal distributions and sulfur isotope patterns associated with various fault geometries.

An examination of the temporal relationship between mineralisation and known structural events has revealed that the onset of mineralisation occurred prior to, or coincident with the initial developments of the major ENE trending semi-listric extensional faults of early Lower Carboniferous age, that now control the general disposition of the orebody.

The basal 5 lens of the Navan Zn+Pb deposit contains ~70 % of the known tonnage of the ~90 Mt orebody and thus is the focus of the metal distribution examination. Lead distribution patterns especially suggest that migration of metal-bearing fluids was principally directed up early to mid Mississippian, near vertical NNE, NE and ENE minor normal faults. These faults predate or are coeval with the major extensional, partly listric, ENE faults which now control the general disposition of the deposit. Only where these major ENE faults cross

putative deep-seated, NE (Caledonoid) and NW structures are they associated with lead enrichments.

A systematic $\delta^{34}\text{S}$ survey in the 5 lens across five minor NNE through to ENE- trending faults associated with distinct lead enrichments, and one ENE trending, partly listric, major extensional fault adjacent to that trend, revealed positive $\delta^{34}\text{S}$ values (+1 to +18‰) for galena, sphalerite and marcasite sampled within 3 m of all the faults on the profile. Sulfides with positive $\delta^{34}\text{S}$ values associated with the deep-seated, metal-bearing fluid generating the Navan deposit have been highlighted by previous workers (Anderson et al., 1998). The evidence reported here strongly suggests that the metal-bearing fluids rose through all the fractures. Conversely negative $\delta^{34}\text{S}$ values (-1 to -26‰) were returned in galena and sphalerite sampled 3 m or more from these faults. These negative values indicate that locally derived bacteriogenic sulfide, reduced from seawater sulfate, dominated away from these faults. Pyrite $\delta^{34}\text{S}$ values suggest a background level of $-29\pm 3.0\text{‰}$ across the profile. However, pyrite $\delta^{34}\text{S}$ values as low as $-34\pm 2.7\text{‰}$ were recorded in one sample collected from within 1 m of a fault. Thus fluids containing highly fractionated, bacteriogenic sulfide also gravitated into these faults on at least one occasion. There is also evidence suggesting that the metal-bearing solutions periodically displaced the locally derived bacteriogenic sulfide-bearing fluid in and near the faults.

Mineral sulfide petrography is used to contextualize the sampling and to give a qualitative indication of the degree of chemical disequilibrium of the system. Mineral textures demonstrating comminution and dissolution are revealed by this study which, when

coupled with evidence of isotopic overprinting, force the conclusion that mineralising fluids first invaded the host lithologies during early Lower Carboniferous times, coincident with active faulting. There is no evidence of reactivation of the minor fault sets encountered in the study area during post Chadian tectonism, though the major, partly listric, ENE extensional faults were reactivated at that time.

A genetic model, based on the hypothesis of Russell, 1974, and Russell, 1986, for the Navan deposit is presented. Highly saline early Lower Carboniferous seawater was allowed access to the basement via regionally major NE trending (Caledonoid) fault systems. These faults remained the focus of down-welling seawater throughout the duration of the mineralising system. Thus the formation waters at depth were re-charged and metals leached from the basement. Ore deposition was effected by bacteriogenic sulfide (reduced from early Lower Carboniferous seawater sulfate) reacting with the rising, metal-bearing mesothermal fluids.

LIST OF CONTENTS

1. INTRODUCTION.	21
1.1 A BRIEF HISTORY OF THE ‘MODERN ERA’ OF IRISH MINING AND THE DISCOVERY OF THE NAVAN DEPOSIT.	21
1.2 LOCATION AND GEOLOGICAL SETTING.	25
1.2.1 LOWER PALAEOZOIC STRATIGRAPHY	27
1.2.1.1 THE LONGFORD DOWN NORTHERN BELT	27
1.2.1.2 THE LONGFORD DOWN CENTRAL BELT	28
1.2.1.3 THE GRANGEGETH TERRANE	28
1.2.2 UPPER PALAEOZOIC STRATIGRAPHY.	29
1.2.2.1 THE NAVAN GROUP (COURCEYAN).	29
1.2.2.1.1 THE RED BEDS.	29
1.2.2.1.2 THE MIXED BEDS	30
1.2.2.1.3 PALE BEDS.	31
1.2.2.1.4 SHALEY PALES.	33
1.2.2.2 THE ARGILLACEOUS BIOCLASTIC LIMESTONE (ABL) GROUP	33
1.2.2.3 THE BOULDER CONGLOMERATE (CHADIAN/ARUNDIAN).	34
1.2.2.4 FINGAL GROUP (ARUNDIAN TO ASBIAN).	35
1.2.2.4.1 UPPER DARK LIMESTONE.	35
1.3 DIAGENESIS OF THE HOST ROCKS.	36
1.4 STRUCTURE	38
1.5 DETAILED MINERALOGY AND MINERAL TEXTURES.	39
1.6 NEXISTING MODELS FOR METALLOGENESIS WITHIN THE IRISH MIDLANDS AND PREVIOUS INVESTIGATIONS AT NAVAN	42
1.7 AIMS	48
2. FAULTING WITHIN THE NAVAN DEPOSIT AND ITS TEMPORAL RELATIONSHIP TO MINERALISATION.	62
2.1 AIMS	62
2.2 METHOD	62
2.3 EVOLUTION OF FAULTING	63
2.4 RESULTS	66

2.4.1 LITHOLOGIES	66
2.4.2 MINERALISATION	66
2.4.2.1 MINERALISED FRACTURES	67
2.4.3 STRUCTURE	68
2.4.3.1 B FAULT SYSTEM	68
2.4.3.2 DEXTRAL REVERSE STRIKE SLIP ASSEMBLAGE	69
2.4.3.3 JOINTING	69
2.5 INTERPRETATION	70
2.6 CONCLUSIONS.	76
3. MAJOR ELEMENT (ZN, PB AND FE) DISTRIBUTION STUDY.	92
3.1 INTRODUCTION.	92
3.2 HYPOTHESIS	92
3.3 SCIENTIFIC METHOD	93
3.4 ANALYTICAL TECHNIQUE	93
3.5 METAL DISTRIBUTION PATTERNS WITHIN SLICES 1 TO 4, AND LOWER 5 LENS.	96
3.5.1 LEAD DISTRIBUTION WITHIN SLICES 1 TO 4, LOWER 5 LENS.	96
3.5.2 ZINC DISTRIBUTION WITHIN SLICES 1 TO 4, LOWER 5 LENS.	97
3.5.3 IRON DISTRIBUTION WITHIN SLICES 1 TO 4, LOWER 5 LENS.	98
3.5.4 DISTRIBUTION OF ZN+PB VALUES WITHIN SLICES 1 TO 4, LOWER 5 LENS.	100
3.5.5 DISTRIBUTION OF ZN:PB VALUES WITHIN SLICES 1 TO 4, LOWER 5 LENS.	101
3.6 INTERPRETATION OF METAL DISTRIBUTION PATTERNS WITHIN SLICES 1 TO 4, AND LOWER 5 LENS.	103
3.6.1 LEAD.	103
3.6.2 ZINC.	103
3.6.3 IRON.	106
3.6.4 ZINC+LEAD.	107
3.6.5 ZINC:LEAD.	108
3.7 CONCLUSIONS.	109

4. $\delta^{34}\text{S}$ VARIATIONS WITH RESPECT TO POSSIBLE FEEDER STRUCTURES	127
4.1 INTRODUCTION	127
4.2 SULPHUR ISOTOPES	128
4.2.1 HYPOTHESES	129
4.2.2 SCIENTIFIC METHODS	130
4.2.2.1 SAMPLING, REFLECTED LIGHT MICROSCOPY AND ISOTOPIC TECHNIQUE.	131
4.3 RESULTS	132
4.3.1 MINERAL TEXTURES	132
4.3.2 ISOTOPE RESULTS	133
4.4 INTERPRETATION OF SULPHUR ISOTOPE ANALYSES AND MINERAL TEXTURES	136
4.5 CONCLUSIONS	140
5. A GENETIC MODEL FOR THE NAVAN DEPOSIT.	158
5.1 INTRODUCTION.	158
5.2 GENETIC MODEL.	159
5.2.1 ONSET OF EXTENSION AND MARINE TRANSGRESSION.	159
5.2.2 CONTINUED EXTENSION.	160
5.2.3 UPDRAUGHTS ESTABLISHED.	161
5.2.4 FULL EXTENSION.	164
5.2.5 A CHANGE OF ENVIRONMENT	165
5.2.6 SUMMARY	166
6. CONCLUSIONS.	179
7. BIBLIOGRAPHY:	182
8. APPENDICES	203

LIST OF FIGURES

CHAPTER 1.

FIGURE 1-1 GEOLOGICAL MAP OF IRELAND.....	51
FIGURE 1-2 DETAILED GEOLOGICAL MAP OF THE NORTHERN PART OF THE DUBLIN BASIN.....	52
FIGURE 1-3 GEOLOGICAL MAP OF THE AREA IMMEDIATELY SURROUNDING THE NAVAN DEPOSIT.....	53
FIGURE 1-4 SCHEMATIC STRATIGRAPHIC COLUMN FOR THE NAVAN DEPOSIT.....	54
FIGURE 1-5 SIMPLIFIED STRUCTURAL PLAN OF THE BASE OF 5 LENS IN THE NAVAN DEPOSIT.....	55
FIGURE 1-6 PLAN OF THE MAJOR STRUCTURES AND THEIR RELATIONSHIP TO THE GEOMETRY OF ORE LENSES WITHIN THE NAVAN DEPOSIT.....	56
FIGURE 1-7 GENERALISED CROSS-SECTION THROUGH THE NAVAN DEPOSIT SHOWING THE RELATIONSHIP OF THE MAJOR (ENE) AND MINOR (NNE TO ENE) FAULTS AND THE LOCATION OF 5 LENS.....	57
FIGURE 1-8 THE TOPOGRAPHY-DRIVEN (MVT) MODEL FOR FLUID GENERATION AND FLOW FOR THE GENERATION OF THE IRISH CARBONATE-HOSTED ZN/PB DEPOSITS.....	58
FIGURE 1-9 THE DEEP CONVECTION (SEDEX) MODEL FOR FLUID GENERATION AND FLOW FOR GENERATION OF THE IRISH CARBONATE-HOSTED ZN/PB DEPOSITS	59
FIGURE 1-10 'NEPTUNIAN DYKE' WITHIN PALE BEDS IMMEDIATELY BELOW THE EROSION SURFACE.....	60
FIGURE 1-11 EXAMPLE OF A LAMINATED SULPHIDE CLAST HOSTED BY THE BOULDER CONGLOMERATE.....	61

CHAPTER 2.

FIGURE 2-1 STRUCTURAL PLAN OF THE NAVAN DEPOSIT SHOWING THE LOCATION OF THE STUDY AREA COVERED BY THIS CHAPTER.....	77
FIGURE 2-2 PLAN OF THE 1330 13LHWA DEVELOPMENT SHOWING LINE OF SECTION IN FIGURE 2-3.....	78

FIGURE 2-3 INTERPRETED SECTION ALONG THE LINE SHOWN IN FIG. 2-2 SHOWING THE RELATIONSHIPS BETWEEN THE B FAULT (AND ITS BRANCHES), AND THE DEXTRAL-REVERSE, STRIKE-SLIP ASSEMBLAGE.....	79
FIGURE 2-4 SIDEWALL SKETCH OF THE 1330 13LHXR (LOOKING WEST).....	80
FIGURE 2-5 SIDEWALL WALL SKETCH OF THE RELATIONSHIP BETWEEN SULFIDE AND CARBONATE RICH VEIN-SETS AS EXPOSED IN THE 1330 13LHWA (LOOKING EAST).....	81
FIGURE 2-6 VIEW OF THE SIDEWALL OF 1330 13LHXL (LOOKING EAST).....	82
FIGURE 2-7 EXTENSIONAL (CARBONATE-RICH) VEINING (ASSOCIATED WITH THE B FAULT) CROSS-CUT AND DISPLACED BY SULFIDE-RICH VEINS.....	83
FIGURE 2-8 A RECENT EXPOSURE (OCTOBER 2001) IN THE 1150 B17P2XLA DEVELOPMENT.....	84
FIGURE 2-9 BRECCIA IN FOOTWALL OF THE B FAULT.....	85
FIGURE 2-10 A MINOR FOOTWALL BRANCH OF THE B FAULT AS EXPOSED IN THE SOUTH SIDEWALL OF THE 1330 13LHWA.....	86
FIGURE 2-11 VIEW OF THE MAIN BRANCH OF THE DEXTRAL-REVERSE STRIKE-SLIP ASSEMBLAGE, AS EXPOSED IN THE 1330 13LHWXL (LOOKING WEST).....	87
FIGURE 2-12 CLOSE-UP VIEW OF THE MAIN BRANCH OF THE DEXTRAL-REVERSE, STRIKE-SLIP ASSEMBLAGE, AS EXPOSED IN THE 1330 13LHWXL (LOOKING WEST).....	88
FIGURE 2-13 OCCURRENCE OF CHALCOPYRITE ON JOINT SURFACES (LOC. = 1075 2636F).....	89
FIGURE 2-14 CLOSE-UP OF COARSE-GRAINED SPHALERITE AND CARBONATE MINERALISATION WITHIN THE FAULT PLANE OF THE MAIN BRANCH OF THE DEXTRAL-REVERSE, STRIKE-SLIP ASSEMBLAGE, AS EXPOSED IN THE 1330 13LHWXL (LOOKING WEST).....	90
FIGURE 2-15 EXPOSURE OF THE B FAULT IN THE 1050 2710F.....	91

CHAPTER 3.

FIGURE 3-1 STRUCTURAL PLAN OF THE NAVAN DEPOSIT SHOWING THE LOCATION OF MINE ZONES DISCUSSED IN THE TEXT.....	110
FIGURE 3-2 THE BASAL GREEN SHALE OF THE NAVAN DEPOSIT. LOCATED WITHIN THE MICRITE UNIT.....	112
FIGURE 3-3 ORE-5 LENS DOLOMITE CONTACT (CORRESPONDING TO THE TOP OF SLICE 7).....	113
FIGURE 3-4 DISTRIBUTION OF %PB IN SLICE1 OF THE NAVAN DEPOSIT.....	114
FIGURE 3-5 DISTRIBUTION OF %PB IN SLICE 2 OF THE NAVAN DEPOSIT.....	114
FIGURE 3-6 DISTRIBUTION OF %PB IN SLICE 3 OF THE NAVAN DEPOSIT.....	115
FIGURE 3-7 DISTRIBUTION OF %PB IN SLICE 4 OF THE NAVAN DEPOSIT.....	115
FIGURE 3-8 DISTRIBUTION OF %PB WITHIN THE LOWERMOST 24M OF 5 LENS (SLICES 1 TO 7) IN THE NAVAN DEPOSIT.....	116
FIGURE 3-9 DISTRIBUTION OF %ZN IN SLICE 1 OF THE NAVAN DEPOSIT.....	116
FIGURE 3-10 DISTRIBUTION OF %ZN IN SLICE 2 OF THE NAVAN DEPOSIT.....	117
FIGURE 3-11 DISTRIBUTION OF %ZN IN SLICE 3 OF THE NAVAN DEPOSIT.....	117
FIGURE 3-12 DISTRIBUTION OF %ZN IN SLICE 4 OF THE NAVAN DEPOSIT.....	118
FIGURE 3-13 DISTRIBUTION OF %ZN WITHIN THE LOWERMOST 24M OF 5 LENS (SLICES 1 TO 7) IN THE NAVAN DEPOSIT.....	118
FIGURE 3-14 DISTRIBUTION OF %FE IN SLICE 1 OF THE NAVAN DEPOSIT.....	119
FIGURE 3-15 DISTRIBUTION OF % FE IN SLICE 2 OF THE NAVAN DEPOSIT.....	119
FIGURE 3-16 DISTRIBUTION OF %FE IN SLICE 3 OF THE NAVAN DEPOSIT.....	120

FIGURE 3-17 DISTRIBUTION OF %FE IN SLICE 4 OF THE NAVAN DEPOSIT.....	120
FIGURE 3-18 DISTRIBUTION OF %FE WITHIN THE LOWERMOST 24M OF 5 LENS (SLICES 1 TO 7) IN THE NAVAN DEPOSIT.....	121
FIGURE 3-19 DISTRIBUTION OF %ZN+PB IN SLICE 1 OF THE NAVAN DEPOSIT.....	121
FIGURE 3-20 DISTRIBUTION OF %ZN+PB IN SLICE 2 OF THE NAVAN DEPOSIT.....	122
FIGURE 3-21 DISTRIBUTION OF %ZN+PB IN SLICE 3 OF THE NAVAN DEPOSIT.....	122
FIGURE 3-22 DISTRIBUTION OF %ZN+PB IN SLICE 4 OF THE NAVAN DEPOSIT.....	123
FIGURE 3-23 DISTRIBUTION OF %ZN+PB WITHIN THE LOWERMOST 24M OF 5 LENS (SLICES 1 TO 7) IN THE NAVAN DEPOSIT.....	123
FIGURE 3-24 DISTRIBUTION OF ZN:PB VALUES IN SLICE 1 OF THE NAVAN DEPOSIT.....	124
FIGURE 3-25 DISTRIBUTION OF ZN:PB VALUES IN SLICE 2 OF THE NAVAN DEPOSIT.....	124
FIGURE 3-26 DISTRIBUTION OF ZN:PB VALUES IN SLICE 3 OF THE NAVAN DEPOSIT.....	125
FIGURE 3-27 DISTRIBUTION ZN+PB VALUES IN SLICE 4 OF THE NAVAN DEPOSIT.....	125
FIGURE 3-28 DISTRIBUTION OF ZN:PB VALUES WITHIN THE LOWERMOST 24M OF 5 LENS (SLICES 1 TO 7) IN THE NAVAN DEPOSIT.....	126
FIGURE 3-29 DIAGRAM DEMONSTRATING THE DISTRIBUTION OF FAULT AZIMUTHS WITHIN THE NAVAN DEPOSIT.....	127.

CHAPTER 4.

FIGURE 4-1 STRUCTURAL PLAN OF THE NAVAN DEPOSIT SHOWING THE STUDY AREA COVERED BY CHAPTER 4.....	143
--	-----

FIGURE 4-2 HISTOGRAM SHOWING THE KNOWN DISTRIBUTION OF SULFUR ISOTOPE RESULTS WITHIN 5 LENS.....	144
FIGURE 4-3 CARTOON MODEL ILLUSTRATING MINERALISATION SUPPOSEDLY POST-DATING THE FULL DEVELOPMENT OF THE B AND T FAULTS.....	145
FIGURE 4-4 CARTOON MODEL ILLUSTRATING THE OCCURRENCE OF MINERALISATION DURING/AFTER THE DEVELOPMENT OF THE EARLY STEEPLY DIPPING MINOR NNE, NE AND ENE NORMAL FAULT SETS.....	146
FIGURE 4-5 STRATIGRAPHIC CROSS-SECTION OF PROFILE SHOWING LOCATION OF LITHOLOGIES AND STRUCTURES DISCUSSED IN TEXT.....	147
FIGURE 4-6 PLAN OF PROFILE DISCUSSED IN TEXT.....	148
FIGURE 4-7 PHOTOMICROGRAPH OF DDH U12477.....	149
FIGURE 4-8 PHOTOMICROGRAPH OF DDH U12473.....	150
FIGURE 4-9 PHOTOMICROGRAPH OF DDH U12472.....	151
FIGURE 4-10 PHOTOMICROGRAPH OF DDH U12493.....	152
FIGURE 4-11 PHOTOMICROGRAPH OF DDH U12478.....	153
FIGURE 4-12 PHOTOMICROGRAPH OF U14298.....	154
FIGURE 4-13 SUMMARY OF THE RANGES OF SULFUR ISOTOPE RESULTS FROM DIFFERENT MINERALS AND TEXTURES.....	155
FIGURE 4-14 FREQUENCY DISTRIBUTION OF $\delta^{34}\text{S}$ VALUES PER SULFIDE PHASE REVEALED BY THIS STUDY.....	156
FIGURE 4-15 DIAGRAMMATIC SUMMARY OF THE DISTRIBUTION OF $\delta^{34}\text{S}$ VALUES (SPHALERITE, GALENA, MARCASITE AND PYRITE) WITH RESPECT TO THE NEAREST FAULT, AND WHETHER THE SAMPLE WAS LOCATED IN EITHER THE FOOTWALL OR THE HANGING WALL....	157
 CHAPTER 5.	
FIGURE 5-1 SCHEMATIC DIAGRAM ILLUSTRATING THE CONDITIONS PERTAINING DURING THE LOWERMOST COURCEYAN.....	168
FIGURE 5-2 SCHEMATIC DIAGRAM SHOWING CONTINUED NNW-SSE EXTENSION LEADING TO DEVELOPMENT OF INCIPIENT HORSTS WITH MINOR NNE-NE FAULTING.....	169

FIGURE 5-3 SCHEMATIC DIAGRAM ILLUSTRATING THE DEVELOPMENT OF LOCALLY MAJOR ENE TRENDING PARTLY LITRIC FAULTS THAT TRUNCATE THE EARLIER NNE-NE FAULTING WITHIN THE HORSTS. (LATE COURCEYAN – EARLY CHADIAN).....	170
FIGURE 5-4 SCHEMATIC DIAGRAM DEMONSTRATING THE DETAILS OF METAL-SULFIDE AND SULFATE PRECIPITATION.....	171
FIGURE 5-5 EXPOSURE OF BARITE MINERALISATION IN 5 LENS....	172
FIGURE 5-6 THE DEVELOPMENT OF THE BOULDER CONGLOMERATE (LATE CHADIAN).....	173
FIGURE 5-7 SURFICIAL DEPOSITIONAL PROCESSES OF SULFIDES WITHIN THE CONGLOMERATE GROUP ORE?.....	174
FIGURE 5-8 EXHALATIVE PROCESSES?.....	174
FIGURE 5-9 EXHALATIVE PROCESSES?.....	175
FIGURE 5-10 EXHALATIVE PROCESSES?.....	175
FIGURE 5-11 EARLY ARUNDIAN TIMES. THE DEPOSITION OF THE BASAL UNIT OF THE UPPER DARK LIMESTONES.....	176
FIGURE 5-12 EXHALATIVE PROCESSES?.....	177
FIGURE 5-13 EXHALATIVE PROCESSES?.....	177
FIGURE 5-14 EXHALATIVE PROCESSES?.....	178

LIST OF TABLES.

TABLE 1-1 TONNAGES AND GRADES OF SELECTED IRISH CARBONATE HOSTED BASE-METAL DEPOSITS.	24
TABLE 1-2 GEOLOGICAL TIMESCALE OF EVENTS LEADING UP TO AND DURING THE PERIOD COVERED BY THIS THESIS.....	25
TABLE 1-3 TABLE OF MICROTHERMOMETRIC RESULTS FROM THE NAVAN DEPOSIT..	47
TABLE 3-1 DISTRIBUTION OF SLICES RELATIVE TO ORE-LENSES, MARKERS HORIZONS, AND MINE AREAS WITHIN THE NAVAN DEPOSIT.	95

Acknowledgements and thanks.

There are many people who have contributed to the following thesis, some wittingly, some not so. Nevertheless, all deserve a mention here, and if I've missed anyone out then I apologise. I'll buy you a drink when you catch up with me!

From a logistical point of view my main sponsors deserve a mention. NERC and Outokumpu-Tara Mines Ltd provided the funding for this thesis and I thank them for their interest and promptness in forwarding instalments on time. Into the category of logistical support I had better include Anne-Marie and James Russell, proprietors of The Sycamores Bed and Breakfast in Navan, an establishment that I hope to continue to use many times in the future. Also in this category I had better acknowledge the various emporia of refreshment that have without fail oiled the machinations of thought and fuelled the engine of research, enabling this project to proceed with as much smoothness and unhindered swiftness as could be expected. Special thanks must therefore go to the proprietors and patrons of Smyth's of the Bridge, Berminghams, O'Flaherty's, Ryan's, and Brady's, in Navan, and Bonham's, Bar Oz, The Rock, The Queen Margaret Union and of course the University of Glasgow Postgraduates Club in Glasgow. Without the open hospitality, patience and fortitude of these people my time in Glasgow and Ireland would have been considerably less enjoyable.

What of the people who have helped through discussion and communication? I would like to thank Jamie Wilkinson and Kate Everett of the Royal School of Mines, Imperial College, Sarah Gleeson (now somewhere in America) and Steve Freeman of the Rock Deformation Research Unit at Leeds University, and Helen Lewis of Herriott Watt for many long and fruitful discussions of the data presented here. Mike Philcox of Trinity College, Dublin, deserves special mention

along with Murray Hitzman of the Colorado School of Mines. Those at Glasgow University who have aided my understanding of the research subject include Alan Hall, Colin Braithwaite and, Laiq Rahman. At this point the many academic staff, postdoctoral and postgraduate personnel at Glasgow deserve special mention, as whilst not being directly involved in this subject area, nevertheless contributed by answering sometimes misdirected, and often badly thought out questions, and also for the moral support.

No research project can proceed without talking to the people 'on the ground', and here especial mention should be made of those people that have made my time at the Tara operation both interesting and rewarding. Eammon Brady, Pdraig Duffy, Jenny Felton, Gerry Gough, Alison Hare, Mark Holdstock, Eugene Hyland, Gerry Kelly, Dessie O'Brien, Billy O'Keefe, Catherine Walsh and Archie Watts for many helpful discussions. These are the people who work with the Navan orebody every day and represent a very knowledgeable platform without which this research would have been considerably poorer. Also here I would like to thank John-Jo and the 'bhoys' from Priority Drilling for helping out and putting up with me when I needed special holes drilling.

Those who are familiar with the staff of the Mine Geology Section at Outokumpu-Tara Mines Ltd will know that there is a name missing from the above list. Jim Geraghty. Jim deserves independent mention here not only because of shared experiences on that fateful morning in the autumn of 1998, but because Jim has always shown a keen interest in what I was about. Even though he was undertaking a part-time degree in the Earth Sciences at the time, (recently completed – good man) and therefore had enough to think about, Jim's searching questions, based on an intimate knowledge of the Navan orebody and Irish

geology, helped in no small way to focus my own thoughts, especially over a few stouts in a local bar. Thanks a million Jim.

On a wider footing in Ireland I have received considerable encouragement from the members of the Irish Association for Economic Geology. Deserving special mention here are Kerr Anderson, Colin and Bernie Andrew, Liz Ashton, Dave Coller, Garth Earls and Mark Cruise, all of whom I've bored considerably by talking incessantly about mineral deposits, not necessarily Irish. Also while in Ireland, and at conferences both in Ireland and the UK, I have been very fortunate to meet many international research workers who allowed me to expand, almost exponentially, on a subject area that many of them are world leaders in.

And so to those people who were directly involved in helping out, pointing me in the right direction and making sure that this research was scientific. Terry Donnelly, Paul Gorman and Chris Taylor are thanked for assistance during S isotope analysis. John Gilleece and Kenny Roberts of the Division of Earth Sciences, University of Glasgow are also thanked for help with sample preparation and photography.

During my time as a research student I have been exceedingly fortunate to be supervised by three senior academics and a leading Mine Geologist. Therefore, it is with special gratitude that I thank Profs. Mike Russell, Tony Fallick and Dr. John Ashton for firstly inviting me to take this project on, and keeping a smile on my face when I was doing it. Secondly for 'kicking' me up the backside when I needed it, and thirdly for introducing me to Dr. Adrian Boyce. Without the dedicated support that Adrian has given to this project things would have been a lot different.

There are three people that also require mention here. Not for any direct involvement in this project, but for providing me with the inspiration to finally get an education within the Earth Sciences. They are (in age order) Victoria, David and Catherine Blakeman. Thanks kids.

In closing, therefore, there are a lot of people from all walks of life and backgrounds that have contributed to what is contained within the following pages. Each has contributed to a greater or lesser degree, and each of those contributions are greatly appreciated. Thanks a lot lads.

1. Introduction.

1.1 A brief history of the ‘Modern Era’ of Irish mining and the discovery of the Navan deposit.

Ireland has a long history of metal mining. Records of activity at Silvermines in particular date from the Middle Ages, and evidence suggests mining operations before historic records began (Rhoden, 1958; Andrew, 1993). Although these early miners traditionally worked for lead, silver was also extracted in payable values (Andrew, 1993). Irish gold is known to have been wrought during the Bronze Age, and several prospects are recognised today, notably in Co. Mayo (Cregganbaun), Co. Wicklow (Kilmacoo), and at Lack and Curraghinalt in Northern Ireland. Copper (with minor Zn, and Pb) was extracted from Avoca, in Co. Wicklow, during the latter eighteenth, nineteenth and twentieth centuries (Andrew, 1993; Gardiner et al., 1982; O’Brien, 1966; Platt, 1980).

This thesis deals with research conducted on one of five economic base-metal deposits that have so far been discovered during the 'modern era' (late 1950's onwards). These Zn+Pb+Fe+/-Ag+/-Ba+/-Cu deposits are all located within the Irish Midlands. All are carbonate hosted and all are described as 'Irish Type', a hybrid variety of carbonate hosted Zn+Pb deposit defined as showing affinities to both the Mississippi Valley Type (MVT), and the Sedimentary Exhalative (SedEx) classifications (Hitzman and Beaty, 1996). This spate of exploration successes, plus a large number of currently sub-economic discoveries, prompted Singer (1995) to calculate that the Irish Midlands contained the highest known concentration of zinc per square kilometre of any country in the world.

The first of the Irish Type deposits to be discovered was at Tynagh, Co. Galway, (Fig. 1-1 and Table 1-1), in 1961 (see Derry et al., 1965). This find was based on favourable information obtained from the Irish Geological Survey, along with complementary geochemical data and the known existence of an ENE trending (Lower Carboniferous) extensional fault (Schultz 1968). This was a similar scenario to the main Silvermines fault, south of Nenagh, Co. Tipperary (Fig. 1-1 and Table 1-1), where lead/silver mineralisation had been worked since pre-history (Rhoden, 1958). Encouraged by the discovery of the Tynagh deposit, renewed drilling in the Silvermines area by Consolidated Mogul had defined, by 1964, a previously unknown area of economic mineralisation to the north of the main Silvermines Fault (O'Brien, 1966).

Tynagh (9.9Mt, at 5.7% Zn, 6.9% Pb, and 0.6% Cu), and Silvermines (17.7Mt, at 6.43% Zn, 2.53% Pb, with 5.5Mt BaSO₄) (Andrew, 1993; Johnston, 1999), constituted, during the 1960's, the most notable exploration successes in the Irish Midlands. However, a survey by the Irish Agricultural Institute published in 1968 (see Libby et al. 1985) highlighted trace element, including zinc and lead, anomalies in stream sediments in the area immediately to the west of Navan, Co. Meath. Although initially viewed as unpromising due to the nearness of Navan town (possible pollution), and the property being the subject of previous exploration by a different company, acquisition in 1969 of prospecting licences (under the 1940 Minerals Development Act) allowed Tara Exploration and Development Company to confirm and enlarge the initial anomalies by shallow soil geochemistry and geophysical prospecting methods. The shallow soil geochemical survey indicated an area to the north of the River Blackwater (900m x 400m) having peak values of 5000ppm zinc and 2000ppm lead against

background levels of 90 and 45ppm respectively. The anomalous zinc values continued east for almost 1400m; however, this tail was found to reflect the dominant drainage direction (Libby et al. 1985).

Following intensive field mapping that revealed mineralised boulders (float), and a mineralised outcrop north of the River Blackwater, an induced polarisation and resistivity survey identified anomalous zones on both sides of the river. During November 1970, the first diamond drill-hole, located on the highest geochemical and most favourable induced polarisation values north of the river, intersected 12m of 8.5% zinc and lead combined. A subsequent drilling programme continued until August 1972, by which time 355 holes had been completed, realising (at a cut-off grade of 4% Zn+Pb), 69.9Mt at 10.09% zinc and 2.63% lead (Libby et al. 1985). The Navan deposit, currently owned and operated by Outokumpu-Tara Mines Ltd, has been extracted at a rate of around 2.5Mt per year (1999 output equalled 2.02Mt at 7.38% Zn, 2.19% Pb, and 2.85% Fe). Current exploration is centred on an area to the southwest of the original discovery, and recent drilling has raised the total size of the orebody to ~90Mt (Ashton, in press).

Within the Irish base-metal ore-field, Navan is the largest deposit so far discovered. Two other deposits are currently being worked at Lisheen, Co. Tipperary (>20Mt), and Galmoy, Co. Kilkenny (6.7Mt). Along with the previously worked deposits (Tynagh and Silvermines), several minor prospects have also been defined (see Fig. 1-1 and Table 1-1).

Deposit	Tonnes x 10 ⁶	Zn%	Pb%	Cu%	Ag g/T	Barite	Status
Navan	~90	10.09	2.63	-	11	Present	Operating*
Lisheen	>20	12.0	1.2	-	30	-	Operating
Galmoy	6.7	10.9	1.0	-	-	-	Operating
Silvermines	17.7	6.43	2.53	-	23	-	Closed
Ballynoe**	5.5	-	-	-	-	85%	Closed
Tynagh	9.9	5.7	6.9	0.6	74	Present	Closed
Gortdrum	3.8	-	-	1.2	23	-	Closed
Abbeystown	1.1	3.5	1.5	-	40	-	Prospect
Aherlow	6.0	-	-	-	-	-	Prospect
Allenwood	?	1.6	0.4	-	-	-	Prospect
Ballinalack	5.7	6.78	1.13	-	27	-	Prospect
Ballyvergin	0.15	-	-	1.2	17.1	-	Prospect
Boston Hill	0.8	2.7	1.1	-	-	-	Prospect
Carrickittle	<0.1	6.0	1.5	-	-	-	Prospect
Clogherboy***	0.34	5.8	1.2	-	-	-	Prospect
Courtbrown	1.0	3.5	2.0	-	14	-	Prospect
Garycam	1.4	2.7	0.2	-	-	36.1%	Prospect
Harberton	5.4	8.17	Zn+Pb	-	-	-	Prospect
Bridge							
Keel	1.8	5.83	1.16	-	-	Present	Prospect
Mallow	4.2	7.7	1.0	0.7	27.5	-	Prospect
Moyvoughly	0.13	6.5	1.0	-	-	-	Prospect
Newtown	?	3.1	3.1	-	-	-	Prospect
Cashel							
Oldcastle	3.0	4.3	0.6	-	-	-	Prospect
Rickardstown	3.5	2.2	1.1	-	-	-	Prospect
Tatestown***	3.6	6.9	Zn+Pb	-	-	-	Prospect

Table 1-1 Tonnages and grades of selected Irish carbonate hosted base-metal deposits (see also Fig. 1-1). (* Currently at 'care and maintenance' status, ** Formerly known as Magcobar (Silvermines), *** Satellite of the Navan deposit). Modified and updated from Johnston (1999).

1.2 Location and Geological Setting.

The Navan deposit is located on the northern edge of the Eastern Irish Midlands, approximately 50-km north-northwest of Dublin on the south-western margin of the Lower Palaeozoic Longford Down Inlier. (Figs. 1-1, 1-2 and 1-3). The deposit is hosted by shallow-water argillaceous bioclastic carbonate lithologies of Courceyan and Chadian/Arundian age (360-345ma), (Anderson et al., 1998; Ashton, 1995; Ashton et al, 1992; Andrew, 1993).

Age (Million Years)	Period	Events relating to the Navan area
355	Carboniferous	<i>Generally weak deformation in foreland of Variscan Orogeny. Deposition of deltaic sands and muds. Development of platform and basin carbonate depositional environments. Minor volcanism. Transgression; limestone ramp sedimentation.</i>
410	Devonian	<i>Final closure of Iapetus; deformation and metamorphism in Caledonian Orogeny. Intrusion of Granites.</i>
438	Silurian	<i>Closure of Iapetus Ocean; deposition in remnant marine basin. Accretion of oceanic sediments and Grangegeeth (arc) Terrane in subduction complex to Laurentian margin.</i>
510	Ordovician	<i>Volcanic arcs within and marginal to Iapetus Ocean Deep marine sedimentation within and on margins of Iapetus Ocean. Volcanism as ocean begins to close.</i>
545	Cambrian	<i>Generation of oceanic crust in newly formed Iapetus Ocean.</i>

Table 1-2 Geological timescale of events leading up to and during the period covered by this Thesis (Adapted from MacConnell et al., 2001).

Most of the mineralisation (~>97%) lies within the Courceyan sequences and takes the form of complex 'stratabound' and occasionally discontinuous lenses separated by argillaceous and dolomitised arenaceous horizons (Fig. 1-4). Further mineralisation (~<3%) occurs within a Chadian/Arundian mega-conglomerate lying above an erosion surface that truncates the deposit to the south (Boyce et al., 1983a; Anderson, 1990; Ashton et al., 1992; Andrew 1993; Rizzi, 1993; Ashton, 1995; Ford, 1996; Anderson et al., 1998). There are also two associated sub-economic satellite bodies at Tatestown (3.6Mt, 5.3% Zn, 1.5% Pb) to the northwest and at Clogherboy (0.34Mt, 5.8%Zn, 1.2% Pb), to the southeast (Andrew, 1993) (Fig. 1-3 and Table 1-1).

The Lower Carboniferous host rocks to the Navan deposit unconformably overlie the Lower Palaeozoic rocks of the Longford Down Inlier (Figs. 1-2, 1-3 and 1-4). These Ordovician clastic, argillaceous and tuffaceous horizons, and Silurian greywackes, mudrocks and siliciclastics, form a series of fault bounded terrains Vaughan (1991). However, the precise nature of the structural geometries affecting these lithologies beneath the Navan deposit are not known (Phillips et al., 1976; Romano, 1980; Leeder, 1982; Freeman et al., 1988; Lee et al., 1990; Kneller, 1991; Murphy et al, 1991; Owen et al., 1992; Vaughan and Johnston, 1992; Chadwick et al., 1993; Lenz and Vaughan, 1994; Todd et al., 1991; Corfield et al., 1996; Readman et al., 1997). It is generally held that the lithologies of the Longford Down Inlier represent a lateral continuation of the Southern Upland Group to the northeast in Scotland, and are therefore demonstrative of a series of accreted exotic terranes (Phillips et al., 1976; Romano, 1980; Leeder, 1982; Freeman et al., 1988; Lee et al., 1990; Kneller, 1991; Murphy et al, 1991; Owen et al., 1992; Vaughan and Johnston, 1992; Chadwick et al., 1993; Lenz and

Vaughan, 1994; Todd et al., 1991; Corfield et al., 1996; Readman et al., 1997). This scenario predicts that the rocks of the Longford Down Inlier lie proximal to the proposed surface trace of the Iapetus Suture ('Navan-Silvermines Fault').

1.2.1 Lower Palaeozoic Stratigraphy

As previously stated, the Navan deposit is hosted by Upper Palaeozoic rocks that unconformably overlie rocks of Lower Palaeozoic age, which outcrop within the Longford Down Inlier to the northeast (Figs. 1-2 and 1-3). The rocks of the Longford Down Inlier have been divided into two distinct "suspect terranes", the Central Terrane and the Grangegeeth Terrane (Murphy et al. 1991). The Central Terrane, consisting of much of the Longford Down Inlier, has been further subdivided into the Longford Down Northern Belt, and the Longford Down Central Belt. Each of these terranes comprises a fault-bounded unit that has been delineated on the basis of lithology, deformational and metamorphic history, and faunal provinciality (see Murphy et al. 1991 and references therein).

1.2.1.1 The Longford Down Northern Belt

The Longford Down Northern Belt consists of Ordovician, possibly Llanvirn to Llandeilo, and late Caradoc or early Ashgillian, greywackes with interbedded shales, cherts, spillites, metabentonites, feldspathic arenites, and cobble conglomerates (Murphy et al. 1991). The same authors describe the geochemistry of these units as being indicative of a volcanic arc setting located to the southeast, while the more felsic igneous and metamorphic detritus was derived from a continental margin to the northwest. The Silurian rocks of the Longford Down

Northern Belt have been dated as Upper Wenlock/Lower Ludlow based on microfossils that occur in a black shale outlier (Murphy et al. 1991).

1.2.1.2 The Longford Down Central Belt

This terrane comprises Llandeilo/Caradoc basic to intermediate volcanics and epiclastics interbedded with carbonaceous shales (the Moffat Shales). The latter begin to dominate toward the southeast (Murphy et al, 1991). Pelagic facies include dark grey carbonaceous shales, olive grey mudstones, metabentonites and minor cherts (Murphy et al., 1991). Greywacke sandstones and metabentonites of Llandovery and Wenlock age overlie pelagic lithologies within the Silurian of the Longford Down Central Belt. (Murphy et al., 1991).

1.2.1.3 The Grangegeeth Terrane

The Grangegeeth Terrane comprises Ordovician and Silurian rocks which outcrop between Navan and Clogher Head in Co. Louth (Murphy et al., 1991), and form the Lower Palaeozoic basement beneath the Navan deposit. The Terrane is bounded to the north by the Navan Fault and to the south by the proposed Slane Fault (Fig. 1-2), which is delineated by aeromagnetic and gravity gradients (Murphy et al, 1991). The Ordovician lithologies consist of the basal volcanoclastics and Llanvirn sediments and mugearite flows of the Slane Group (Murphy et al., 1991). These are unconformably overlain by the Grangegeeth Group of proposed early Llandeilo to lower Caradoc age. This Group comprises volcanic conglomerates and related sediments (Romano, 1980; Murphy et al, 1991). The overlying Mellifont Abbey Group of Upper Caradoc black shales, is

followed by mudrocks and volcanoclastic sandstones of Ashgillian age (Murphy et al, 1991).

1.2.2 Upper Palaeozoic Stratigraphy.

The Carboniferous succession at Navan comprises a sequence of predominantly carbonaceous lithologies that represent a major marine transgression from south to north throughout the Courceyan, Chadian and Arundian (Fig. 1-4). These rocks are divided into three groups, the Navan Group, the Argillaceous Bioclastic Limestone (ABL) Group and the Fingal Group. The marine transgression occurred in response to the ultimately catastrophic subsidence of several fault-bounded basins within the Irish Midlands, e.g. the Dublin Basin, a result of an extensional tectonic regime predominating to the north of the developing Hercynian Orogeny.

1.2.2.1 The Navan Group (Courceyan).

1.2.2.1.1 The Red Beds.

Resting unconformably on the Lower Palaeozoic basement is the basal member of the Navan Group (Fig. 1-4). This unit comprises immature, proximal, terrestrial/littoral polymict conglomerates, sandstones and mudstones, and is known locally as the Red Beds. Sporadically containing caliche horizons, this unit is chiefly composed of detrital fragments sourced from the underlying Lower Palaeozoics (Mallon, 1997). Also, Everett (2000) suggests that the feldspars have a predominant Caledonian granitic source on the basis of lead isotopes. A zone of intense haematisation extends some way into the underlying Ordovician and Silurian lithologies. Although Courceyan in age, the Red Beds represent a

continuing depositional environment similar to that of the Old Red Sandstone facies of predominantly Devonian aspect in the rest of the British Isles, most notably in the Central Midland Valley of Scotland. The thickness of this member at Navan ranges from 0 to at least 40m, and although the Red Beds steadily thicken to the south, they do not attain any great thickness until the northerly bounding faults of the Munster Basin are crossed, where thicknesses of 4000m or more are attained (Andrew, 1986a).

1.2.2.1.2 The Mixed Beds

The Laminated Beds.

The Laminated Beds mark the beginning of the marine transgressive sequence (Strogen et al. 1990; Rizzi, 1993), (Fig. 1-4). They comprise bioturbated, thinly interbedded, bioclastic calcisiltites and bioclastic mudstones/shales and occasional more persistent yellow sandstones typical of a littoral/shallow water environment. Rizzi (1993) has identified several minor sub-aerial erosion surfaces within the unit indicating that at times the prevailing marine transgression was reversed. The existence within this unit of a chalcedonic silica layer, interpreted as replaced anhydrite (Ashton et al., 1986) along with sporadic, nodular and lensoid occurrences of gypsum indicate that at times evaporative, sabkha conditions dominated the environment.

The Muddy Limestone.

Above the Laminated Beds, the Muddy Limestone (Fig. 1-4), marks a change to deeper water conditions. These limestones predominantly comprise bioturbated, argillaceous, sparsely bio-clastic micrites, occasionally oncholithic, with horizons

of syringopora corals. However, occasional polymict micro-conglomerates pervade the sequence, indicating minor erosive events, some of which penetrate the underlying Laminated Beds (Anderson, 1990; McNestry and Rees, 1992; Rizzi, 1993; Anderson et al., 1998).

1.2.2.1.3 Pale Beds.

The Pale Beds (Fig. 1-4), comprise a sequence of deeper water pelletal, oolitic and bioclastic carbonate lithologies with occasional argillaceous or arenitic members (Strogen et al., 1990). The basal unit within the Pale Beds sequence consists of clean, pale grey, variably oncholithic, 'birds-eye' micrites ('birds-eyes' are indicative of methane gas bubbles Shinn, 1983), up to 60m in thickness termed the Micrite Unit. This lithology forms the host to the basal ore lens (5-Lens) within the Navan deposit. A persistent thin green shale horizon exists within the basal parts of this unit that has been ascribed to an airborne volcanic ash deposit, similar to other such horizons in the Irish Midlands (Andrew, 1993). Another type of green shale derived from Silurian rocks forms the footwall to the Upper G and Ballynoe deposits at Silvermines (Andrew, 1995). Rizzi (1993) however, describes the Green Shale as a palaeosol, and as such representative of a period of minor re-emergence. This green shale horizon is used by the Mine Geologists as the footwall marker to the lowermost 5-Lens part of the deposit.

Several pervasively dolomitised calc-arenitic units occur within the Micrite Unit. One of these, the 5-Lens Dolomite (mine staff informal nomenclature) that towards the top becomes increasingly oolitic and peloidal, forms an important hanging-wall control to the localisation of ore grade mineralisation within the western areas of the deposit (Rizzi, 1993; Anderson et al., 1998). In the eastern

part of the deposit the hanging-wall of 5-Lens is formed by a bioturbated, five-metre thick micaceous calcisiltite termed the Lower Dark Marker (LDM). However, this unit dies out rapidly to the south-west where the Lower Dark Marker Equivalent (LDQ), slightly higher in the succession, serves the same function. This unit is superseded by a ~160m succession of variously oolitic and bioclastic calcarenites and calcargillites. Various (sometimes dolomitised) units are used as 'marker' horizons within this succession, notably (from bottom to top):

- i) The Lower Sandstone Marker (LSM), a massively bedded sandy calcarenite, which demarks the hanging-wall of 4-Lens;
- ii) The Nodular Marker, a mud-rich, nodular, crinoidal calcisiltite, forming the hanging-wall of 3/2-Lens;
- iii) The Upper Dark Marker (UDM), a sequence of dark shale units, denoting the hanging-wall of 1-Lens; and
- iv) The Upper Sandstone Marker (USM), a clean massively bedded sandstone, which falls within the lithologies constraining the U-Lens (Ashton et al., 2001)

Lateral variation occurs within both the 'marker' horizons and the Pale Beds sequences. At least three erosional episodes with their axes trending between north and northwest have been recognised (Anderson, 1990; Anderson et al., 1998). One such channel feature has removed large volumes of the Micrite Unit in

the eastern part of the deposit (Fig. 1-4). Infilled by calcic-micro-conglomerates this feature occurs between the Lower Sandstone Marker and the Nodular Marker (Andrew and Ashton, 1985; Anderson, 1990; Rizzi, 1993; Anderson et al. 1998).

1.2.2.1.4 Shaley Pales.

These rocks comprise bioclastic, locally bryzoan-rich, shales and calcarenites. Philcox, (1984, and 1989) has divided the Shaley Pales into three sub-members comprising:

- i) The Lower Shaley Pales, a series of interbedded bioclastic sandstones, siltstones and shales;
- ii) The Middle Shaley Pales, a sequence of sandstones and calcarenites; and
- iii) The Upper Shaley Pales comprising chiefly richly bioclastic dark shales.

1.2.2.2 The Argillaceous Bioclastic Limestone (ABL) Group (Courceyan/Chadian).

Although this Group is absent within the immediate area of the Navan deposit, it does occur conformably overlying the Navan Group to the northwest of the Liscarton and Castle Faults. Philcox (1989) describes the basal member of the ABL Group as comprising a thick argillaceous mudstone horizon, overlain by an increasingly crinoidal, well-bedded, muddy limestone. This upward trend to dominantly crinoidal, bioclastic debris extends up-sequence until true Waulsortian mudstone facies is developed. This is considered to have been formed in relatively deep water (Strogen et al., 1990). The Supra-Reef Shale (Philcox, 1989) overlies the Waulsortian Limestone and marks the top of the ABL Group.

1.2.2.3 The Boulder Conglomerate (Chadian/Arundian).

Both the Navan Group and the ABL Group are truncated locally by a submarine erosion surface that excavates to the southeast (Boyce et al. 1983a; Philcox, 1989; Ford, 1996).

The erosion surface probably formed in response to gravitational instability caused by major extension and growth faulting in the Navan area during the Chadian (Boyce et al., 1983a; Philcox, 1989; Ashton et al., 1992; Ford, 1996). The erosion surface is overlain by a highly immature polymict mega-conglomerate termed the Boulder Conglomerate that contains clasts of both the Navan and ABL Group rocks interbedded with hemipelagic limestone (Boyce et al., 1983a; Binney, 1987; Ford 1996). To the south of the Navan Deposit the Boulder Conglomerate includes clasts of Lower Palaeozoic rocks indicating that the erosion event removed the complete Courceyan and Chadian sequences in that area (Anderson et al., 1998). The clast size and sorting within the Boulder Conglomerate is highly variable and Ashton et al. (1986) present evidence that some Waulsortian mudstone clasts may not have been fully lithified at the time they were entrained into this unit. The matrix comprises dark, often crinoid-rich shale that, within the area of the deposit, also contains pyrite and marcasite laminae. Philcox (pers. Comm.) has observed the cyclical deposition of various conglomeratic and thin calc-turbidite units (similar to the overlying Thinly Bedded Unit) within the Boulder Conglomerate.

1.2.2.4 Fingal Group (Arundian to Asbian).

1.2.2.4.1 Upper Dark Limestone.

The gradation from the Boulder Conglomerate into the Upper Dark Limestones is variable between an abrupt contact and a steady decrease in clast size (Ashton et al. 1986; Anderson, 1990; Anderson et al., 1998). The basal units of the Upper Dark Limestone are termed the Thinly Bedded Unit and consist of interbedded shales and calc-turbidites (Rees, 1987; Strogon et al. 1990). Common thin pyrite laminae are present within the shale units along with rare pyritic 'rip-up clasts' within the calc-turbidites. Only minor stratiform mineralisation persists between the Boulder Conglomerate and the Thinly Bedded Unit. It comprises sometimes friable, unlithified, cross-bedded, thinly laminated, fine-grained framboidal pyrite and minor sphalerite and galena. In some horizons graded bedding and soft-sediment deformation structures occur. The occurrence and petrography of this pyrite strongly suggest that surface processes were involved in its deposition, and therefore indicates either that exhalative activity similar to that occurring at Tynagh and Silvermines (Boyce et al., 1983b; Banks, 1986; Boyce et al., 1999) may have occurred at Navan during the lowermost Arundian or, conversely, reworking of existing concentrations of pyrite-rich material took place. Whether these concentrations came about through diagenetic or hydrothermal processes remains unresolved.

1.3 Diagenesis of the host rocks and dolomitisation.

Several studies have been completed on the diagenesis and subsequent dolomitisation of the host rocks to the Navan Deposit, most notably those by Anderson (1990), Rizzi (1993) and Peace (1999). All these studies utilised cathodoluminescence and staining techniques to indicate multiple stages of carbonate cementation. Anderson (1990) recognised three stages of calcite cementation,

- i. early dark luminescent fringing cement,
- ii. well-zoned, dull to bright yellow luminescent overgrowths,
- iii. medium yellow, blocky cement.

Three stages of dolomitisation were recorded,

- i. fine-grained (<50 μm), dull brown luminescent mosaic-type replacement of carbonate allochems. This dolomite forms up to 75% of the rock. The dolomite rhombs are reported as frequently displaying corroded margins.
- ii. a dark, non-luminescent cement that occurs in veins within, and overgrowths to, the stage 1 dolomite rhombs. This dolomite frequently occurs in association with sulfides (see Vasconcelas et al., 1995; Vasconcelas and McKenzie, 2000).
- iii. the last stage occurs as coarse cement. Non-luminescent except for a bright red band, this dolomite is restricted to veins and vugs.

Anderson (1990), and Anderson et al. (1998), conclude that the stage 1 dolomite is consistent with formation in a shallow burial environment, and that the later stages were synchronous with, and later than, the mineralising event.

That the stage 1 dolomite was precipitated at a shallow burial depth is also consistent with the more clastic members within the Pale Beds succession being

preferentially dolomitised because of a greater original porosity over the more carbonate-rich members (Anderson, 1990; Anderson 1998).

Rizzi (1993) and Braithwaite and Rizzi (1997) have identified the existence of a 'dolomite plume' that they attribute to hydrothermal processes associated with the mineralising event. The plume is roughly concordant with NNE-NE faulting within the horst structure in the northern and north-western parts of the deposit and forms a major control on the localisation of ore in the western parts of 5-Lens. Peace (1999), and Peace and Wallace (2000), describe the diagenetic history of the Upper Pale Beds (host to the U-Lens), and the Boulder Conglomerate. Again, several generations of cement are recognised;

- i. Initial fine, inclusion rich, syntaxial, fibrous (isopachous) calcite that is non-luminescent with dull-luminescent rims in CL light.
- ii. A second cement of coarser, equant calcite, well zoned in CL, is further subdivided into;
 - a) Pre-mineralisation (complexly zoned non-luminescent to dull-bright bands)
 - b) Syn-mineralisation (bright), and
 - c) Post-mineralisation (dull to non-luminescent)

Dolomitisation is regarded by Peace (1999), and Peace and Wallace (2000), as pre-mineralisation, with only the later saddle dolomite apparently synchronous with sulfide emplacement.

1.4 Structure

Several large NE/SW trending fractures cross the mine area and its periphery, namely the Randlestown and Castle Faults to the northwest, and the D Fault to the southeast (Figs. 1-3). These Caledonoid faults have a long history of reactivation up to and including the Hercynian (Phillips and Sevastopulo, 1986). Within the deposit itself major Lower Carboniferous extensional faulting is represented by the partly listric ENE trending B and T Faults to the southeast, and the Liscarton Fault to the northwest (Figs. 1-3 and 1-5), as well as related M, P and Y structures further to the southwest (Fig. 1-6), which downthrow to the south-southeast. These faults define a southwesterly plunging asymmetric horst structure in the northern part of the deposit (Fig. 1-7). As there is no sign of thinning of lithological units over the horst block, it is inferred that this structure did not develop until at least late Chadian times.

There are numerous minor steeply dipping normal faults that are, in places, apparently truncated by the larger, partly listric structures. The minor faults trend from NNE, through NE to ENE, and are confined to early to mid Lower Carboniferous lithologies. They predate or are coeval with the earliest movements on the major, partly listric, ENE trending extensional faults that locally penetrate some way into the overlying Arundian strata. The Liscarton Fault apparently delineates the northwest limit of the zone of economic mineralisation. Jointing within the carbonates trends to the northwest and is considered to be of Upper Carboniferous age (Ashton et al., 1986; Ashton, 1995). Regionally the host rocks have been tilted through minor folding of likely Upper Carboniferous age (Ashton et al., 1986), and currently dip at 15° to 20° to the southwest. Locally, however, the folding is more intense - especially in close proximity to faults.

1.5 Detailed Mineralogy and Mineral Textures.

The detailed mineralogy and associated textures are described in Anderson (1990) and Anderson et al. (1998). The Navan orebody displays a stacked, tabular multi-lensoid stratabound geometry with ~97% of the deposit being hosted by the Pale Beds sequences termed the Pale Beds Ore (PBO). The remaining ~3%, located within the Boulder Conglomerate, is termed the Conglomerate Group Ore (CGO). As previously discussed, the chief ore minerals are sphalerite and galena. Pyrite and marcasite occur throughout the deposit but are mainly concentrated in the northeast parts of 5-Lens, 1-Lens and the Conglomerate Group Ore. Swarms of marcasite veins, trending slightly obliquely to, but occurring proximal to, the T Fault (and very locally the B Fault), are located in the footwall of this structure (Andrew and Ashton, 1985). Gangue minerals are mainly calcite and dolomite. Barite does occur throughout the deposit but is nowhere economic. A minor mineralogy comprising semseyite ($\text{Pb}_9\text{Sb}_8\text{S}_{21}$), bournonite (PbCuSbS_3), freibergite ($(\text{Ag,Cu,Fe})_{12}(\text{Sb,As})_4\text{S}_{13}$), pyrargyrite (Ag_3SbS_3), boulangerite ($\text{Pb}_5\text{Sb}_4\text{S}_{11}$), cylindrite ($\text{Pb}_4(\text{Fe,Sn})_4\text{Sb}_{12}\text{S}_{16}$), argyrodite (Ag_8GeS_6) and jordanite ($\text{Pb}_{14}(\text{As,Sb})_6\text{S}_{23}$) has been reported (Boast, 1979; Ashton et al. 1986).

Ore textures are diverse. The following styles have been recorded.

- a) Massive replacement of host carbonates.
- b) Mineralised, sub-vertical fractures (veins).
- c) Bedding-parallel veins.
- d) Geopetal infilling of cavities by sulfide rhythmities.
- e) Erosion surfaces within geopetal cavities and bedding parallel veins.
- f) Extensive (>5m bedding parallel) stratiform sulfide rhythmities.

- g) Deformation of sulfide rhythmites including boudinage, slumping and rollover structures.
- h) Deformation of laminated stratiform framboidal pyrite including soft-sediment deformation (load casts), slumping, cross bedding, and rollover structures. (These features are chiefly concentrated in the CGO and overlying Thinly Bedded Unit).
- i) Brecciation of all the above styles (especially in the Boulder Conglomerate)
- j) Disseminated sulfides.

Mineral textures are diverse. The following have been recorded; where applicable the predominant phases within the texture type are included in brackets;

- a) Coarse-bladed sulfides (marcasite and galena).
- b) Zoned sulfides (sphalerite).
- c) Rhythmically banded sulfides (sphalerite).
- d) Granular sulfides.
- e) Cubic sulfides (galena).
- f) Stalactitic sulfides.
- g) Honeyblende sphalerite.
- h) Dendritic sulfides (galena).
- i) Laminated sulfides.
- j) Replaced allochems (sphalerite).
- k) Colloform (pyrite and sphalerite).
- l) Framboidal (pyrite).

Course-grained, euhedral sulfides (predominantly honeyblende sphalerite), are restricted to open fractures i.e. faults and joints.

1.6 Existing models for metallogenesis within the Irish Midlands and previous investigations at Navan

Much debate has surrounded the base-metal deposits of the Irish Midlands with regard to their origin and process of emplacement (see discussions in Russell; 1978, Hitzman and Beaty, 1996). Enough features occur regularly within each of the deposits for workers in the ore-field to classify these deposits as Irish-Type, as distinct from Mississippi Valley and Sedimentary Exhalative types. These features are;

1. The deposits are hosted by the lowermost 'clean' carbonate horizon in the Carboniferous succession (Waulsortian Mudbank Limestones or their immediate equivalents in the south Irish Midlands, Navan Group rocks in the north) (Andrew, 1993).
2. Most deposits are associated with ENE extensional faults that were demonstrably active during the early to mid-Lower Carboniferous. (Andrew, 1993).
3. Studies at Silvermines, Tynagh and Navan have revealed a bimodal distribution of $\delta^{34}\text{S}_{(\text{SULFIDE})}$ values. By far the largest component of measurements (80 to 90%), comprise negative values centred on -15 per mil, attributed to the open system bacteriogenic reduction of seawater sulfate. The remaining 10 to 20% with a mean of $\sim +10$ per mil is considered to have been sourced from diagenetic

sulfides located in the Lower Palaeozoic basement (Anderson et al., 1989; Boyce et al., 1994, Fallick et al., 2001).

4. $\delta^{34}\text{S}_{(\text{SULFATE})}$ values are indistinguishable from those of Lower Carboniferous seawater. (Coomer and Robinson, 1976)

5. Fluid temperatures range from $<100^{\circ}\text{C}$ to around 250°C with salinities of between 10 and 30 wt% NaCl (Everett et al., 1999). However, because of the fine-grained nature of the ore sulfides within the Irish Midlands, there is no data from many deposits, and some authors question these results (e.g. Hitzman and Beaty, 1996).

Metallogenic models for the Irish Type deposits are essentially polarised around two end member propositions. First of these is the Mississippi Valley-Type (MVT) hypothesis (Fig. 1-8) which invokes either a migrating basinal brine, driven by increased geothermal gradients during basin extension, or by gravity induced flow resulting the hypothetical presence of nearby elevated topography (Lydon, 1986; Hitzman, 1995; and refs. in Hitzman and Beaty, 1996). Second, a model employing an isolated deepening convective cell sourcing seawater as a major component, as proposed by Russell (1978), which has the capacity to accommodate synsedimentary/syndiagenetic mineralisation similar to Sedimentary Exhalative (SedEx) deposits (Fig. 1-9).

Knowledge of the timing of metallogenesis within the Irish Midlands can aid elucidation of the more relevant model. The convective cell of Russell (1978) can operate at any time, requiring only a suitable convection driver, either heat or enhanced density contrasts. Although capable of functioning either at the same

time as the host rocks were being laid down (syngeneses), or at a later juncture (epigenesis), the Russell (1978) model has however, become synonymous with a syngenetic/syndiagenetic age relationship. Conversely the topographic flow model of Hitzman (1995) and Hitzman and Beaty (1996) requires elevated topography, which, due to the developing Variscan Orogeny, the model locates to the south of the Irish Midlands. This situation would only pertain during the Upper Carboniferous and, therefore, given the age of the host-rocks, mineralisation could only be epigenetic.

While it has been demonstrated by various workers that deposits such as Tynagh and Silvermines can be classed, at least in part, as truly exhalative in nature (Boyce et al., 1983b; Banks, 1985; Boyce et al., 1999), and therefore the same age as the host rocks (~355Ma early Lower Carboniferous), the Navan deposit remains enigmatic in this respect (Ashton, 1995; Ashton et al., 1992; Andrew, 1993; Anderson, 1990; Anderson et al., 1998; Ford, 1996, Peace 1999; Peace and Wallace, 2000). The presence of Boulder Conglomerate-infilled 'neptunian dykes' that dislocate lower Pale Beds hosted sulfide veins below the Erosion Surface suggests that mineralisation began before the Boulder Conglomerate was emplaced (Fig. 1-10). This conclusion is supported by rotated, truncated clasts of sulfide-bearing Pale Beds within, and stratiform sulfide mineralisation occurring both within and immediately above the Boulder Conglomerate (Ashton et al. 1992), (Fig. 1-11). These textures also strongly suggest that mineralisation occurred prior to, during sedimentation of and perhaps after, deposition of the Boulder Conglomerate i.e. the late Chadian (345Ma). However, the precise nature and timing of sulfide emplacement has yet to be ascertained. Anderson 1990; Ashton et al., 1992; Ford, 1996; and Anderson et al 1998 favour a Chadian age

(i.e. syndiagenetic/synsedimentary mineralisation), whereas Peace, 1999 and Peace and Wallace, 2000 propose a Holkerian (340Ma) age. In the latter's view, mineralisation is entirely epigenetic. These arguments aside, the Navan deposit is generally considered to be Courceyan/Chadian in age because of the above-mentioned crosscutting relationship of the overlying Boulder Conglomerate (Boyce et al. 1983; Philcox, 1989; Ashton et al., 1992, Anderson 1990; Anderson et al., 1998; Ford 1996). Further to these textural relationships, Halliday and Mitchell (1983) have published a single K-Ar date of $366\text{Ma} \pm 11$ (Courceyan to Chadian) whilst Symmons et al (in press), has produced a palaeomagnetic age of $330\text{Ma} \pm 8$ (Holkerian).

Lead isotopes reflect a similar signature to that of the underlying Lower Palaeozoic/Dalradian basement. The distribution of the most radiogenic Pb at Navan ($^{206}\text{Pb}/^{204}\text{Pb} = 18.2$) persists vertically throughout the ore body (O'Keefe 1986; LeHuray et al. 1987). However, a progressively less radiogenic signature increases with ascent through the orebody so that 1 Lens displays $^{206}\text{Pb}/^{204}\text{Pb} = 17.6$. (Mills et. al. 1987). The results of Mills et al. (1987) may indicate that whilst the lead source was mainly orogenic a small fraction was obtained from Dalradian rocks at depth below the Navan ore-body (but see discussion in Fallick et al., 2001).

Sulfur isotope studies have revealed two dominant populations of $\delta^{34}\text{S}_{(\text{SULFIDE})}$ (Anderson 1990; Anderson et al, 1998), -23‰ to -5‰ , and 0 to 15‰ , and a smaller third grouping, -32‰ to -28‰ . Following Coomer and Robinson's (1976) isotopic study at Silvermines, populations of lighter values have been interpreted as representing bacteriogenic reduction of seawater sulfate, (-23‰ to -15‰), whereas the $+8\text{‰}$ to $+15\text{‰}$ range represents hydrothermal sulfur postulated as

being sourced from diagenetic sulfides in the Lower Palaeozoic basement (e.g. Anderson et al., 1989). Values straddling the two main populations indicate mixing of the two fluids. There is also an apparent correlation between sulfur_(SULFIDE) values and mineral textures (Anderson 1990; Anderson et al., 1998). Sulfur_(SULFATE) reflects that of seawater sulfate during the Lower Carboniferous (Claypool et al., 1980). Analyses of carbonate isotopic compositions ($\delta^{18}\text{O} = -6.6\text{‰}$ to -10.4‰ and $\delta^{13}\text{C} = -0.2\text{‰}$ to $+2.5\text{‰}$) within a proposed hydrothermal dolomite plume at Navan are indicative of a depositional fluid similar in composition to that of Carboniferous seawater (Braithwaite and Rizzi, 1997; but see also discussions in Vasconcelos et al., 1995 and Vasconcelos and McKenzie, 2000).

Because of the fine-grained textures of the sulfides, microthermometric data are rare, and in consequence may be unrepresentative of the mainstage ore depositional system. Further, Peace (1999) underlines the unreliability of fluid inclusion data from barite, as the inclusions are prone to stretching, and applies this argument to inclusions from the carbonate and sulfide phases. She reports wide variations in homogenisation temperatures in inclusions with similar salinities within diagenetic cements from the Upper Pale Beds. In contrast to the Everett et al (2000) findings, Peace (1999) favours a sulfide precipitation temperature at between 90 and 120°C. Fluids recognised at Navan, by Braithwaite and Rizzi (1997), Everett et al (2000), Peace (1999) and Everett (unpublished data) are given in Table 1-3.

Host mineral	Interpreted paragenesis	Th(°C)	Salinity (wt% NaCl equiv.)	Reference
Calcite	Pre-ore (U Lens)	56.4-145.0 (n=49)	0.7-26.3 (n=22)	Peace (1999)
Saddle dolomite	Syn-ore (U Lens)	89.4-174.8 (n=40)	4.7-21.6 (n=4)	Peace (1999)
5 Lens dolomite	Syn-ore (5 Lens)	82.6-159.3 (n=6)	No Data	Braithwaite and Rizzi (1997)
Dolomite plume	Syn-ore (5 Lens)	100.5-134.3 (n=8)	No Data	Braithwaite and Rizzi (1997)
Stratal dolomite	Syn-ore (5 Lens)	59.7-102.3 (n=2)	No Data	Braithwaite and Rizzi (1997)
Sphalerite	Syn-ore (5 Lens)	147.3 (n=1)	No Data	Braithwaite and Rizzi (1997)
Sphalerite	Syn-ore (5 Lens)	186.9-260.5 (n=13)	15.1-17.2 (n=4)	Everett et al. (1999)
Calcite	Post-ore (U Lens)	66.2-158.0 (n=38)	3.6-22.0 (n=12)	Peace (1999)
UDL, saddle dolomite	?	142.5 (n=1)	No Data	Peace (1999)
UDL, sphalerite	?	67.6-139.9 (n=8)	5.3-5.9 (n=2)	Peace (1999)
UDL-hosted calcite	?	90.7 (n=1)	22.2 (n=1)	Peace (1999)
Dolomitized hostrock	Pre-syn ore (5 Lens)	111.2-151.1 (n=6)	6.3-13.0 (n=5)	Everett (unpublished data)
Dolomite veins, vugs	Syn-late-orestage	97.8-184.2 (n=22)	7.2-26.5 (n=27)	Everett (unpublished data)
Sphalerite	Syn-ore (5 Lens, 2-3 Lens)	75-156 (n=86)	5.4-18.2 (n=52)	Everett (unpublished data)
Calcite	Syn-late ore (5 Lens, 2-3 Lens)	75-134 (n=29)	5.6-23.3 (n=31)	Everett (unpublished data)
Sphalerite	Syn- to post-ore	79-122 (n=11)	24.3-24.9 (n=12)	Everett (unpublished data)
Calcite	Late sulphosalts	92.8-124 (n=7)	19.9-24.7 (n=9)	Everett (unpublished data)
Calcite	Post-ore veins	54-99 (n=7)	3.2-23.7 (n=11)	Everett (unpublished data)

Table 1-3 Table of microthermometric results from the Navan deposit. (Braithwaite and Rizzi, 1997; Everett et al., 2000; Peace, 1999; and Everett, unpublished data).

1.7 Aims

The identification of the routes taken by the metal bearing solutions and the locally derived bacteriogenic sulfide-bearing fluid is important for the understanding of the genesis of the Navan deposit. The delineation of these conduits has relevance to identifying

- i) The discovery of more ore within the Navan deposit,
- ii) The discovery of similar deposits,
- iii) The likely source-rocks of the metals, and
- iv) The timing of the metallogenic event.
- v) Refinement of the genetic model.

A well-constrained palaeohydrological model therefore has implications with regard to exploration expenditure in and around the Navan ore-body, as well as throughout the Irish base-metal ore-field.

The most likely candidates for the source-rocks are either the Lower Carboniferous 'Red Bed' sequences underlying the host lithologies (Hitzman and Beaty, 1996), or the Lower Palaeozoic pile forming the (non-crystalline) basement (Russell, 1978; 1986). Personal observation suggests that the Lower Carboniferous Red Beds at Navan have undergone little or no alteration other than in areas restricted to faulting or at the boundary with the overlying Laminated Beds. This is in accordance with the findings of Mallon (1997). However, significant alteration of certain lithostratigraphic members within the Lower Palaeozoic basement has been observed. If a geochemical link between the Navan

deposit and altered Ordovician and Silurian non-crystalline basement can be established it would imply that the Lower Palaeozoic prism played a larger role in permitting metal-bearing fluid migration than did the basal Carboniferous Red Beds. Such an observation may indicate the existence of potential economic mineralisation hosted by the Lower Palaeozoic basement similar to mineral deposits located within Cambrian to Silurian horizons elsewhere in the British Isles and thought to be of a similar age e.g. Tyndrum and Leadhills/Wanlockhead in Scotland, and the South West Shropshire Orefield on the Welsh Borders (Patrick et al., 1983; Patrick and Russell 1989).

The question of which of the two models outlined above is best supported can be addressed by three essential areas of study;

i) An examination of the spatial and temporal relationship between economic mineralisation and faulting of both Lower and Upper Carboniferous age,

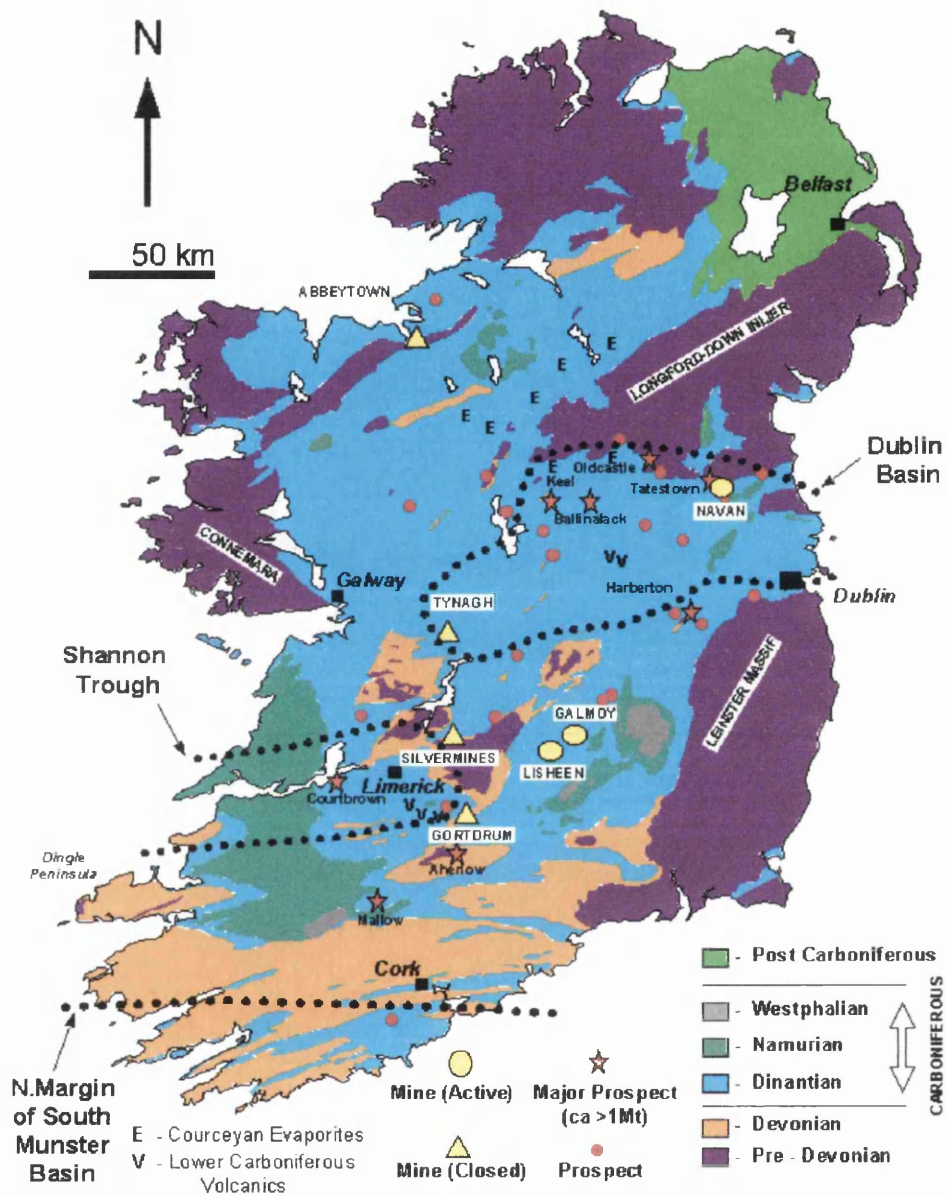
ii) A comparison of the trends of major element distributions and prominent structures within both the deposit and the Lower Palaeozoic basement, and

iii) A sulfur isotope geochemical study to elucidate the pathways of fluid flow during mineralisation.

Timing the mineralisation event with respect to movements on faults that now control the disposition of the Navan deposit constrains the age of metallogenesis. Coupled with a more comprehensive investigation into the major element (Zn, Pb and Fe) distribution within the Navan deposit (see an earlier study by Andrew and

Ashton 1985) elucidates the likely immediate source of the metal-bearing fluids, and probable fluid pathways within the deposit host.

To investigate fluid conduits highlighted by the major element study, a high-resolution analysis of $\delta^{34}\text{S}$ dispersion patterns across such structures was carried out to search for distinct emanative centre(s) associated with the genesis of the orebody. The $\delta^{34}\text{S}$ work was based on the ability to recognise the proposed metal-bearing fluid (positive $\delta^{34}\text{S}$ values) (Anderson, 1990; Anderson et al., 1989; Anderson et al., 1998) representing around twenty percent of the total sulfide in the orebody (see also Fallick et al., 2001), and the proposed locally derived fluid bearing bacteriogenically reduced Lower Carboniferous seawater sulfate (negative $\delta^{34}\text{S}$ values) (Anderson, 1990; Anderson et al., 1998; Fallick et al., 2001). A well-constrained palaeohydrological model for the Navan orebody would not only enable a more accurate identification of potential source areas, but also aid in improving the model for ore genesis and help establish the evolution of the depositional environment. This in turn assists in the identification of prospective ground likely to host economic mineralisation within the Irish orefield.



cts,

Figure 1-1 Geological map of Ireland showing the distribution of Lower Carboniferous carbonates and the location of economic and sub-economic Zn+Pb deposits (see Table 1.1 for comparison of tonnages and grades).

(Diagram courtesy of Dr J H Ashton, Outokumpu-Tara Mines Ltd.)

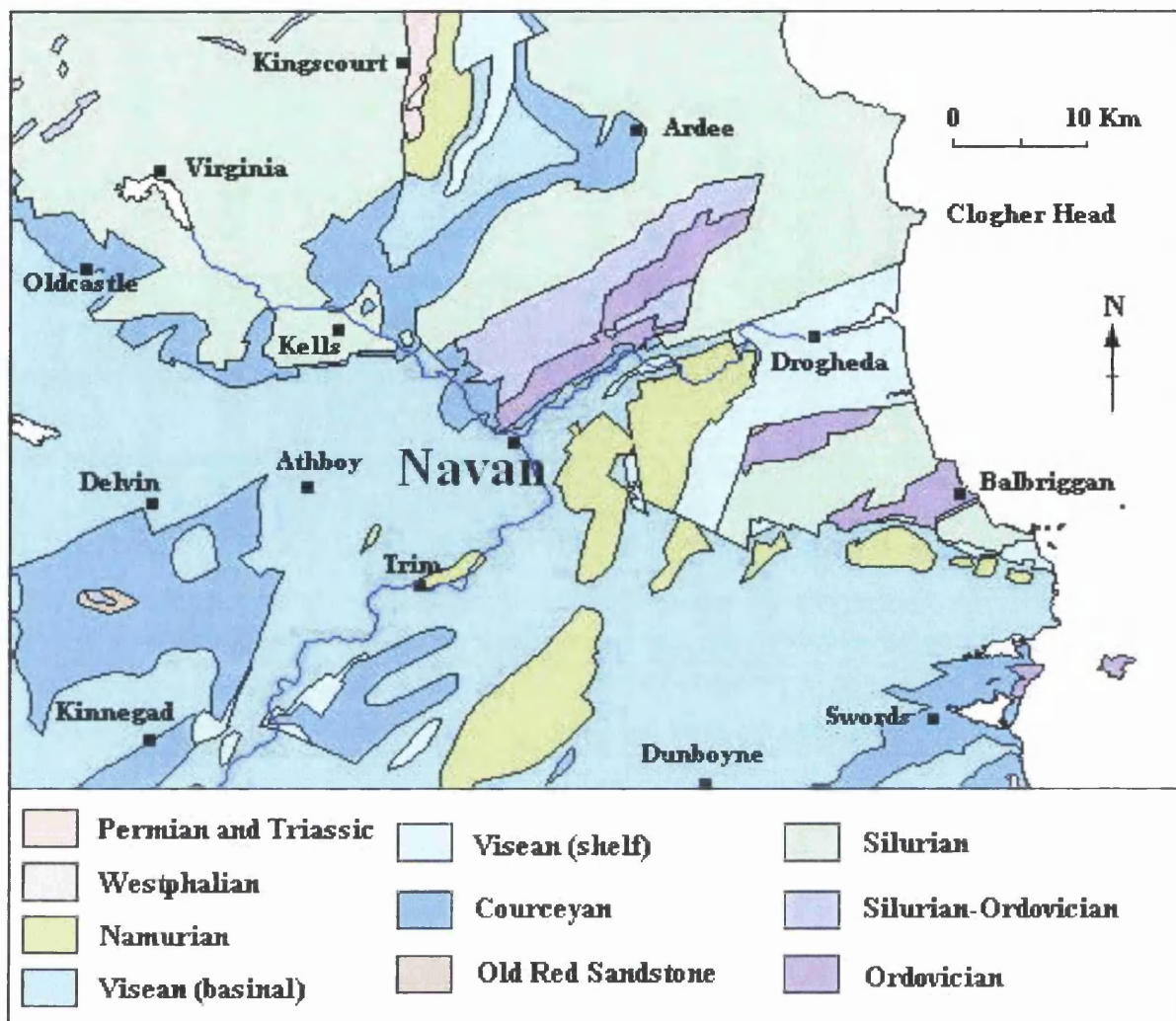


Figure 1-2 Detailed geological map of the northern part of the Dublin Basin, and adjoining parts of the Longford Down Inlier. (Adapted from Geraghty and McConnell, 1999).

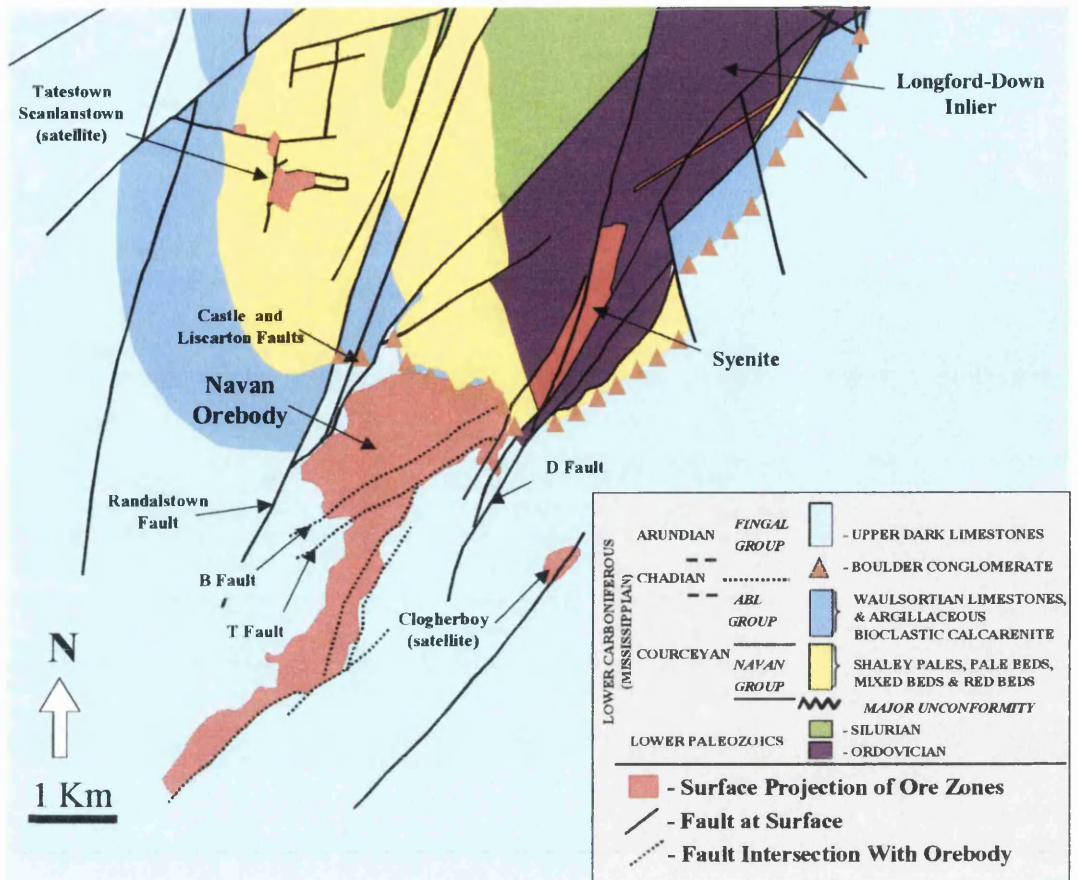


Figure 1-3 Geological map of the area immediately surrounding the Navan deposit. (Adapted from Ashton et al. 2001)

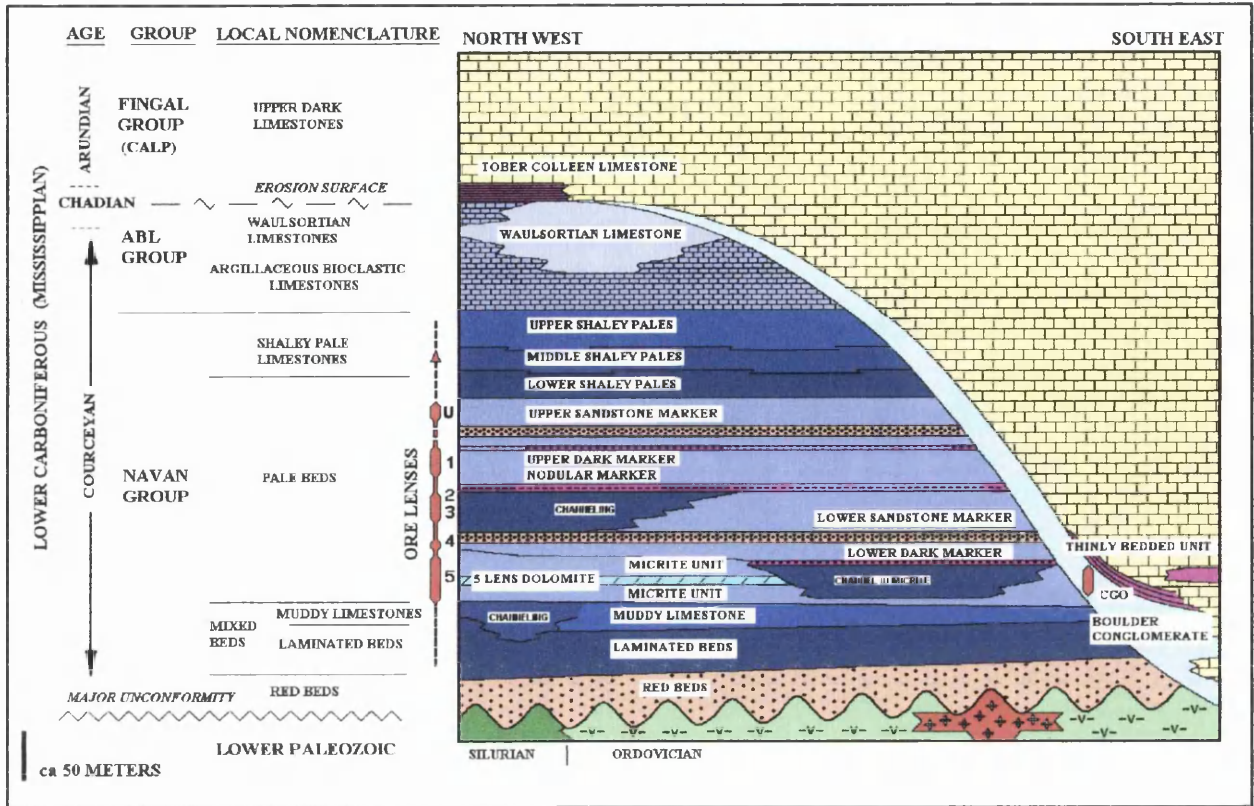


Figure 1-4 Schematic stratigraphic column for the Navan deposit
(adapted from Ashton et al., 1992 and Anderson et al., 1998)

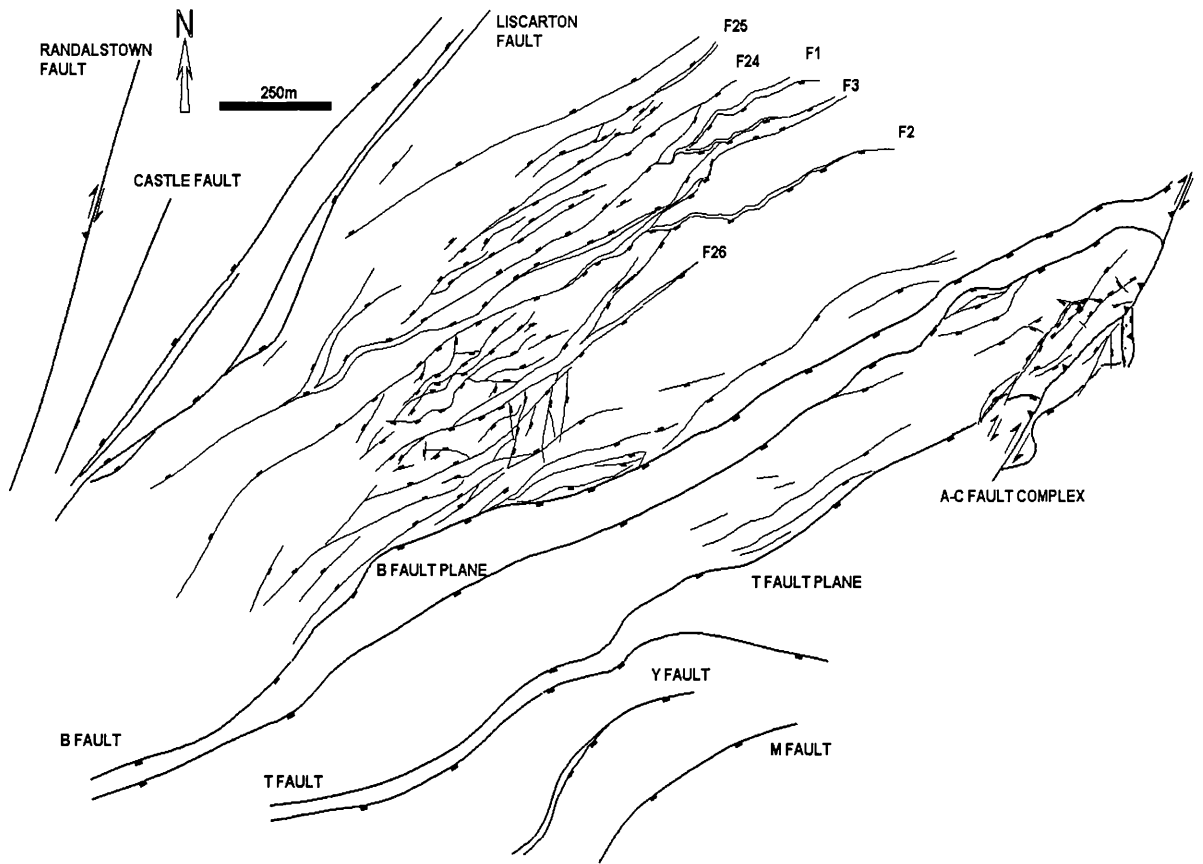


Figure 1-5 Simplified structural plan of the base of 5 Lens in the Navan deposit (see enclosure at back of this Thesis for the detailed plan).

(Diagram courtesy of Dr J H Ashton, Outokumpu-Tara Mines Ltd.)

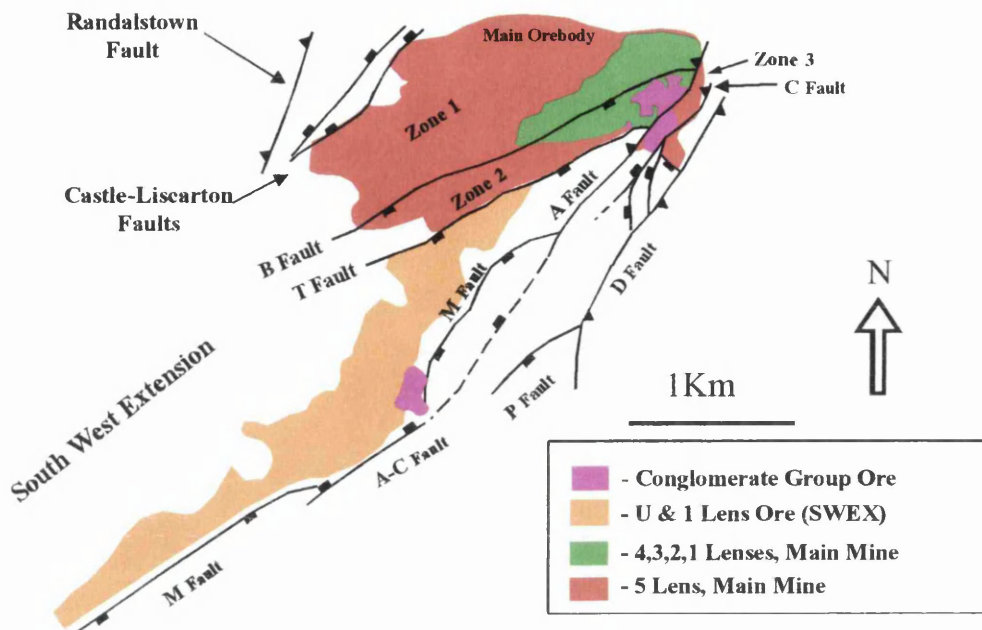


Figure 1-6 Plan of the major structures and their relationship to the geometry of ore lenses within the Navan deposit. (Adapted from Ashton et al. 2001).

NW

SE

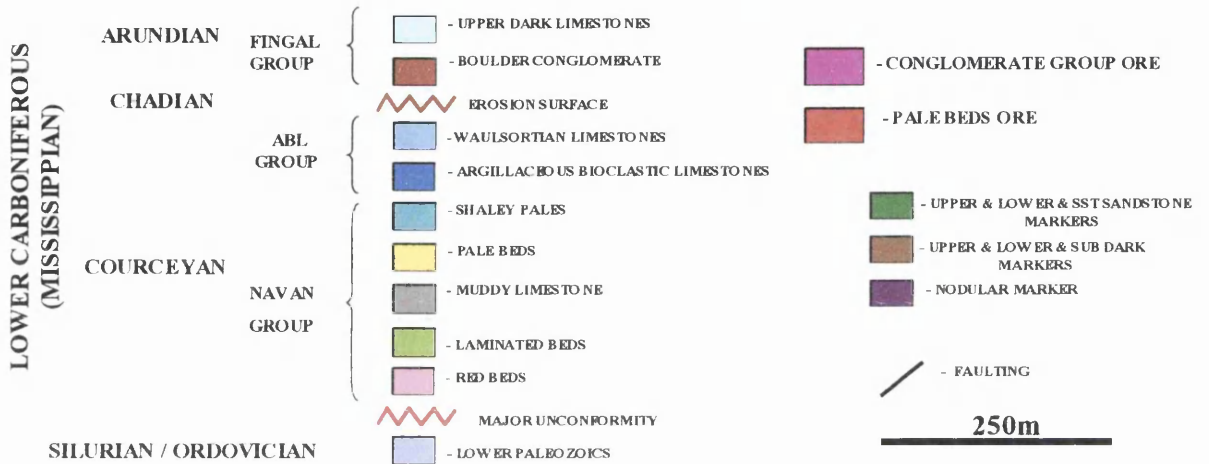
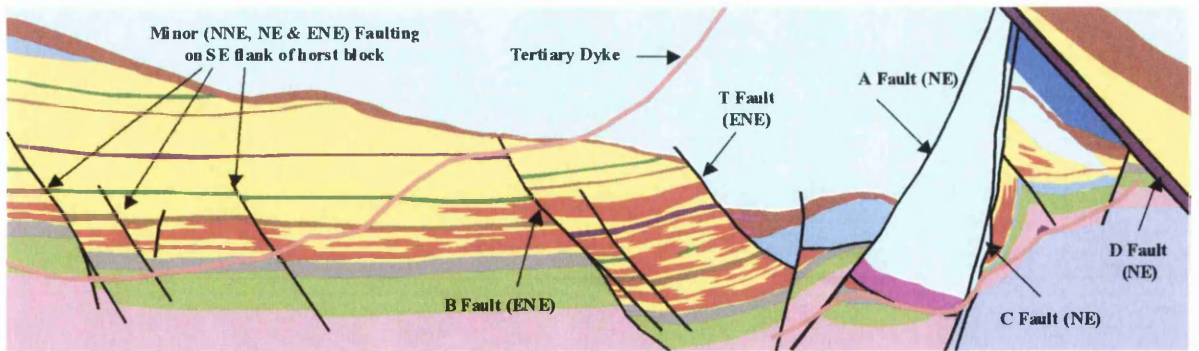
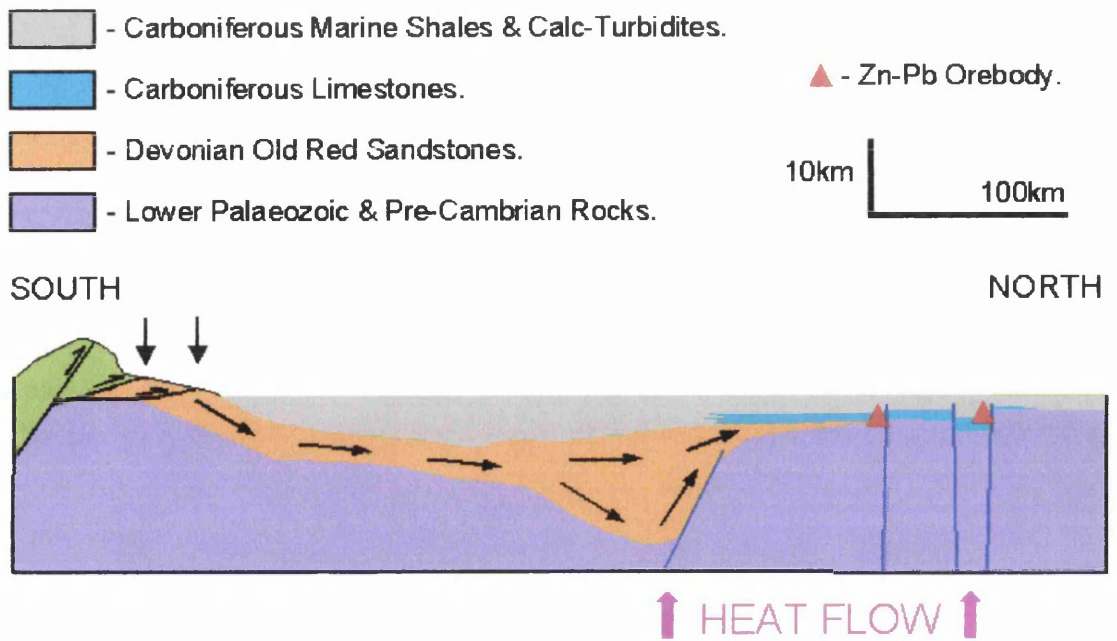


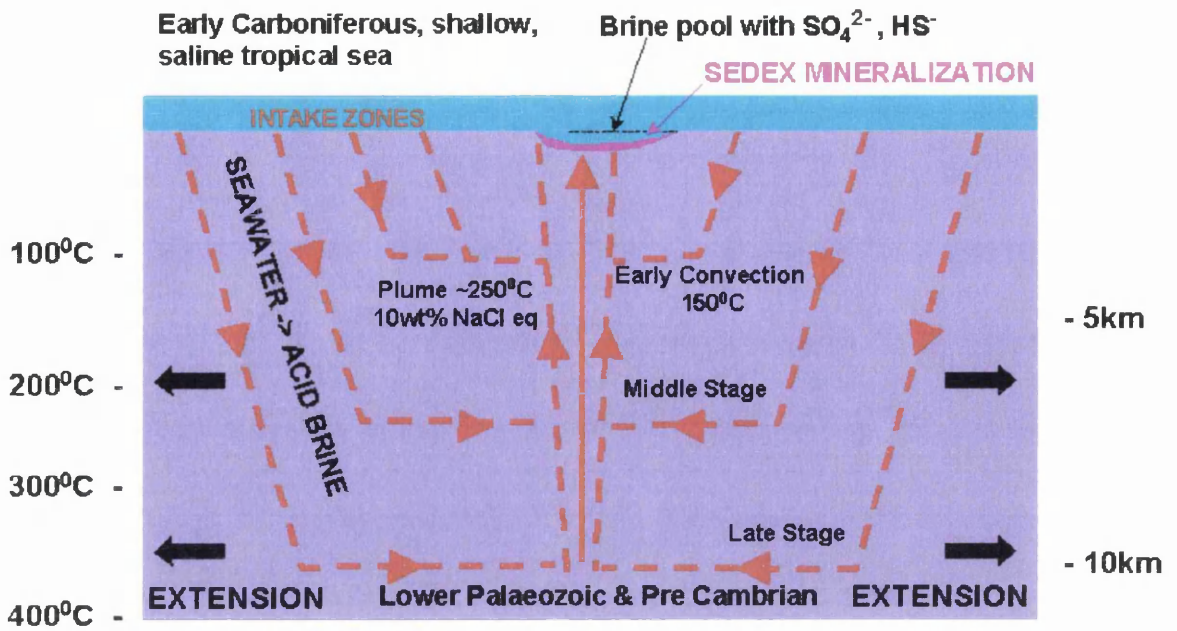
Figure 1-7 Generalised cross-section through the Navan deposit showing the relationship of the major (ENE) and minor (NNE to ENE) faults and the location of 5 lens. Adapted from Ashton et al. (2001).



Topography-Driven Model for Fluid Generation & Flow for Generation of Irish Carbonate-Hosted Zn/Pb Deposits (after Hitzman & Beaty, 1996).

Figure 1-8 The topography-driven (MVT) model for fluid generation and flow for the generation of the Irish carbonate-hosted Zn/Pb deposits (after Hitzman and Beaty, 1996).

(Diagram courtesy of Dr J H Ashton, Outokumpu-Tara Mines Ltd.)



Deep Convection Model for Fluid Generation & Flow for Generation of Irish Carbonate-Hosted Zn/Pb Deposits eg Silvermines (after Russell, 1986)

Figure 1-9 The deep convection (SedEx) model for fluid generation and flow for the generation of the Irish carbonate-hosted Zn/Pb deposits (after Russell, 1986).

(Diagram courtesy of Dr J H Ashton, Outokumpu-Tara Mines Ltd.)



Figure 1-10 'Neptunian dyke' within Pale Beds immediately below the Erosion Surface, infilled with Boulder Conglomerate material. Note that this feature cut across a series of Zn+Pb veins in the lower half of the photograph, (Hammer for scale). Extracted from Ashton et al., (1986).

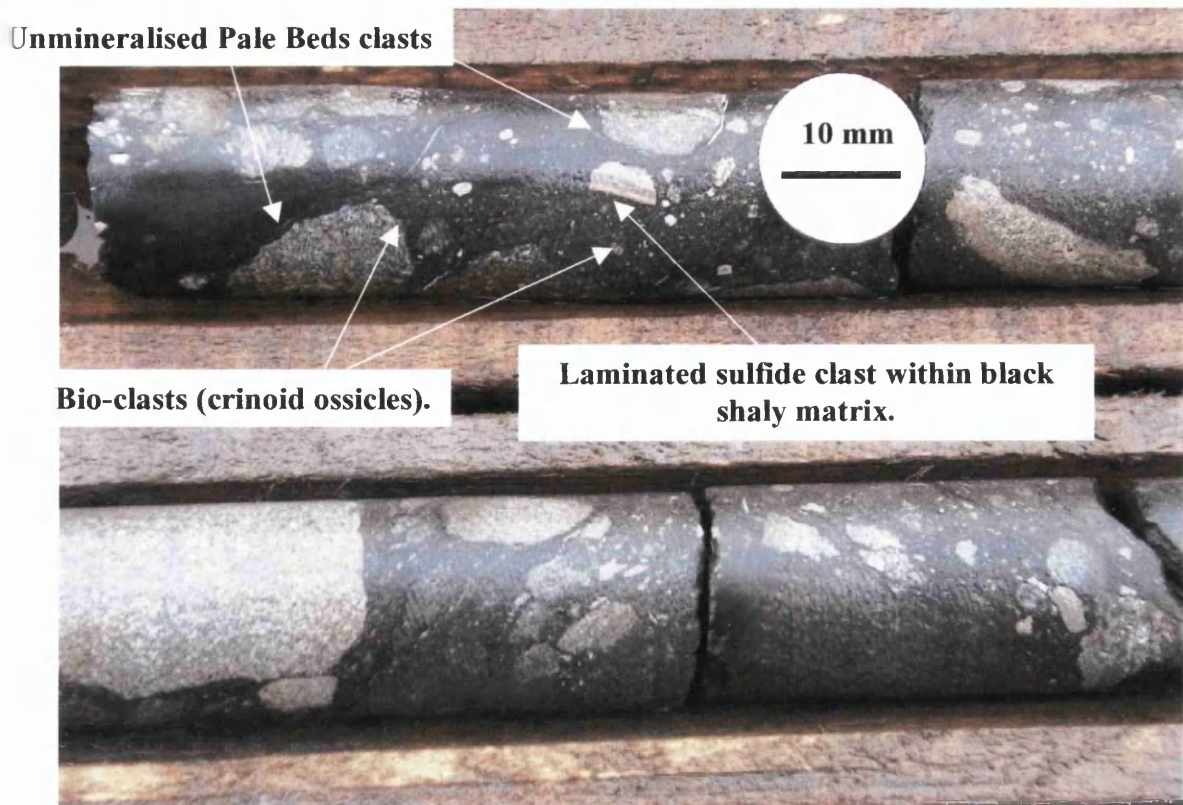


Figure 1-11 Example of a laminated sulphide (mainly sphalerite) clast hosted by the Boulder Conglomerate (DDH U14898 @ 58.5m), in close proximity to crinoid ossicles and unmineralised Pale Beds clasts. Note that fine-scale replacement (dominantly sphaleritisation) of bioclastic debris is a common feature in the underlying Pale Beds ores (Anderson et al., 1998): these ossicles are not replaced by sulfide.

2. Faulting within the Navan deposit and its temporal relationship to mineralisation.

2.1 Aims

While previous work on the Navan deposit has revealed that a minimum age of mineralisation ~345Ma can be demonstrated (see Chapter 1), a constraint on the initiation of metallogenesis remains poorly defined. A study of underground exposure presented an opportunity to elucidate the relationships between mineralisation, Lower Carboniferous extensional faulting and an Upper Carboniferous strike-slip fault. Thus a constraint on the timing of economic mineralisation relative to the final movements on those structures could be established.

2.2 Method

In order that the relationship between mineralisation, the B Fault Complex, (one of the major, partly listric, extensional faults of late-Chadian age that control the current disposition of the orebody), and a dextral-reverse strike slip assemblage could be considered, exposures within the 1330 1-3 Lens Hanging Wall Access Drift, and associated crosscuts, were examined in detail (Fig. 2-1 and 2-2). The drift was driven in a roughly west-south-westerly direction into an area of economic mineralisation previously delineated by underground diamond drilling. Four crosscuts within the drift provide further exposures of the features under discussion. Underground mapping was completed at a scale of 1:250, while the 1330 1-3 Lens development was progressing, and was accompanied by

examination of underground diamond drill core to constrain the positions of major features (Fig. 2-3).

2.3 Evolution of faulting

Major, Caledonide faults trend NE around the area of the Navan orebody (i.e. the Randlestown, Castle and D Faults) (Philips and Sevastopulo, 1986; Ashton 1995). It is important to note that these fractures do not affect the deposit itself and are not associated with increases in the grade of mineralisation. These Caledonide faults now demonstrate dextral-reverse displacements that are thought to reflect reactivation during Upper Carboniferous tectonism (Philips and Sevastopulo, 1986). The Navan deposit itself is affected by Lower Carboniferous extensional faults that fall into five main categories;

- a) Minor, steeply dipping, near vertical, normal faults that trend NNE, NE and ENE, with throws of around 5 metres or less. These faults have dips that trend from E to predominantly SE (Ashton 1995).

- b) Minor ENE-trending normal faults dip steeply to the SE and NW with throws of <10-30 metres. These fault-sets confine the central parts of an asymmetric horst block in the northern part of the deposit, (e.g. F-1, F-2 and F-3 etc.) (Ashton 1995). (Fig. 2-1).

- c) Major ENE, partly listric SE and NW dipping, extensional faults with throws of 100 to 200 metres that control the current disposition of the orebody, (e.g. the B and T faults). It is the development of these major faults, which is considered to

have led to catastrophic footwall collapse, and in turn, the evolution of the erosion surface and superincumbent Boulder Conglomerate (Ashton 1995). (Fig. 2-1)

d) NE to ENE, listric, NW dipping faults that now demonstrate dextral-reverse displacement, thought to be a result of Upper Carboniferous tectonism, (e.g. A and C Faults) (Ashton 1995). (Fig. 2-1)

e) A series of low angle displacements (M, P and Y Faults) that affect the southwestern extension of the orebody. These may not be faults *sensu stricto*, but slides underlying rafts of Shaley Pales that have slid into a the developing graben to the SSE, due to catastrophic footwall collapse of more major structures that remain unseen (Ashton et al., in press).

The Liscarton/Castle Fault System which downthrows to the northwest (Fig 2-1), together with the SE dipping faults defines a southwest plunging asymmetric horst in the northern part of the deposit (Fig. 2-1) (Anderson 1990; Ashton 1995). That this horst block did not fully develop until at least late Chadian times is suggested by a lack of thinning of lithological units over the structure. However, many of the minor bounding faults penetrate only Courceyan lithologies (Ashton 1995), implying movement on these structures during the early Lower Carboniferous. These numerous minor steeply dipping normal faults are, in places, truncated by the larger, partly listric structures (Ashton 1995). The minor faults trend from NNE, through NE to ENE. They predate or are coeval with the earliest movements on the major, partly listric, ENE trending extensional faults that locally penetrate some way into the overlying Arundian strata (Philips and

Sevastopulo 1986; Ashton 1995). Upper Carboniferous deformation within the orebody is restricted to several NE to ENE trending dextral reverse faults, for example the A-C Fault complex (Fig. 2-1), and locally, intense folding of the hanging wall lithologies (Philips and Sevastopulo 1986; Ashton 1995).

2.4 Results

2.4.1 Lithologies

The 1330 13LHWA (Figs. 2-2 and 2-3) development is driven into a B Fault footwall series of massively bedded bioclastic calcarenites, located below a bioclastic calcargillite member known, as the Nodular Marker that defines the top of 3 Lens. A common occurrence throughout the deposit is a build up of mineralisation beneath the Nodular Marker (see also Anderson et al., 1998), often attaining ore grade especially between the B and T Faults. The B Fault hanging wall lithologies exposed in the development are a sequence of clean calcarenites associated with the Upper Sandstone Marker and are the broad equivalent of the lithologies mineralised within the U Lens (see Peace, 1999, Ashton et al., in press.).

2.4.2 Mineralisation

All the major minerals associated with the Navan deposit are present in the examined exposure i.e. sphalerite, galena and pyrite/marcasite. Gangue mineralisation is in the form of calcite and, in places, dolomite. Textures within the 1330 1-3LHWA are typical of epigenetic, replacive mineralisation at Navan, chiefly comprising fine-grained massive, bedding parallel, crosscutting, and disseminated styles (See Figs. 2-4 to 2-7). Within the crosscutting styles there are both vein (Fig. 2-7), and breccia variations (Fig. 2-9). The vein style mineralisation contains both galena and sphalerite, with minor iron di-sulfides and gangue minerals. The breccia styles exposed within the mapped development (Fig. 2-9), are typical of those seen throughout the deposit, being vertical to sub-vertical

structures frequently attaining widths greater than 100mm. They are composed of rounded Pale Beds clasts having replacive pyritic and sphaleritic margins hosted by a fine-grained massive sphalerite matrix. Within the exposed area occurrences of the breccia styles of mineralisation appear to increase toward the B Fault structures, whilst the vein style mineralisation apparently increases away from the fault zone. Individual veins may be only 10mm in width, are vertical to sub-vertical in orientation, and connect with bedding parallel or more massive poddy style mineralisation. They comprise chiefly fine-grained sphalerite, galena and iron di-sulfide mineralisation. However, some contain large quantities of carbonate in the form of massive calcite. Minor euhedral sphalerite crystals (~5mm) associated with euhedral calcite and minor dolomite occur in some of the fractures.

2.4.2.1 Mineralised Fractures

The data collected during this study is tabulated in Appendix 1. Fractures associated with vein style crosscutting mineralisation comprise two sets (Fig. 2-5). One set is observable at the junction between the 1330 13LHWA and the 1330 13LHXR trending NW and NNE. The second set, located in the far west of the drift, trends ENE and NW both near to sub-vertical. In both instances the more westerly trending fracture set contains substantially more carbonate than the more northerly trending set. This suggests that whilst both sets connect with bedding parallel and poddy mineralisation and are thus associated with economic stage mineralisation, they are the result of two distinct events. At no point during this investigation was any evidence of movement along the mineralised fractures

observed, suggesting that shear stress was not a significant component of their formation.

2.4.3 Structure

Of particular interest during this study was the inter-relationship between mineralisation, the B Fault extensional phase, and a sequence of sub-vertical, dextral, strike-slip faults exposed in the drift under investigation (Figs. 2-2 and 2-3). Although confined to the early to mid Lower Carboniferous, the exact timing of B Fault formation within the tectonic evolution of the deposit is not well constrained. It is considered to be largely pre-Boulder Conglomerate, as that lithology is apparently not displaced within the main mine area (Ashton et al., 1986). However, to the southwest the B Fault does displace the Upper Dark Limestones, which overly the Boulder Conglomerate implying that movement on the fault, in places, continued until lower Arundian times (Ashton et al., in press).

2.4.3.1 B Fault System

Several B Fault branches are exposed that display dips between 32° and 50° to the south-southeast (Fig. 2-10). The strike of these faults overall remains at around 267°. Within the area under discussion the local maximum throw on the B Fault is located in the branch exposed at the western end of the drift, where it forms a 1 metre wide zone of black shaley gouge within which are located competent rotated blocks of Pale Beds lithologies forming a well defined fault breccia. Several B Fault-associated accommodation structures are present. One such structure exposed in the 1330 13LHXR, trends 069° and dips to the north at 44° (Fig. 2-4).

2.4.3.2 Dextral Reverse Strike Slip Assemblage

Strike slip displacement within the area comprises a series of anastomosing faults trending on average 256° , with near vertical dip angles (Figs. 2-2 and 2-3). Clearly defined slickensides indicate a shallow dextral-reverse sense of movement, based on slicken-crysts, of $076^{\circ}/20^{\circ}$. It is important to remember that slickensides record only the latest sense of movement on a fracture surface. A major feature of the fault complex within this area is the large quantity of euhedral (vuggy) calcite precipitated within the fault planes, accommodated by the characteristically undulatory nature of the opposing fault surfaces (Figs. 2-11 and 2-12). Where the strike slip assemblage intersects existing B Fault branches two outcomes have been noted (see Fig. 2-2 and 2-3):

- i. Where the B Fault branch is favourably orientated, transverse movements are accommodated along the B Fault branch.
- ii. Where the B Fault branch is not favourably orientated the B Fault branch is truncated and extensional movements (trend and plunge of slickensides = $179^{\circ}/44^{\circ}$), along the B Fault branch are preserved,

2.4.3.3 Jointing

Jointing exposed within the 1330 1-3 Lens development follows similar trends as seen elsewhere within the deposit and are essentially northwest trending fractures infilled with carbonate (see Ashton 1995). Occasional joint faces show deposition of euhedral 'honeyblend' sphalerite and very rarely chalcopyrite (Fig. 2-13).

2.5 Interpretation

Determination of the nature of the relationships between the several generations of fractures and the differing styles of mineralisation was the prime purpose of this investigation. These are:

1. There are two distinct fracture sets containing fine-grained sulfides. One set sulfide rich (northwest to northeast trending). The other, carbonate rich (east-northeast trending) parallels the B Fault (Fig. 2-5).
2. No movement along mineralised fractures was observed implying that they are largely dilational.
3. The carbonate-rich ENE extension veins crosscut massive mineralisation in the immediate footwall of the B Fault (Fig. 2-5).
4. In places, sulfide vein mineralisation crosscuts the carbonate-rich ENE extensional veins (Fig. 2-7).
5. Massive mineralisation is built up within the footwall of the B Fault complex.
6. There is no mineralisation in the hanging wall lithologies of the B Fault, which are direct correlatives of the U Lens host lithologies.
7. At no point is fine-grained mineralisation seen occurring within the B Fault or any of its branches.

8. Where mineralisation does occur along B Fault related branch fault planes it is coarse-grained euhedral 'honey' blende sphalerite.

9. Mineralisation associated with the dextral-reverse strike slip faulting is predominately carbonate rich with only minor coarse-grained euhedral sphalerite (Fig 2-14).

10. The B Fault branches and mineralisation are truncated and displaced by the dextral-reverse strike-slip fault assemblage.

These observations are interpreted below.

1. The existence of NE to NW trending, sulfide-rich, veins within the Navan deposit has been recorded elsewhere (see Andrew and Ashton, 1985), and therefore this study confirms their association with the distribution of high-grade mineralisation. The co-occurrence of ENE trending carbonate-rich, sulfide-bearing veins, that parallel the B Fault, points to an overall evolution of tectonic stresses during the mineralising process, from roughly EW extension to SE-NW extension, which became the dominant stress-field during the development of the B Fault.

2. That these NW-NE and ENE mineralised fractures demonstrate only dilational characteristics implies that they did not form during the B Fault extensional phase. Instead, they must either pre-date, or post-date the B Fault. This, in turn, suggests that;

- a) The mineralised fractures formed pre-late Chadian or,
- b) Post-early Arundian.

However,

- 3. The observation that carbonate infilled extensional fractures associated with the B Fault crosscut both sulfide-bearing veins, and massive mineralisation strongly suggests that the initiation of the mineralising event pre-dates the latest normal movements on the B Fault, and therefore must be pre-late Chadian in age.

- 4. That, in places, sulfide-bearing veins crosscut carbonate infilled extensional fractures associated with B Fault indicates that mineralisation continued throughout the evolution of the B Fault.

- 5. The observation that mineralisation is built-up in the immediate footwall of the B Fault complex suggests that either;
 - a) The B Fault acted as a seal to migrating metal-bearing fluids or,
 - b) The B Fault crosscuts a pre-existing mineralised trend.

- 6. That there is no mineralisation in the hanging wall lithologies of the B Fault, which are direct correlatives of the U Lens host lithologies, implies again, that either;

- a) The B Fault acted as a seal to metal-bearing fluids or,
- b) The B Fault crosscuts a pre-existing mineralised trend.

Although at this locality the B Fault plane is infilled by a thick shaley gouge, this is not typical. More commonly, the B Fault comprises an open cavernous structure containing calcite +/- barite +/- minor pyrite (Fig. 2-14). Of course, it may be that this apparent permeability is the result of fluids moving through the structure during late Carboniferous tectonism. The part of this study dealing with metal distributions in the Navan orebody (Chapter 3) demonstrates the existence of strong NE mineralised trends within the deposit similar to those noted by Andrew and Ashton (1985). These trends are associated with NNE, NE and ENE, steeply dipping normal faults that are, in places, truncated by the major extensional faults (e.g. B Fault) implying that they pre-date the main extensional event. This evidence is in concordance with points 3 and 4 above, and therefore the displacement of a pre-existing mineralised trend as an explanation for the observed features is preferred.

7. That no fine-grained mineralisation is found within the plane of the B Fault, or any of its branches is a common feature of the orebody. However, this does not imply that it was never there, only that this absence may be the result of fluids capable of sulfide dissolution moving through the structure during a later event.

8. The existence of coarse-grained, euhedral 'honey-blend' sphalerite along some of the B Fault branches suggests that at times metal-bearing fluids did access these fractures (Fig. 2-14).

9. The vuggy carbonate and coarse-grained euhedral sphalerite seen within the dextral-reverse, strike slip assemblage again implies metal-bearing fluids had access to this structure.

10. The observation that the dextral-reverse, strike-slip assemblage truncates and displaces all Lower Carboniferous structures suggests that it post-dates the formation of the B Fault, and is therefore younger than early Arundian. When coupled with the presence of other dextral-reverse, strike-slip faulting within and around the orebody, final movements of which are thought to have occurred during the Upper Carboniferous (see Phillips and Sevastopulo, 1986; Ashton 1995; Ashton et al., 1992), I suggest that this structure is related to that event.

The occurrence of untypical euhedral 'honeyblend' sphalerite within the B Fault branches and within the dextral-oblique strike-slip assemblage, suggests that at certain times sulfides have been allowed to precipitate under conditions dissimilar to those prevalent during the economic mineralisation event. Textures exhibited by economic stage mineralisation indicate that the environment of deposition was far from chemical equilibrium both with respect to fluid mixing and wall-rock reactions (Anderson et al., 1998). For example, skeletal and dendritic crystal forms, stalactitic morphologies, coupled with the fine-grained nature of the mineralisation indicating rapid precipitation. A far more stable environment or

one closer to chemical equilibrium must have existed during the later event. The presence of euhedral 'honey-blend' sphalerite in association with B Fault branches suggests that fluids moving along these fractures had come into contact with sulfides along their flow path, and re-precipitated dissolved base metal species as sulfides within favourable locations.

A sequence of events can be built up that covers the structural evolution of this part of the ore body in connection with the economic stage, and subsequent mineralisation events.

1. Development of northwest and northeast trending fracture sets.
2. Coeval or later economic mineralisation.
3. Development of east-northeast trending fractures during continued mineralising activity (possibly precursor fractures to the B Fault proper).
4. Development of the B Fault complex with continuing mineralisation and possible late mobilisation of sulfide phases causing precipitation of coarse-grained euhedral sphalerite on the B Fault branches.
5. Development of the dextral reverse strike slip fault assemblage and jointing, again with minor mobilisation and precipitation of sulfides.

2.6 Conclusions.

This study elucidates the age of mineralisation in relation to timable events during the evolution of the Navan deposit. Access to a drift located in the hanging wall of 1-3 Lens has allowed the mapping of six generations of mineralised and unmineralised fractures. The temporal relationship of these structures indicates that three fracture sets, northeast, northwest, and east-west trending, existed prior to, or during the mineralising event. These fractures are purely dilatational in character. Carbonate-infilled extensional veins associated with the B Fault (one of a series of major, partly listric, extensional faults that control the current disposition of the orebody) cut across the mineralised NE, NW and E-W fractures, as well as massive and disseminated ore. Conversely, this mineralisation crosscuts the carbonate-infilled extensional veins elsewhere within the same exposure. Northwest trending joint sets as well as an east-west trending sub-vertical, dextral-reverse strike-slip fault complex, post-date all the above structures, and are interpreted as the result of Upper Carboniferous tectonism. Other than the occurrence of light coloured, coarse-grained, euhedral 'honey-blend' sphalerite along fracture surfaces, no sulfide mineralisation is associated with those putative Upper Carboniferous structures at this particular exposure. These observations force the conclusion that mineralisation within this part of the Navan deposit was concurrent with the initial development of the B Fault, and continued during the evolution of that major structure through to the late Chadian.

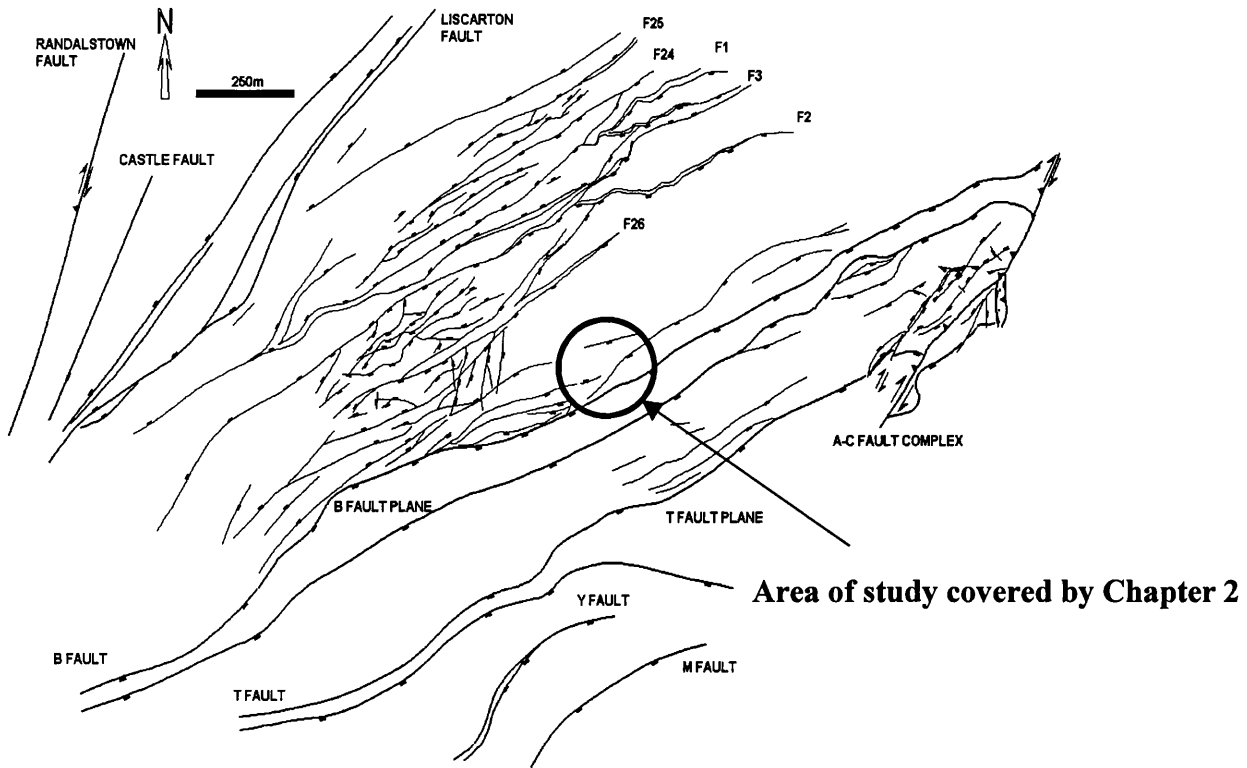


Figure 2-1 Structural plan of the Navan deposit showing the location of the study area covered by Chapter 2.

Structural plan of the 133013LHWA and associated crosscuts.

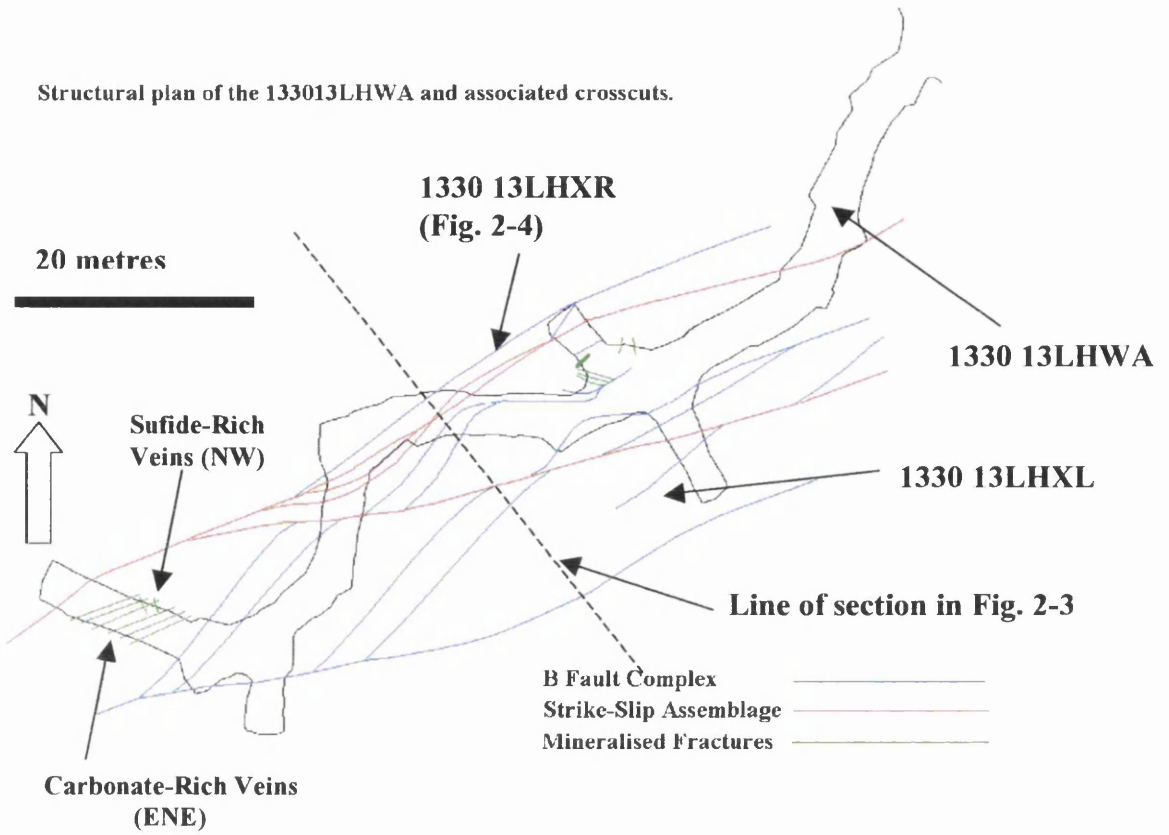


Figure 2-2 Plan of the 1330 13LHWA development showing line of section in Figure 2-3. (See text for details)

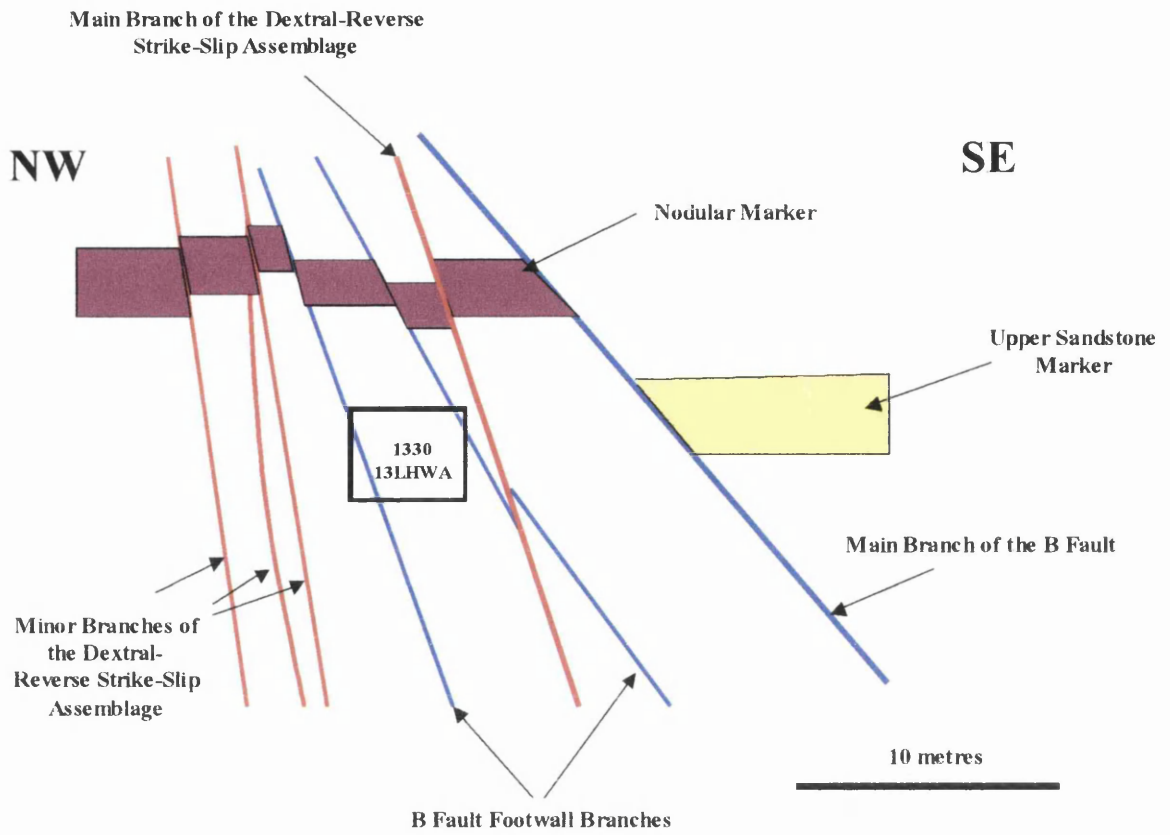


Figure 2-3 Interpreted section along the line shown in Fig. 2-2 showing the relationships between the B Fault (and its branches), and the dextral-reverse, strike-slip assemblage.

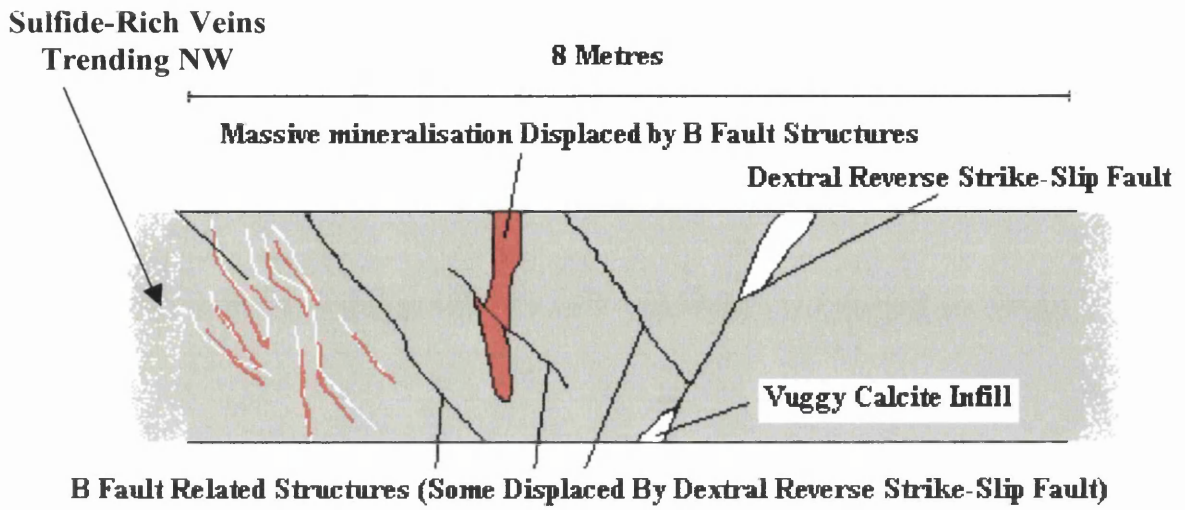


Figure 2-4 Sidewall sketch of the 1330 13LHXR (looking west). Note the north dipping B Fault related fracturing (accommodation structures) are displaced by the dextral-reverse strike-slip fault. Both fault complexes displace massive/poddy sulfide mineralisation. (See also Fig. 2-6).

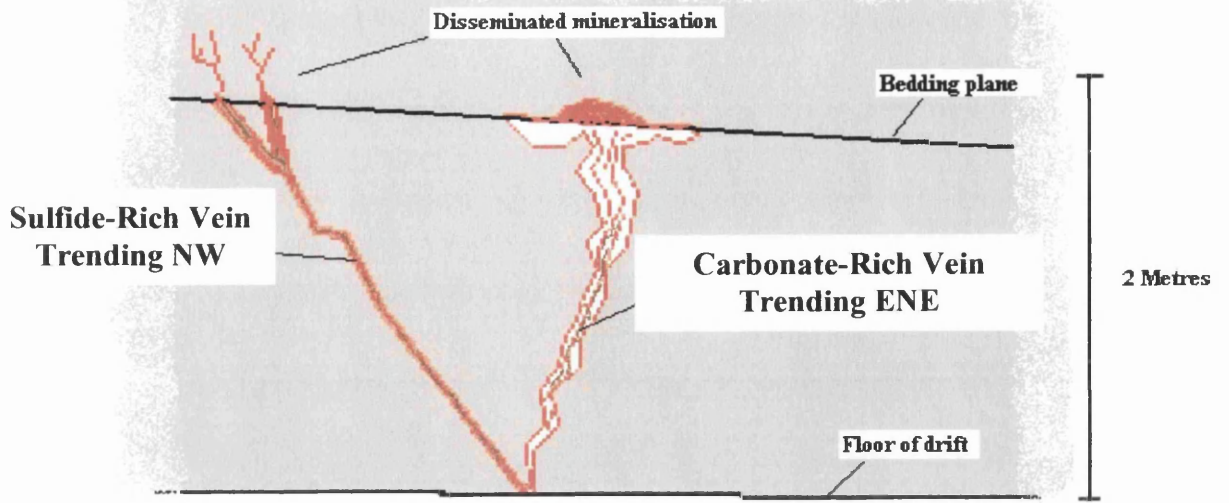


Figure 2-5 Sidewall wall sketch of the relationship between sulfide and carbonate rich vein-sets as exposed in the 1330 13LHWA (looking east).

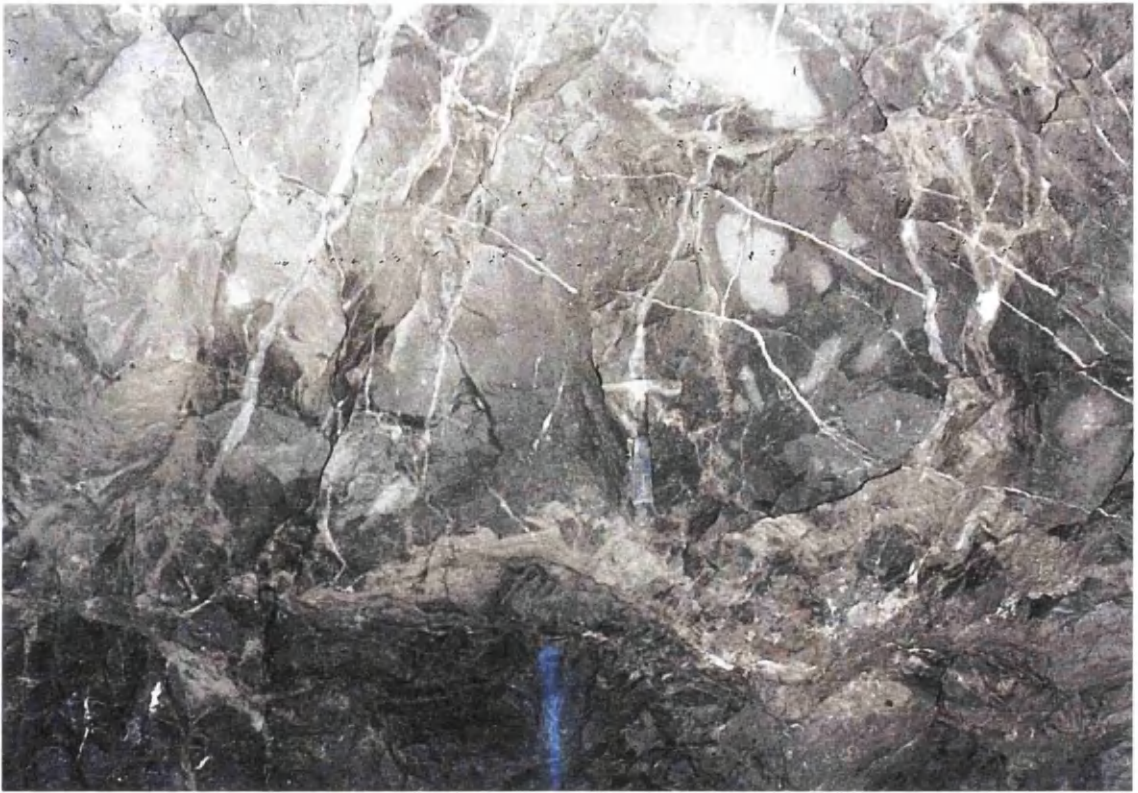


Figure 2-6 View of the sidewall of 1330 13LHXL (looking east). Note that enechelon carbonate veins (dipping to the SSE, parallel to the B Fault) both cross-cut massive sulfide mineralisation, and in turn are themselves cross-cut by minor sulfide-rich veining (See Fig. 2-7 and compare with Fig. 2-8).

(Hammer for scale).

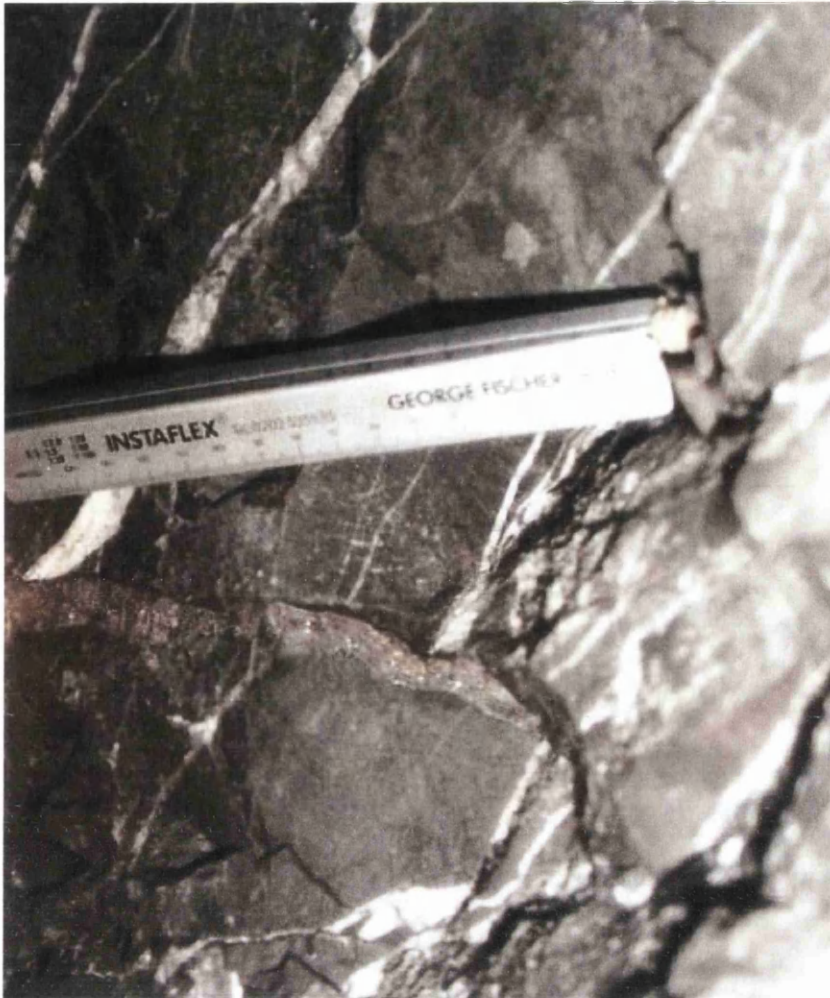


Figure 2-7 Extensional (carbonate-rich) veining (associated with the B Fault) cross-cut and displaced by sulfide-rich veins. Locality = 1330 13LHXL looking west.
(Ruler for scale).



Figure 2-8 A recent exposure (October 2001) in the 1150 B17P2XLA development. Note the relationships between extensional, en-echelon veining (carbonate-rich), and sulfide mineralisation (here associated with a NNE trending minor structure (throw = ~3m) in the footwall of the Liscarton Fault) Compare with Fig. 2-6.

Width of view = 2 metres.



Figure 2-9 Breccia in footwall of the B Fault. Note the sphalerite-rich matrix, and angular clasts of unreplaced carbonate host-rock.



Figure 2-10 A Minor footwall branch of the B Fault as exposed in the south sidewall of the 1330 13LHWA. These minor footwall branches dip between 32° and 50° to the south-south-east. The strike of the B Fault complex overall remains at around 267° . (Ruler for scale).



Figure 2-11 View of the main branch of the dextral-reverse strike-slip assemblage, as exposed in the 1330 13LHWXL (looking west). The fault is exposed just to the right of the hammer (for scale). Note the juxtaposition of intensely mineralised pale beds to the left and barren Pale Beds to the right.



Figure 2-12 Close-up view of the main branch of the dextral-reverse, strike-slip assemblage, as exposed in the 1330 13LHWXL (looking west). Note the inclusion of coarse grained sphalerite, along with carbonate mineralisation within the fault plane.

Hammer for Scale.



Figure 2-13 Occurrence of chalcopyrite on joint surfaces (loc. = 1075 2636F).
Width of view = 500mm.



Figure 2-14 Close-up of coarse-grained sphalerite and carbonate mineralisation within the fault plane of the main branch of the dextral-reverse, strike-slip assemblage, as exposed in the 1330 13LHWXL (looking west).

Hammer for Scale.



Figure 2-15 Exposure of the B Fault in the 1050 2710F. Note open cavities and calcite infill along fault plane. Width of view = 5m. Note also, massive sulfide mineralisation in footwall and barren hanging wall.

3. Major element (Zn, Pb and Fe) distribution study.

3.1 Introduction.

The common sense view that the major, partly listric ENE faults acted as conduits for metal-bearing fluids at the Silvermines Zn+Pb+barite SedEx deposit, has been shown by Taylor (1984), using Pb:Zn distribution patterns, to be incorrect. Furthermore, using metal distribution patterns in the same way at Navan, Andrew and Ashton (1985) went on to show that the partly listric, major extensional faults also did not coincide with high Zn+Pb trends. Instead, as at Silvermines, it appeared that more minor fractures acted as the feeders.

Since those early studies, upgraded software and the amassing of a greatly enhanced dataset over a much larger area of the Navan deposit has allowed the opportunity to augment the original findings. This study confirms that metal enrichment trends (particularly as revealed by the Pb isochores within the basal, 5 Lens) at Navan are more closely related to the minor NNE, NE and ENE fractures than the major ENE extensional faults.

The parts of this chapter dealing with Pb distributions contribute to the relevant sections of Blakeman et al., (in press), and a subset of the complete data used is included on a CD-ROM located in the back of this Thesis. The full dataset is available from Outokumpu-Tara Mines Ltd.

3.2 Hypothesis

Taking a lead from Taylor and Andrew (1978) and Taylor (1984) who demonstrated that Pb enrichment is the clearest indicator of feeder zones at Silvermines, the major element distributions within the Navan deposit have been investigated. Such a study

was expected to confirm the previously identified metal enrichment trends at Navan (Andrew and Ashton, 1985), and enhance their patterns. In addition, finding similar patterns outside the original study area of Andrew and Ashton (1985) was anticipated. Such patterns may also be expected to continue below the economically mineralised horizons indicating likely feeder zones stemming from the Lower Palaeozoic basement hosted structures.

3.3 Scientific method

The major element study was primarily focused on the lowest twenty-one metres above the orebody assay-footwall within the Micrite Unit (Fig. 1-4). The lithological footwall of the orebody is delineated by a green shale horizon (see fig. 3-2) recognisable throughout most of the deposit, and located in the lower part of the Micrite Unit (Fig. 1-4). The Micrite Unit forms a distinctive pale grey horizon containing oncholithic and 'birds-eye' textures. Located twenty-one metres above the orebody footwall is the base of a dolomitic calc-arenite termed the 5 Lens Dolomite (Fig. 3-3), which forms an important control to ore localisation in the western part of the deposit (Rizzi, 1993; Anderson et al, 1998). This lowest part of 5 Lens represents the most pervasively mineralised horizon within the Pale Beds sequence. Major element plots have been produced for Zn, Pb, and Fe, as well as total Zn+Pb, and metal ratios (Zn:Pb). Major element distribution plots have also been produced for the complete sequence of mineralised stratigraphy.

3.4 Analytical technique

Outokumpu Tara Mine's computerised ore reserve system, based on vertical 3m stratigraphic slicing (Ashton & Harte, 1989), has been used to determine the

percentage metal distributions within the ore-bearing horizons. Average metal contents have been calculated for 10x10m blocks using appropriate 3m stratigraphic slice ranges and inverse distance weighting methods. Within the Navan deposit therefore, the amalgamation of appropriate, consecutive slices allows elucidation of the average metal grade distributions within the respective Lenses. However, complications are caused by areal variations in the thickness of particular units which, along with the restricted horizontal extent of some lithologies within the Pale Beds sequence, means that distinct calculations are required for four separate geographical divisions of the deposit (Fig. 3-1).

The Navan deposit is not only separable into a series of vertical, stratigraphically delineated lenses, but also horizontally into zones defined by the major faults in the deposit (Fig. 3-1). The area north of the B Fault is referred to as Zone 1. Zone 2 is located between the B and T Faults, while Zone 3 is located to the south of the A Fault in the main mine area and to the south of the T Fault towards the south west. To accommodate the variances in stratigraphical thickness each Zone is further subdivided into an eastern and western sub-zone. This is shown in Fig. 3-1 and detailed in Table 3-1 below.

This study is necessarily focused on height intervals above the deposit footwall (i.e. the slices of Ashton and Harte, 1989), rather than true stratigraphic divisions. Distribution plots for the complete deposit above Slice 4 therefore, are not truly comparable from Zone to Zone. However, plots are included that cover the vertical thickness from the base of Slice 1 to the top of Slice 7 (some 24m) in order to show the overall metal distribution patterns for the lower part of 5 Lens. The top of Slice 7 in the western part of 5 Lens corresponds with the base of the 5 Lens Dolomite which

acts as a major control on the localization of ore-grade mineralisation in the area (see Fig. 3-3).

Further complications arise when distribution plots are produced for 3 Zone East, immediately south of the A Fault. Here structural complexity has contrived to produce intense folding and faulting within the Pale Beds making it impossible, using the slicing system, to distinguish between the various stratigraphical horizons. Therefore, due to the structural complexity and the limited nature of mineralisation in Zone 3 East, it has been decided that that data should be ignored for the purposes of this study. Enough information is available from the far larger areas of Zones 1, 2 and 3 to the north of the A Fault. In accordance with the computerised ore reserve system in use at Outokumpu-Tara Mines Ltd, the slice ranges for the individual lenses per mine area are listed in Table 3-1.

Main mine area		Zone 1 (north of the B Fault)	Zone 2 (between the B and T Faults)
Lens	Markers	Slices	Slices
1	UDM-NOD	45-31	46-32
3	NOD-LSM	30-20	31-21
4	LSM-LDM/Q	19-12	20-13
5	LDM/Q-5F	11-03	12-03
Far west (Zones 1 and 2)			
Lens	Markers	Slices	
U	LSP-USM	66-52	
0	USM-UDM	51-47	
4W	LSM-LDQ	20-16	
5U	LDQ-DOL	15-08	
5L	DOL-GS/5F	07-03	
Far west (Zone 3)			
Lens	Markers	Slices	
U	LSP-USM	66-52	
1	LSM-UDM	32-46	

Table 3-1 Distribution of slices relative to ore-lenses, markers horizons, and mine areas within the Navan deposit.

UDM = Upper Dark Marker, NOD = Nodular Marker, LSM = Lower Sandstone Marker. LDM/Q = Lower Dark Marker or Lower Dark Marker Equivalent, GS/5F = Green Shale or 5 Lens Assay footwall, LSP = Lower Shaley Pales. USM = Upper Sandstone Marker, DOL = 5 Lens Dolomite. 4W = 4 Lens West. 5U = 5 Lens Upper. 5L = 5 Lens Lower.

3.5 Metal distribution patterns within slices 1 to 4, and lower 5 Lens.

3.5.1 Lead distribution within slices 1-4, and lower 5 Lens.

The distribution of Pb values between 1 percent and >7 percent within the lowest 6 metres (slices 1 and 2) of the basal, 5 Lens of the Navan deposit are shown in Figs. 3-4 and 3-5. Distinct isolated enrichments can be recognised in association with the B Fault. These isolated enrichments contain Pb values greater than 7 percent. Further areas of enrichment (up to 3%) can be seen close to and at the T fault as well as at several minor faults in the northern portion of the deposit. A clearly defined NE trend connecting the areas of greater enrichment seen in Slice 1 (Fig. 3-4) can also be observed in Slice 2 (Fig. 3-5). Figure 3-6 shows the Pb distribution in Slice 3, the interval immediately above the Green Shale and the generally accepted lowest economically mineralised horizon in the Navan deposit. The NE trend observed in Slice 2 is now strengthened, and elongated by the appearance of a distinct enrichment (up to 20% Pb) to the south-western end of the T Fault. A parallel zone of enrichment has now become visible associated with a series of NE trending minor structures between the B and T Faults in the eastern part of the deposit. Further enrichments (up to 12.5%) occur throughout the zone between the B and T Faults, along with other zones, now appearing to the north of the B Fault. The patterns shown in Slice 4 (Fig. 3-7) mimic those already seen in the underlying slices. Distinct trends of enrichment are beginning to coalesce, most noticeably between the B and T Faults. To the north of the B Fault, in the western part of the deposit, a NNE trend is associated with a series of minor

steeply-dipping NNE and NE trending normal faults. Further enrichments are now seen associated with ENE trending faults in the north of the orebody. Figure 3-8 is a composite of all slices within the lower portion of 5 Lens (slices 1 through 7). All enrichments are distinctly associated with NNE and NE trends, and run obliquely to the major extensional faults.

3.5.2 Zinc distribution within slices 1 to 4, and lower 5 Lens.

The distribution of Zn values between 1 percent and >8 percent within the lowest 6 metres (slices 1 and 2) of the basal, 5 Lens of the Navan deposit are shown in Figs. 3-9 and 3-10. As with the Pb data, distinct isolated enrichments can be recognised in association with the B Fault. These isolated enrichments contain Zn values greater than 8 percent. A further centre is recognisable, associated with the F5 fault in Zone 2 East. Further areas of enrichment (up to 3%) can be seen close to and at the T fault, while the minor faults in the northern portion of the deposit appear to localise values in excess of 6%. The clearly defined NE trend in Slice 2 Pb data (Fig. 3-5) connecting the areas of greater enrichment seen in Slice 1 (Fig. 3-4) is not as pronounced in the Zn data (Figs. 3-9 and 3-10). The patterns observed in Slice 1 are repeated, although the grades are reduced. Figure 3-11 shows the Zn distribution in Slice 3. Remember Slice 3 represents the lowermost part of the orebody proper and the importance of this unit in localising high-grade mineralisation is immediately apparent with Zn grades in excess of 35% in parts of Zone 2. Although more diffuse, the NNE, NE to ENE trends observed in the Pb data in Slice 3 are quite visible within the Zn data. However, also strongly visible are a series of NW trending grade enrichments within Zone 2 and the central parts of Zone 1. The patterns shown in Slice 4 (Fig. 3-12) mimic those already seen in

the underlying slices, with the exception of the NW trending enrichments seen in Slice 3. As with the Pb data distinct trends of enrichment are beginning to coalesce, most noticeably between the B and T Faults. To the north of the B Fault, in the western part of the deposit, a NNE trend is associated with a series of minor steeply-dipping NNE and NE trending normal faults. Further enrichments are now seen associated with ENE trending faults in the north of the orebody. Figure 3-13 is a composite of all slices within the lower portion of 5 Lens (slices 1 through 7). All enrichments are distinctly associated with NNE and NE trends, and run obliquely to the major extensional faults.

While not visible in the Pb data, overall the Zn distribution plots for slices 3 (Fig. 3-11), and 4 (Fig. 3-12), as well as the plot for slices 1 through 7 (Fig. 3-13) show stronger enrichments to the north-east of the study area.

3.5.3 Iron distribution within slices 1 to 4, and lower 5 Lens.

The distribution of Fe values between 1 percent and >8 percent within the lowest 3 metres (slice 1) of the basal, 5 Lens of the Navan deposit are shown in Fig. 3-14. The enrichments at this horizon seen in the Pb (Fig. 3-4) and Zn (Fig. 3-9) data, associated with the B Fault, are not repeated in the Fe data. Instead more minor faults in the northern portion of the deposit appear to localise values in excess of 6%; for example, the F3 fault and the junction of the F26 and one of its branches. Lower grade enrichments, up to 3% can also be seen associated with the F1 and F25 faults in the north-eastern part of Zone 1. Zone 2 East shows only minor enrichments, less than 3%, associated with the set of NE trending faults remarked upon in the Pb data. Figure 3-15 shows the Fe distributions in Slice 2. Note that the maximum grade shown is half that of Slice 1 (Fig. 3-14). Note the highly

localised, but nevertheless ubiquitous occurrence of distinct Fe enrichments associated with NE faulting in and around the horst. There appear to be NW trending breaks in the Fe values within this dataset. However this orientation coincides with diamond drilling profiles. Thus the strong NW trends visible here are likely an artefact of the DDH profiles rather than reflecting a hidden structural control. Further Fe enrichments in Slice 2 are visible in Zone 2, especially in association with the T Fault and the NE end of the B Fault. These zones of Fe enhancement are repeated in Slice 3 (Fig. 3-16) where values in excess of 16% are seen to the north of the T Fault. This is not surprising as several arrays of marcasite veins occur throughout that area which trend more north-easterly than the T Fault itself (Andrew and Ashton, 1985). North of the B Fault Fe enhancements are associated with the F1, F2, F3, F24 and F25 fault systems. Two limited areas also occur in association with the B Fault towards the south-west. In Slice 4 (fig. 3-17) the last two mentioned areas of Fe enrichments have disappeared. However, the zones previously remarked upon north of the T and B Faults, and in the north-east part of Zone 1, are still clearly visible. A further small area has also appeared associated with a flexure in the T Fault towards the south-west, which is also present, but at a reduced grade, in the underlying slices. Figure 3-18 is a composite of all slices within the lower portion of 5 Lens (slices 1 through 7). Apart from the area in the T Fault footwall where marcasite veins run oblique to that structure, all enrichments are distinctly associated with minor NNE and NE faulting.

While not visible in the Pb data, overall the Fe distribution plots for slices 3 (Fig. 3-16), and 4 (Fig. 3-17), as well as the plot for slices 1 through 7 (Fig. 3-18) show stronger enrichments to the north-east of the study area.

3.5.4 Distribution of Zn+Pb values within slices 1 to 4, and lower 5 Lens.

While the single element plots can be used to define likely structures that acted as fluid conduits during the mineralising process, the use of Zn+Pb distributions can help identify either those structures that accommodated most fluid flow, or the areas within the host lithologies that acted as the most efficient traps. The Fe data has not been combined with the Zn and Pb data because it shows different distributions and therefore may indicate differing processes involved in its localization. The significance of the disparity of Fe compared to Pb and Zn distributions is discussed below. Fig. 3-19 shows the total Zn+Pb in the lowermost Slice 1. As expected from the individual Zn and Pb plots, isolated areas of enrichment are clearly visible along the trend of the B Fault. Similarly, isolated pockets of enhanced grade are seen in association with the NE trending faults in Zone 2 East. Both these occurrences contain total metal grades in excess of 16%. Slice 2 (Fig. 3-20), again shows expected peaks in grade associated with the B and T faults with values upwards of 14% especially adjacent to the T Fault. Fig. 3-21 shows the total-metal variations in Slice 3. The strong NE trends seen in the Pb data are still visible, although more diffuse due to the inclusion of the previously described Zn data. Of note in comparison with the Zn only data is the almost total disappearance of the NW trends seen in Zone 1. However, they are still present in Zone 2. A strong NW trend is also apparent running between Zones 1 East and 2 East. This is clearly a major feature and is mirrored by a more minor NW trend visible in Zone 2 West. Zn+Pb grades for Slice 4 are show in Fig. 3-22. Again the previously noted NW trending feature running between Zones 1 and 2 in the east

of the deposit is a dominant feature. Similarly, several more minor NW trends are also apparent.

Figure 3-23 shows the %Zn+Pb values for slices 1 through 7. Although Zn+Pb values follow the minor faulting to the north of the B Fault, it can be seen that an increase in Zn:Pb values occurs to the north-east of the study area.

3.5.5 Distribution of Zn:Pb values within slices 1 to 4, and lower 5 Lens.

Metal ratio plots have the potential to show at a glance likely feeder structures especially when two metals with differing solubilities are combined. For an example the success of this technique has been demonstrated by Taylor and Andrew (1978) and Taylor (1984). Using Zn:Pb plots, these authors have delineated feeder zones at Silvermines. In the present study a lower-end cut-off of 1% total metal has been applied to the data in order to exclude excessive ratios (greater than 40).

Fig. 3-24 shows the Zn:Pb distribution in Slice 1. As expected the lowest ratios are seen where comparably higher Pb grades are present. However, of note is the extended area of predominantly lower Zn:Pb values (1 to 4) in Zone 2 East. This indicates an overall increase in the amount of Pb within this area, although the NE trending faults still attain Zn:Pb ratios of greater than 22. Compared with an overall initial ratio of close to 5:1 (69.9Mt at 10.09% zinc and 2.63% lead, Libby et al., 1985), Zone 2 East is comparatively Pb enriched in Slice 1. Slice 2 (Fig. 3-25) demonstrates elongated (Zn:Pb = <5) trends that mimic Pb enhanced patterns in higher slices. Zn:Pb ratios greater than 5 only pertain away from the putative

feeder structures. Within Slice 3 (Fig. 3-26) the first appearance of Zn:Pb values of less than unity appear. Again these trends, albeit isolated, are aligned in the same orientation as those seen in the Pb only data. High Zn:Pb (>30) ratios are isolated and only occur associated with structures that show both Zn and Pb enrichments. Similarly Slice 4 data (Fig. 3-27), repeats the pattern. The values towards the south-west of Zone 1 West are on the limit of the deposit and represent relatively weakly mineralised horizons. Here then, the metal ratios are comparatively insignificant.

Figure 3-28 shows the Zn:Pb values for slices 1 through 7. It can be seen that an increase in Zn:Pb values occurs to the north-east of the study area.

3.6 Interpretation of metal distribution patterns within slices 1 to 4, and lower 5 Lens.

3.6.1 Lead.

The expected role of the minor NNE, NE and ENE structures in localising ore-grade mineralisation has been demonstrated. That no Pb trend coincides with the strike directions of the major ENE, partly listric extensional faults, is in line with the findings of Andrew and Ashton (1985). One of the advantages of the method used to delineate likely feeders is the facility to separate the lower section of the basal, 5 Lens of the Navan deposit into 3-metre slices. Distinct Pb enrichments associated with the major extensional faults, certainly in the lowermost slices, are revealed that otherwise would have been invisible at lower resolutions had the results been totalled for all the slices. The Pb enhancements are not linear, but instead form areas of isolated enrichment. These highs are arranged along a north-easterly trend that parallels Caledonoid structures/faults seen in the vicinity of the orebody (Fig. 3-29). These patterns strongly suggest the influence of either Caledonoid fault complexes (e.g. Randlestown, Castle and D Faults) (Fig. 1-3), or near vertical, highly permeable Lower Palaeozoic lithologies acting as fluid conduits. The isolated areas of enrichment along the B and T Faults are interpreted as delineating intersections of those fractures with such basement structures and/or lithologies.

3.6.2 Zinc.

As with the Pb data, the expected role of the minor NNE, NE and ENE structures in localising ore-grade mineralisation has been demonstrated. That no Zn trend

coincides with the strike directions of the major ENE, partly listric extensional faults, is again in line with the findings of Andrew and Ashton (1985). As with the Pb data, distinct Zn enrichments associated with the major extensional faults, certainly in the lowermost slices, are revealed that otherwise would have been invisible at lower resolutions. Again the Zn enhancements are not linear, but instead form areas of isolated enrichment. Thus the same interpretation applies to the Zn data as the Pb data. However, NW trends are clearly visible within the Zn data, especially in Slices 3 and 4, and these have no immediately obvious cause. Minor NW trending sulfide veins have been reported in the Navan deposit by previous workers (Andrew and Ashton, 1985), and similar structures are reported in this study (see Chapter 2). These structures are nonetheless very minor features and would not be expected to produce such pronounced anomalies as are visible in the data. Three possibilities therefore remain to explain these phenomena

- a) Jointing within the deposit host rocks is aligned along NW trends, and mineralising fluids circulated within these structures.

- b) Exploration, development and production diamond drilling within the orebody conducted on NW profiles thereby artificially increasing the importance of those trends.

- c) There are major lithological variations within the Pale Beds sequences that strike NW. Preferential replacement of these horizons would produce similar patterns.

In discussion of the above it can be pointed out that:-

a) More sophisticated statistical analytical techniques can be applied to this dataset. This would reveal whether the apparent major NW trends can be removed, suggesting 'noise' caused by the drilling profiles.

b) Anderson et al. (1998) report variations in lithological thickness within the basal Pale Beds (see fig. 1-?), as well as differences in lithology across the same horizons. These variations however do not occur at the same frequency as the observed NW trends in the Zn data, and therefore, if there is a control present, it is not acting alone.

c) The presence of jointing in the Navan deposit has been attributed to Upper Carboniferous compressional tectonism. Following the findings of Chapter 2, and in agreement with previous workers (e.g. Andrew and Ashton, 1985; Ashton et al., 1992; and Anderson et al., 1998), the jointing clearly post-dates metallogenesis at Navan, and therefore could not have been a control on fluid flow at the time.

To summarise, the noted occurrence of major NW metal trend are likely a product of NW drilling profiles employed in the delineation of the orebody. Minor sulfide veins (Andrew and Ashton, 1985; and Chapter 2) possibly represent very minor fracture arrays present at the time of mineralisation.

The noted concentration of higher %Zn values towards the north-east of the study area cannot, at this time, be explained. The area of the Navan deposit to the north-

east (Nevinstown) remains the subject of ongoing legal action and therefore all data remains commercially confidential. Also, some, if not a substantial part of the Navan deposit has been removed by post-Carboniferous erosion. That the higher concentrations of Zn to the north-east represent an overall fluid-flow regime from the south-west, based on relative metal solubility, may be the case, but this hypothesis cannot be substantiated by this study.

3.6.3 Iron.

The Fe distribution patterns throughout the 4 slices under investigation are distinctly different from those exhibited by either the Zn or Pb datasets. Iron enrichment remains isolated in occurrence, being concentrated in the main to an area just north of the T Fault. Here, as exposed in the 1230-3 Zone Access Drift, marcasite veining constitutes the most important phase (Andrew and Ashton, 1985). In a similar fashion the area of enhanced Fe values centred on the F1, F2, F3, F24 and F25 faults in the north-east of Zone 1 contains, where observable in underground exposure, high incidences of marcasite, although pyrite is also present. From the isotopic work described in Chapter 4 it is suggested that marcasite in the Navan deposit is precipitated directly from the metal-bearing fluid with no interaction with the local fluid that bears the bacteriogenically-reduced seawater sulfate. Therefore, a high incidence of marcasite is a clear, macro-scale, indicator of zones of metal-bearing fluid ingress at Navan.

The work described in Chapter 4 demonstrates that marcasite is restricted to likely feeder zones delineated by the Pb enrichments described above. The presence of pyrite however, through its almost ubiquitous $\delta^{34}\text{S}$ signature of between -30 and -40 per mil. indicates strongly the presence of the local fluid bearing bacteriogenically reduced seawater sulfate. The Fe patterns within the Navan

deposit, coupled with the distribution of the two FeS₂ polymorphs, marcasite and pyrite, variously indicate not only conduits for the metal-bearing fluid, but also zones of mixing between that fluid and the local bacteriogenic sulfide-rich fluid. The Fe (marcasite) distribution within the lowermost slices of 5 Lens suggests that some of the metal-bearing fluid gained access into the deposit in and around the T Fault. Indeed this zone falls at the south-western end of distinct Pb enrichment. The relative absence of Pb (and Zn) in the immediate area strongly suggests that an Fe rich fluid was a precursor to the metal-bearing fluid that ultimately produced the Navan deposit. This might be expected given the relative solubilities of the respective metals during the initiation of upward fluid flow within developing fractures. This possibility is discussed further in the Chapter 5 dealing with the genetic model.

As with the Zn data, the noted concentration of higher %Fe values towards the north-east of the study area cannot, at this time, be explained. The area of the Navan deposit to the north-east (Nevinstown) remains the subject of ongoing legal action and therefore all data remains commercially confidential. Also, some, if not a substantial part of the Navan deposit has been removed by post-Carboniferous erosion. That the higher concentrations of Fe to the north-east represent an overall fluid-flow regime from the south-west, based on relative metal solubility, may be the case, but this hypothesis cannot be substantiated by this study.

3.6.4 Zinc+Lead.

The Zn+Pb plots serve to underline the role played by the NNE, NE and ENE minor faults highlighted most strongly by the Pb data. As with the Pb and Zn data therefore, the interpretation of the Zn+Pb plots is that these metal patterns strongly

suggest a deep-seated control on conduits providing metal-bearing fluids access into the Navan deposit. Again the major lineaments of the combined metal plots run oblique to, and are displaced by, the major extensional faults in the orebody implying that the majority of movement on these larger faults occurred after the mineralisation in these slices was emplaced, or that they, as relatively shallow angle faults did not have the permeability to be exploited by the metal-bearing fluid.

As with the Zn and Fe data, the noted concentration of higher %Zn+Pb values towards the north-east of the study area cannot, at this time, be explained. The area of the Navan deposit to the north-east (Nevinstown) remains the subject of ongoing legal action and therefore all data remains commercially confidential. Also, some, if not a substantial part of the Navan deposit has been removed by post-Carboniferous erosion. That the higher concentrations of %Zn+Pb to the north-east represent an overall fluid-flow regime from the south-west, based on relative metal solubility, may be the case, but this hypothesis cannot be substantiated by this study.

3.6.5 Zinc:Lead.

The linear patterns of the Zn:Pb plots remain consistent with those observed in the Pb, Zn and Zn+Pb plots. The interpretation of these plots therefore, is as above.

Further, as with the Zn, Fe and Zn+Pb data, the noted concentration of higher Zn:Pb values towards the north-east of the study area cannot, at this time, be explained. That the higher value of Zn:Pb to the north-east represent an overall fluid-flow regime from the south-west, based on relative metal solubility, may be the case, but this hypothesis cannot be substantiated by this study.

3.7 Conclusions.

The role of the minor NNE, NE and ENE structures in localizing ore-grade mineralisation is demonstrable. The lead and zinc enhancements are not constant along the strike directions of the major ENE, partly listric extensional faults, although areas of isolated enrichment do occur within these faults. The highs are arranged along a north-easterly trend that parallels the Caledonoid structures and faults seen in the vicinity of the orebody (Fig. 3-29). This finding is consistent with that of Andrew and Ashton (1985). These patterns strongly suggest the influence of Caledonoid fault complexes on mineralisation (e.g. Randalstown, Castle and D Faults) (Figs.1-2 and 1-3). The isolated areas of enrichment along the B and T Faults I interpret as delineating intersections of those fractures with such basement fault zones. Thus the listric faults have not acted as major conduits to the mineralising solutions, contrary to the expectations of the MVT model.

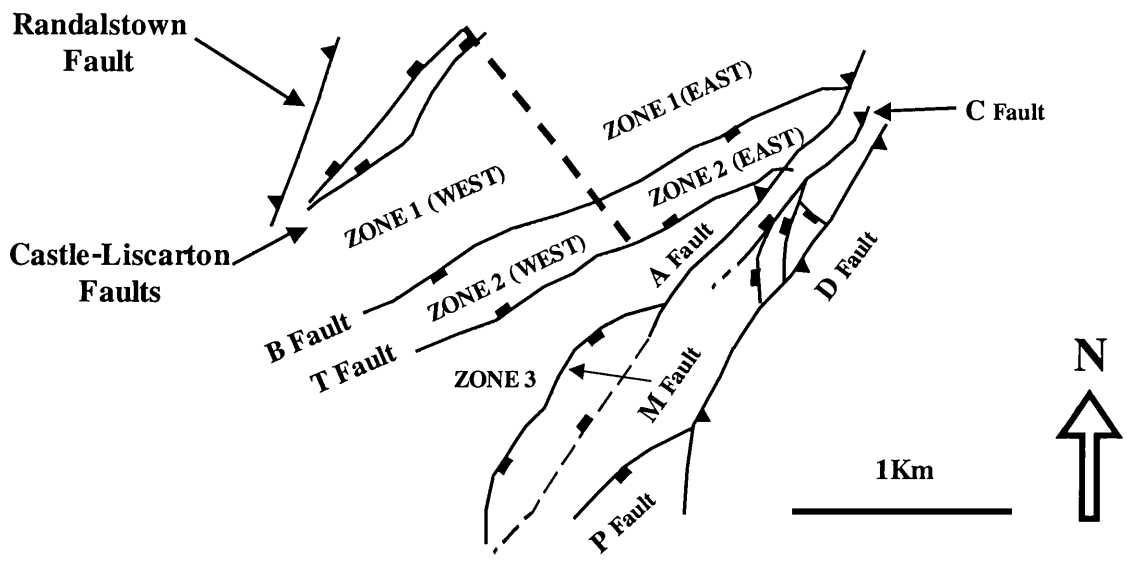


Figure 3-1 Structural plan of the Navan deposit showing the location of Mine Zones discussed in the text.

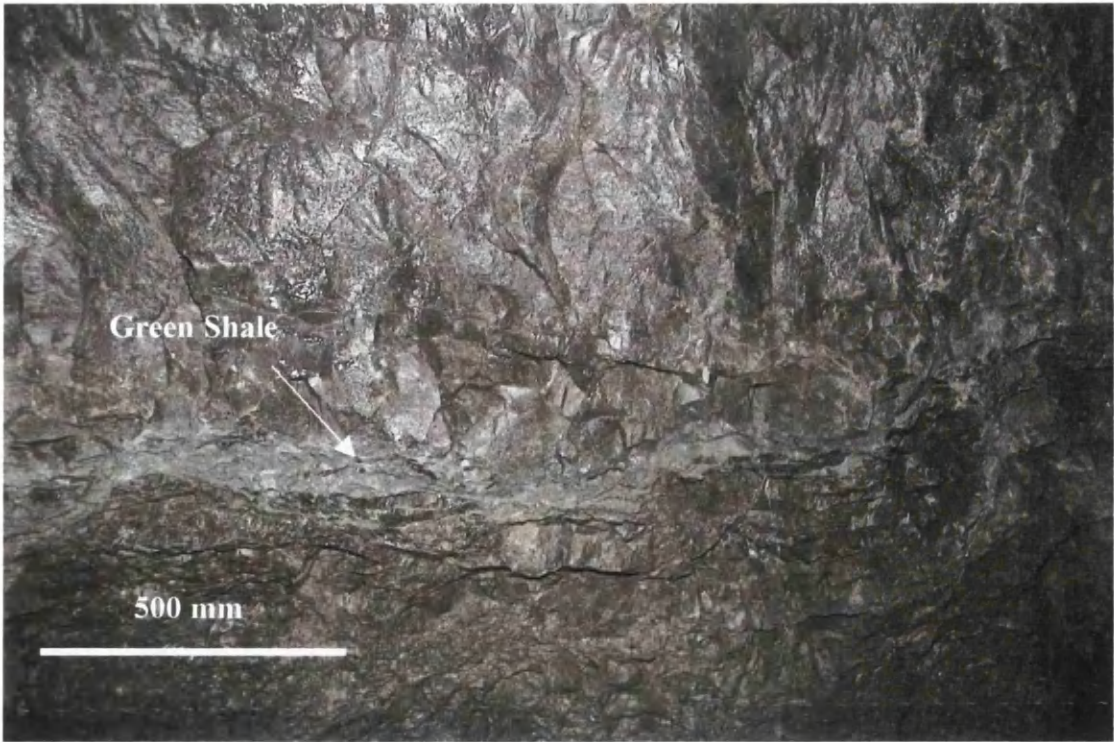


Figure 3-2 The basal Green Shale of the Navan deposit. Located within the Micrite Unit. Located in the 1050 2710NE development. This horizon marks the base of Slice 3 (see text). See Rizzi and Braithwaite (1996) for a discussion on origin.

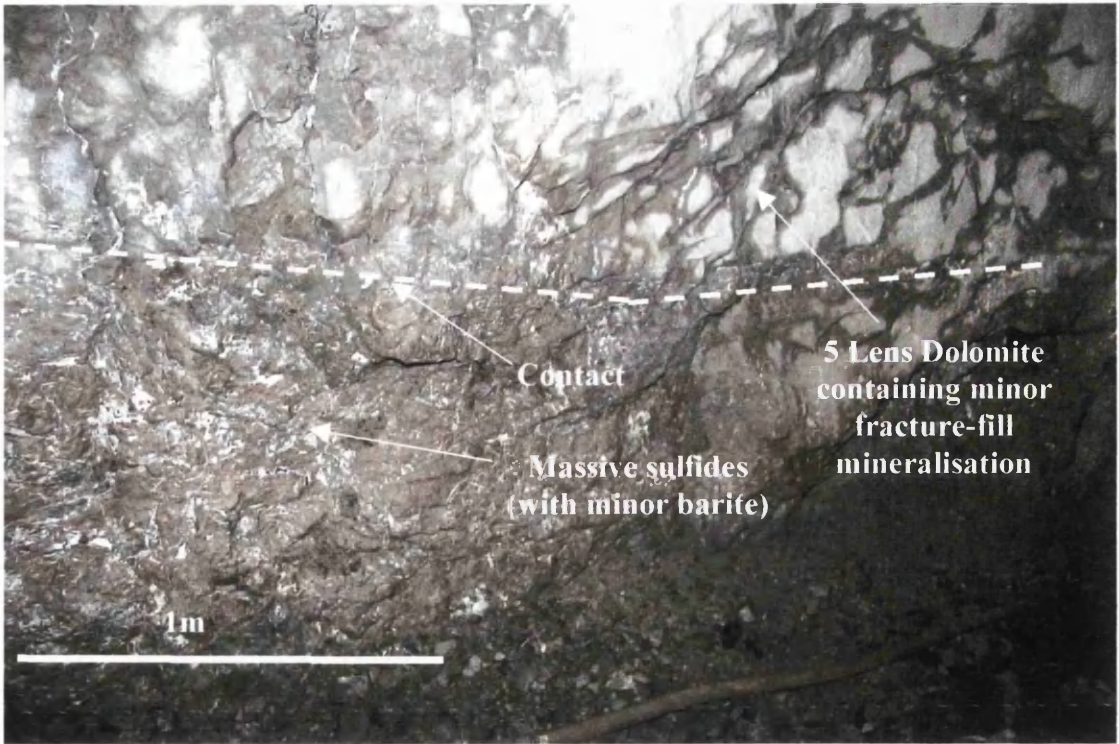


Figure 3-3 Ore-5 Lens Dolomite contact (corresponding to the top of Slice 7 (see text). Located in the 1050 2710F development. See Anderson et al., (1998) for a discussion on the importance of this unit in localizing ore-grade mineralisation.

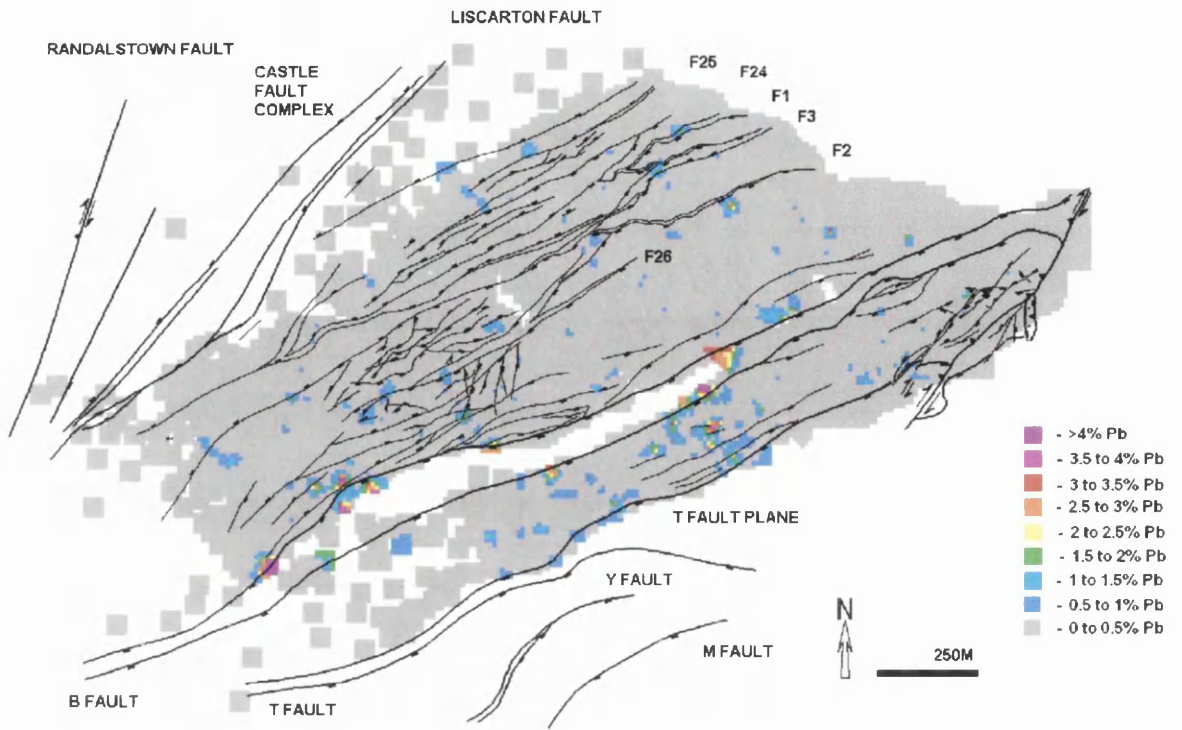


Figure 3-4 Distribution of %Pb in Slice 1 of the Navan deposit.

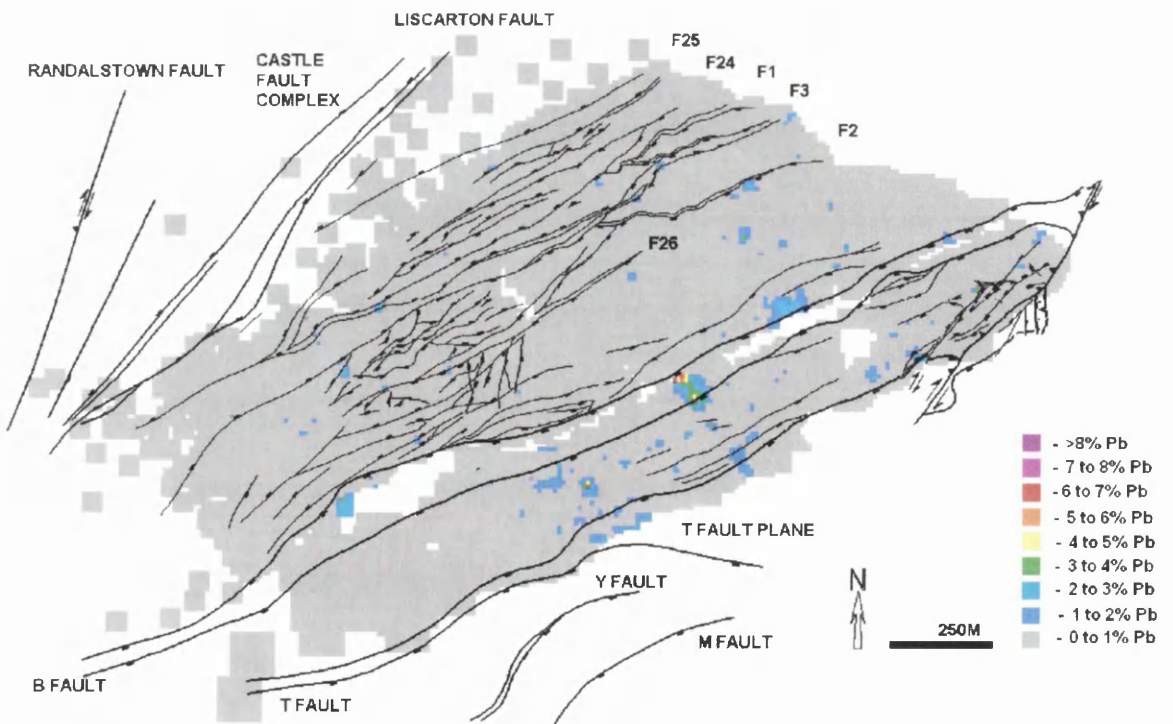


Figure 3-5 Distribution of %Pb in Slice 2 of the Navan deposit.

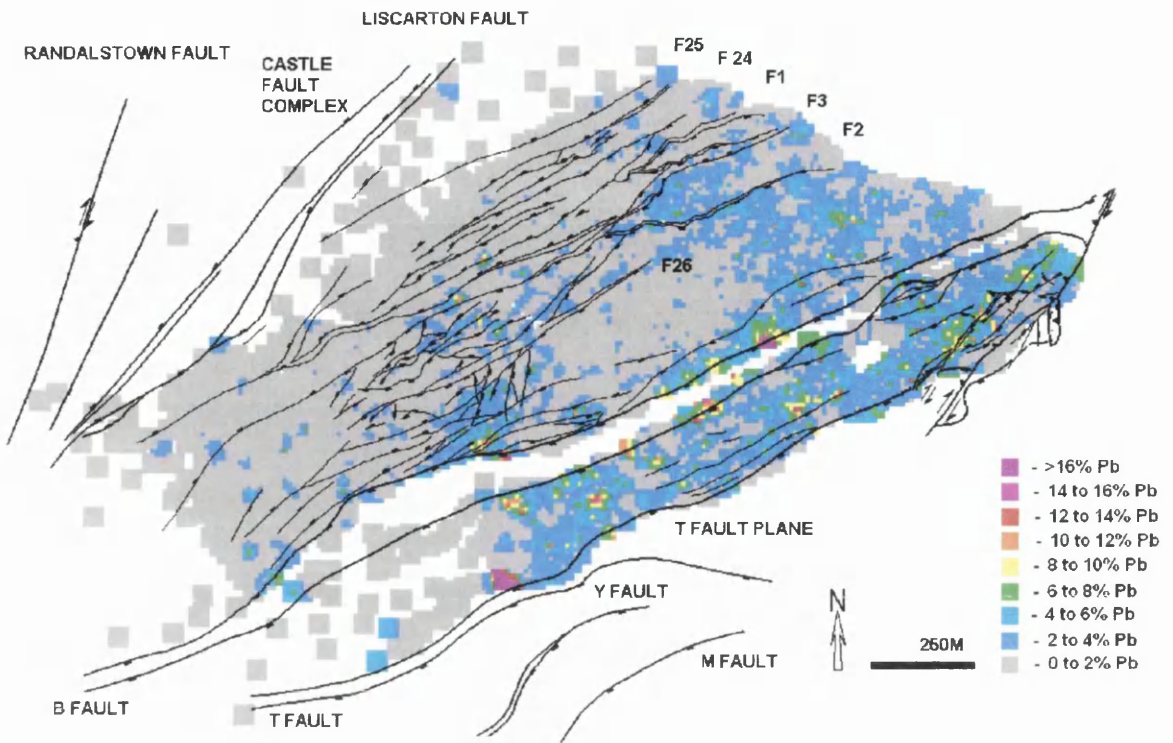


Figure 3-6 Distribution of %Pb in Slice 3 of the Navan deposit.

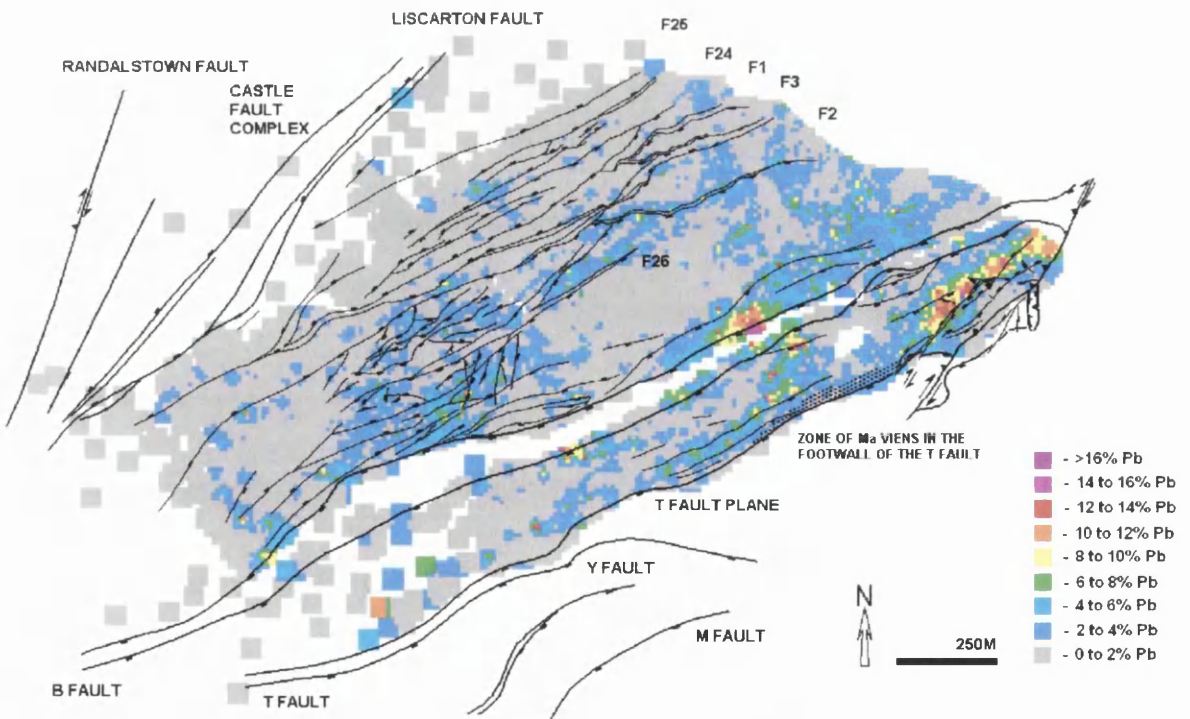


Figure 3-7 Distribution of %Pb in Slice 4 of the Navan deposit.

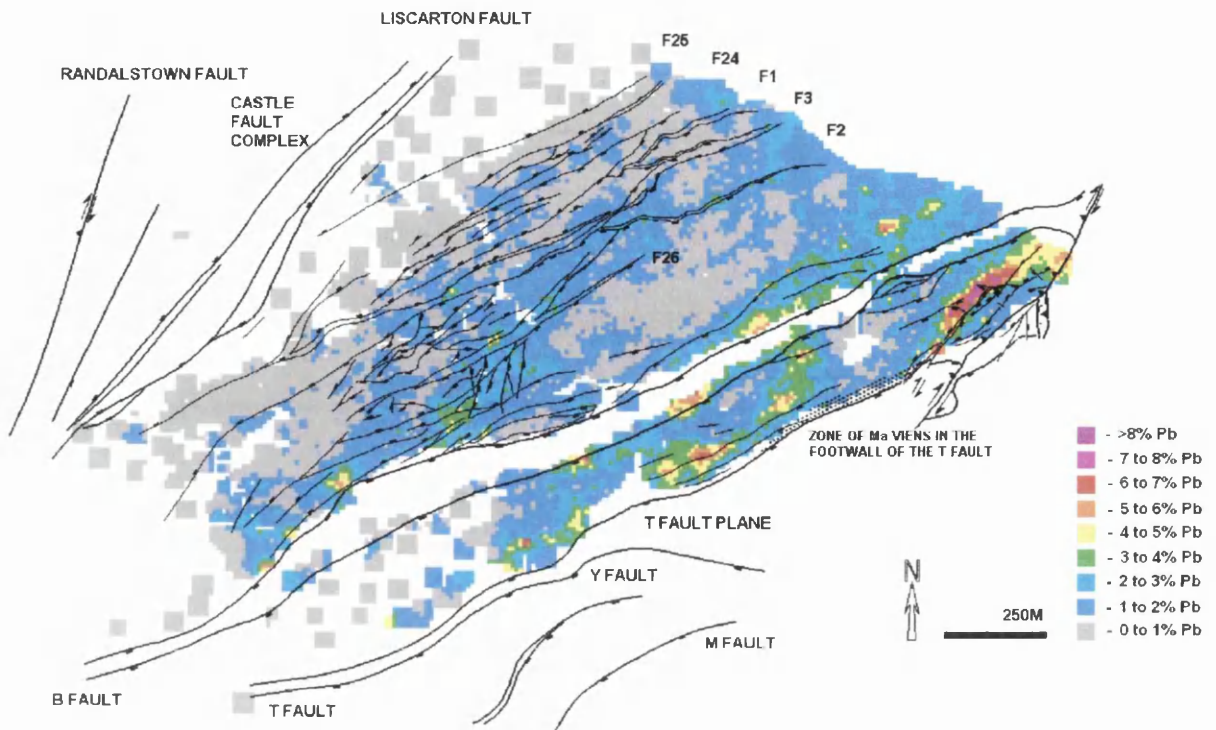


Figure 3-8 Distribution of %Pb within the lowermost 24m of 5 Lens (Slices 1 to 7) in the Navan deposit.

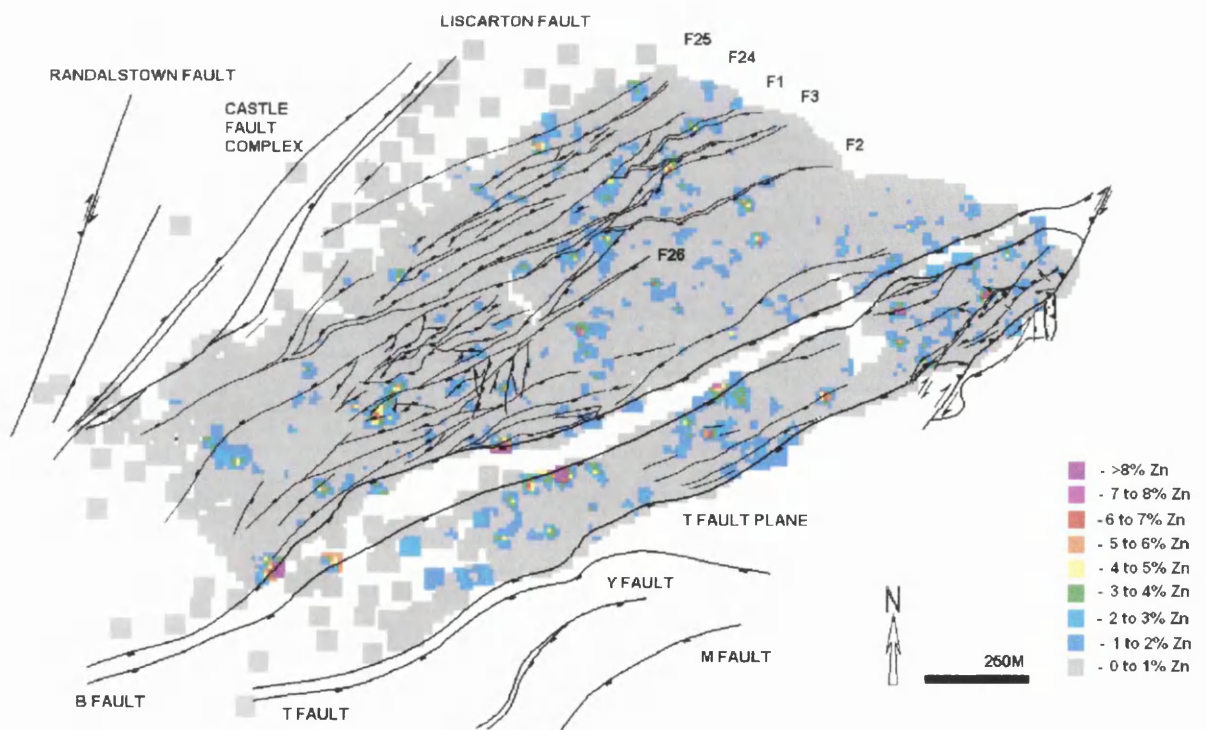


Figure 3-9 Distribution of %Zn in Slice 1 of the Navan deposit.

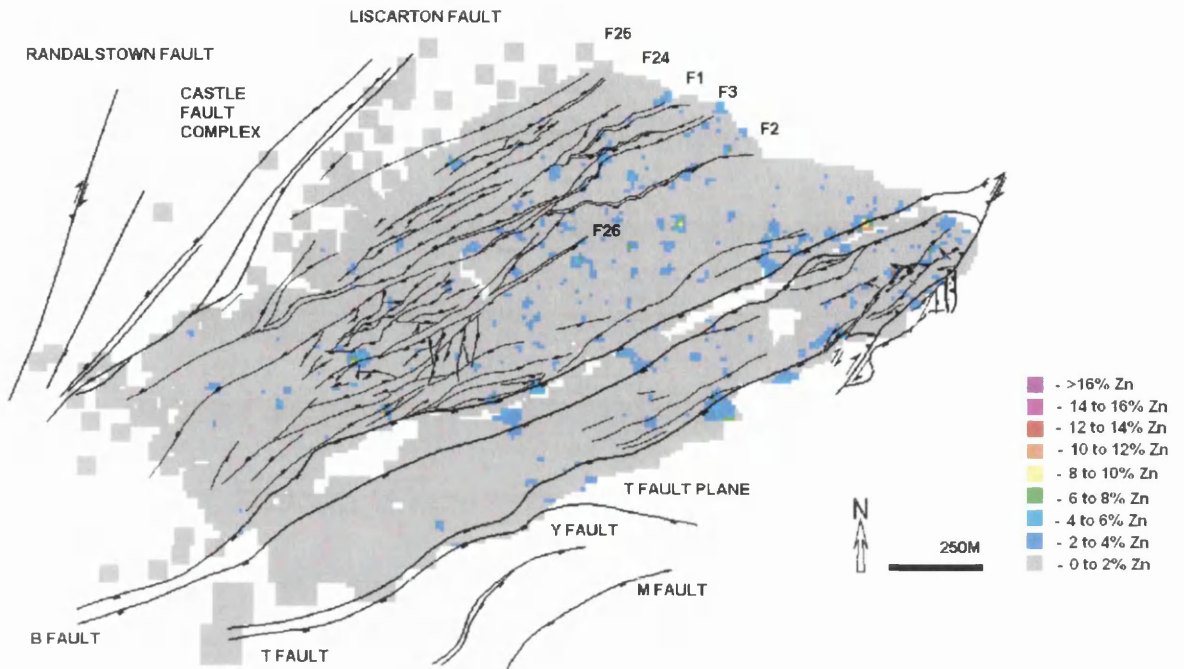


Figure 3-10 Distribution of %Zn in Slice 2 of the Navan deposit.

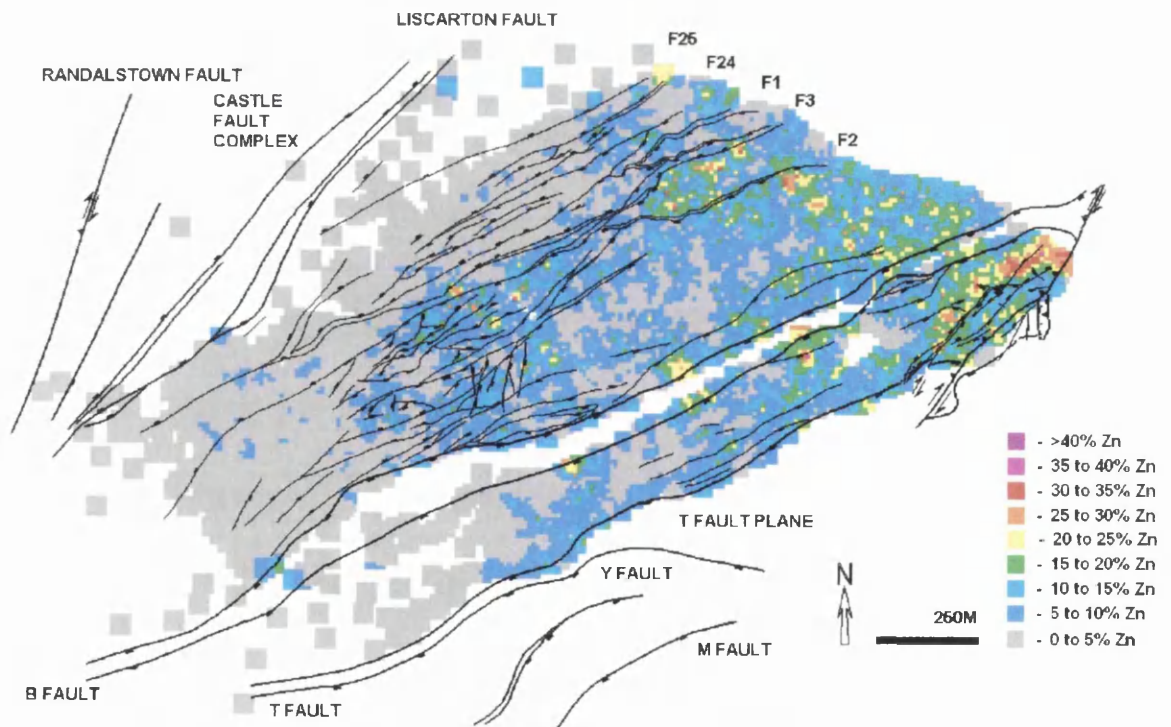


Figure 3-11 Distribution of %Zn in Slice 3 of the Navan deposit.

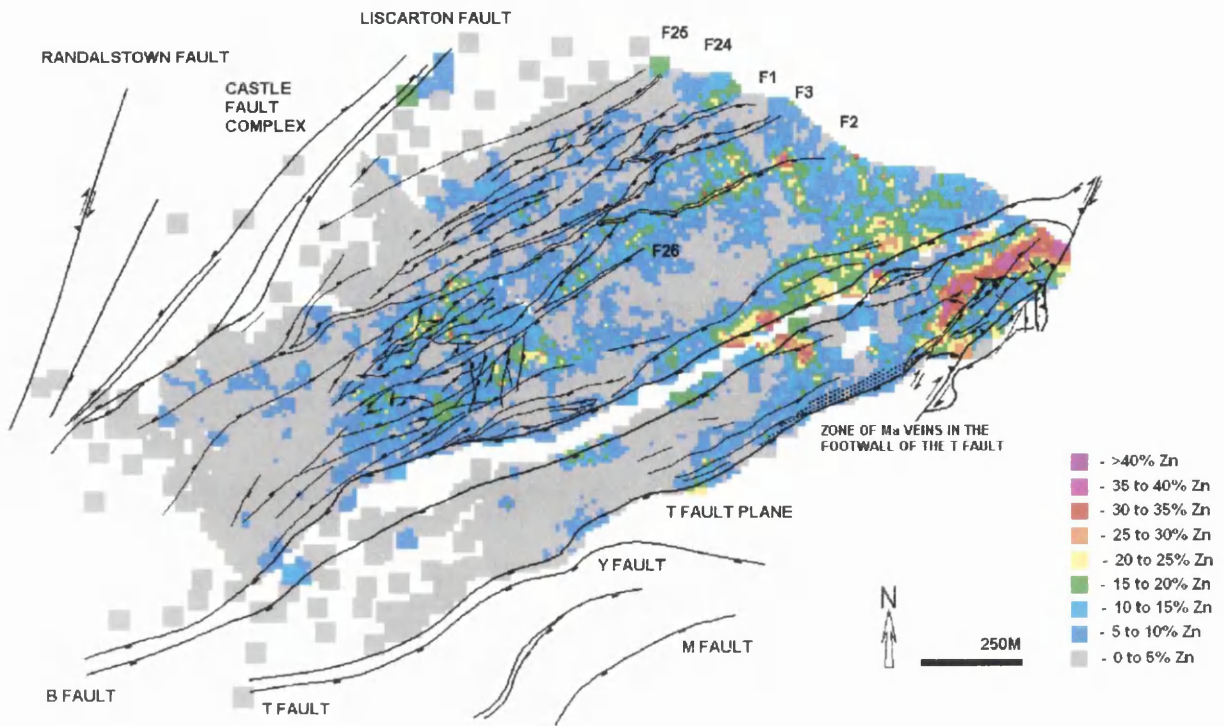


Figure 3-12 Distribution of %Zn in Slice 4 of the Navan deposit.

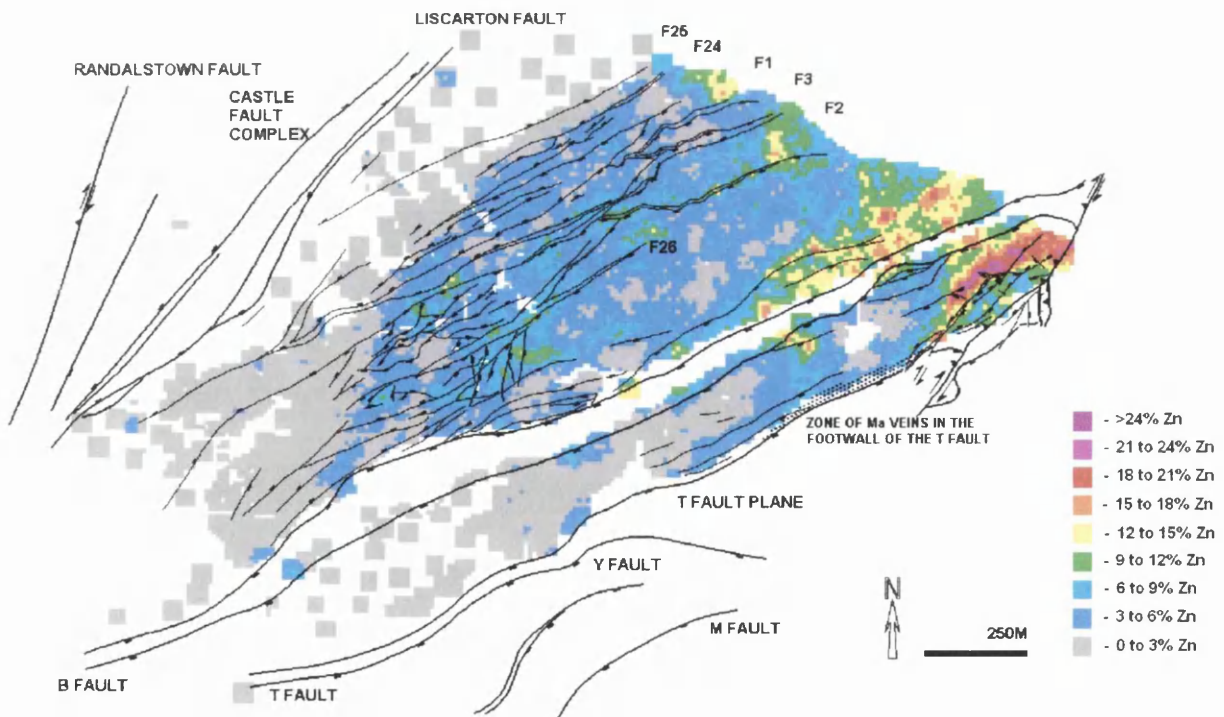


Figure 3-13 Distribution of %Zn within the lowermost 24m of 5 Lens (Slices 1 to 7) in the Navan deposit.

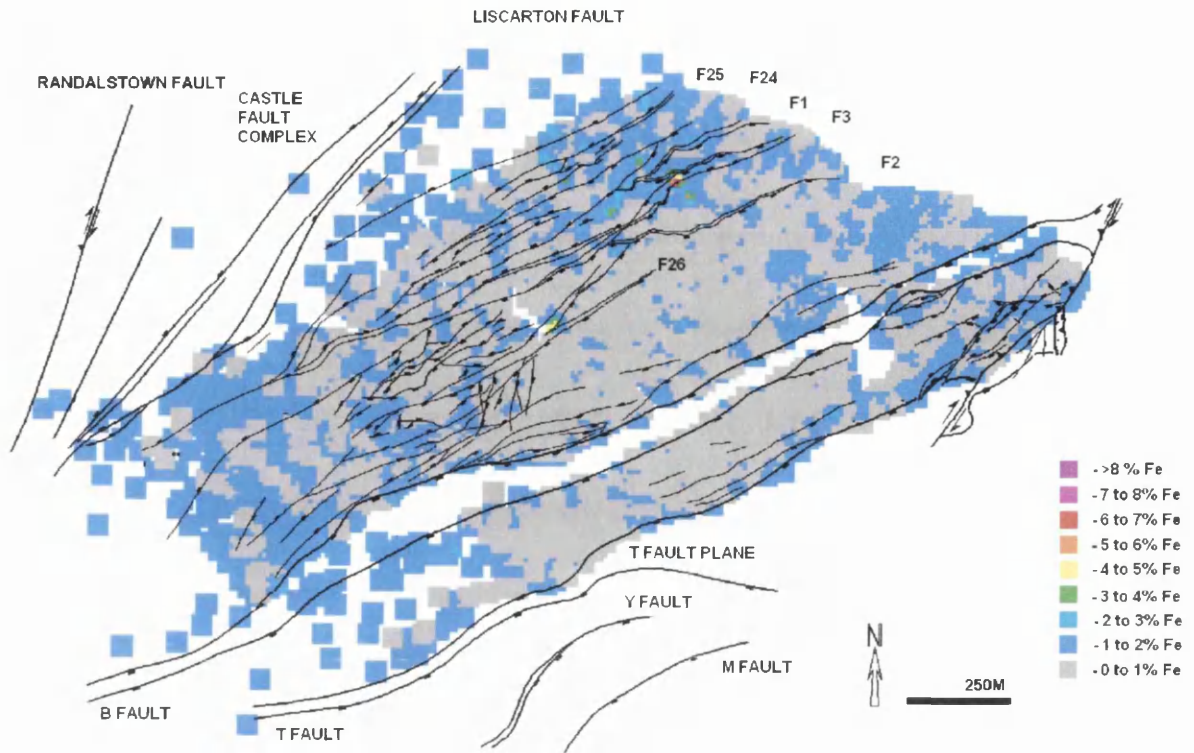


Figure 3-14 Distribution of %Fe in Slice 1 of the Navan deposit.

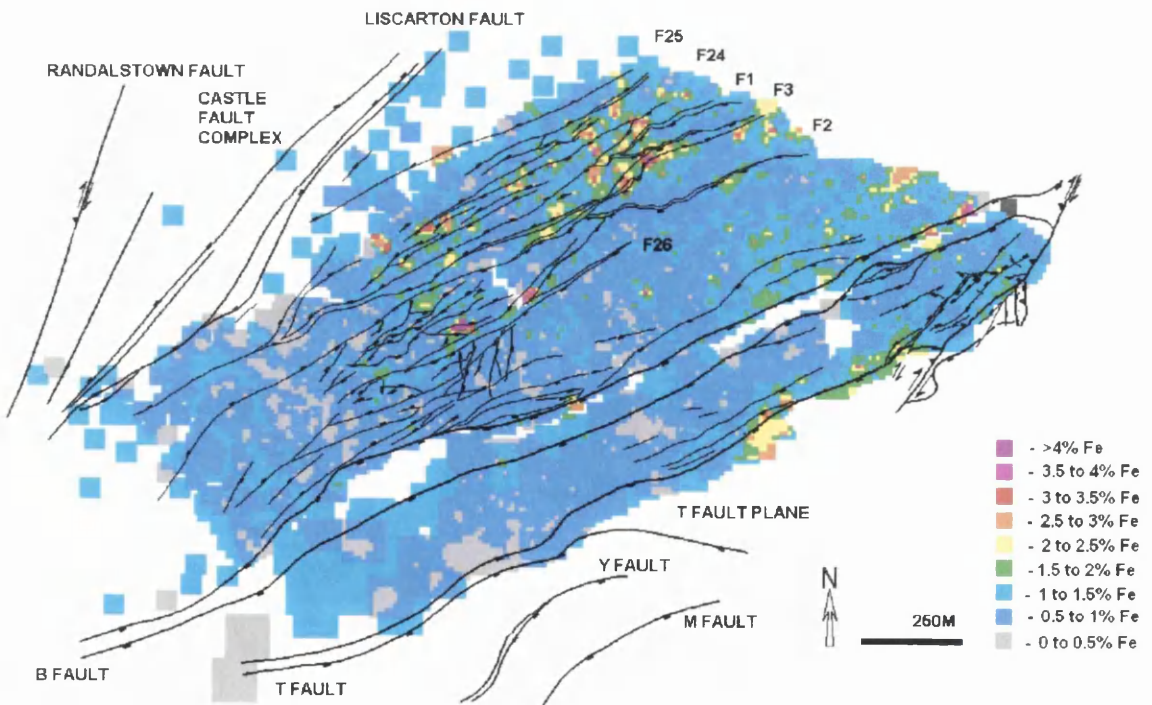


Figure 3-15 Distribution of % Fe in Slice 2 of the Navan deposit.

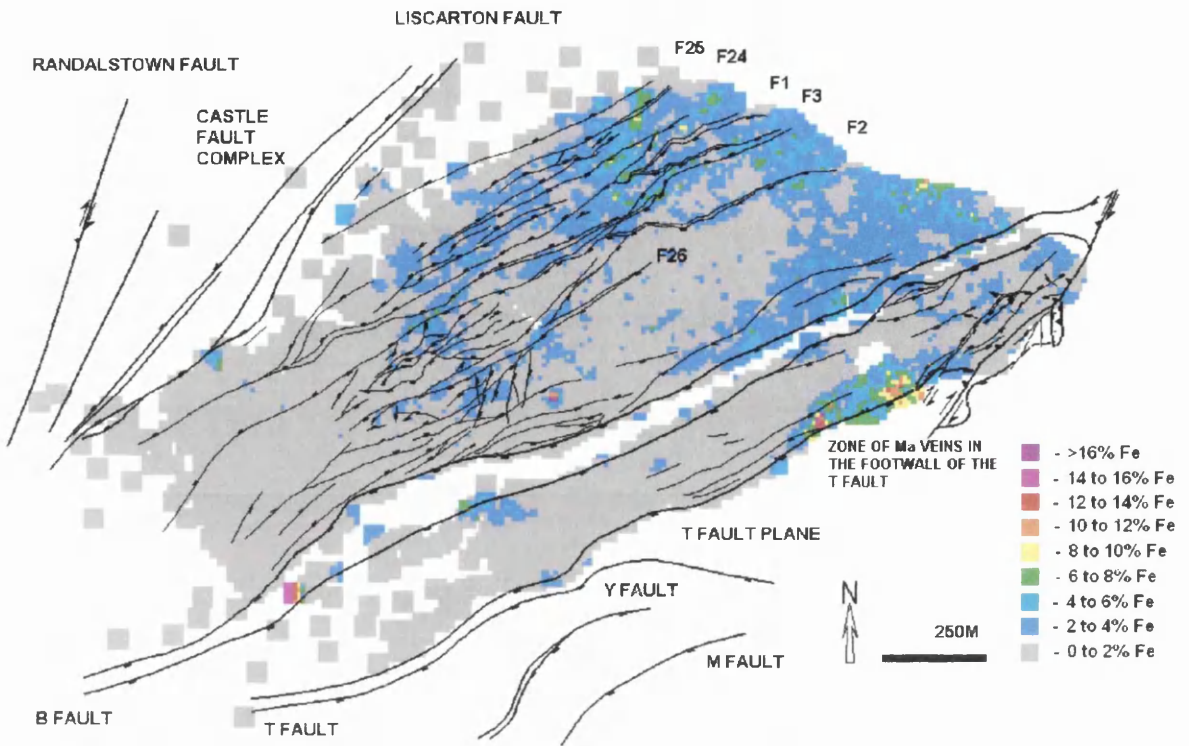


Figure 3-16 Distribution of %Fe in Slice 3 of the Navan deposit.

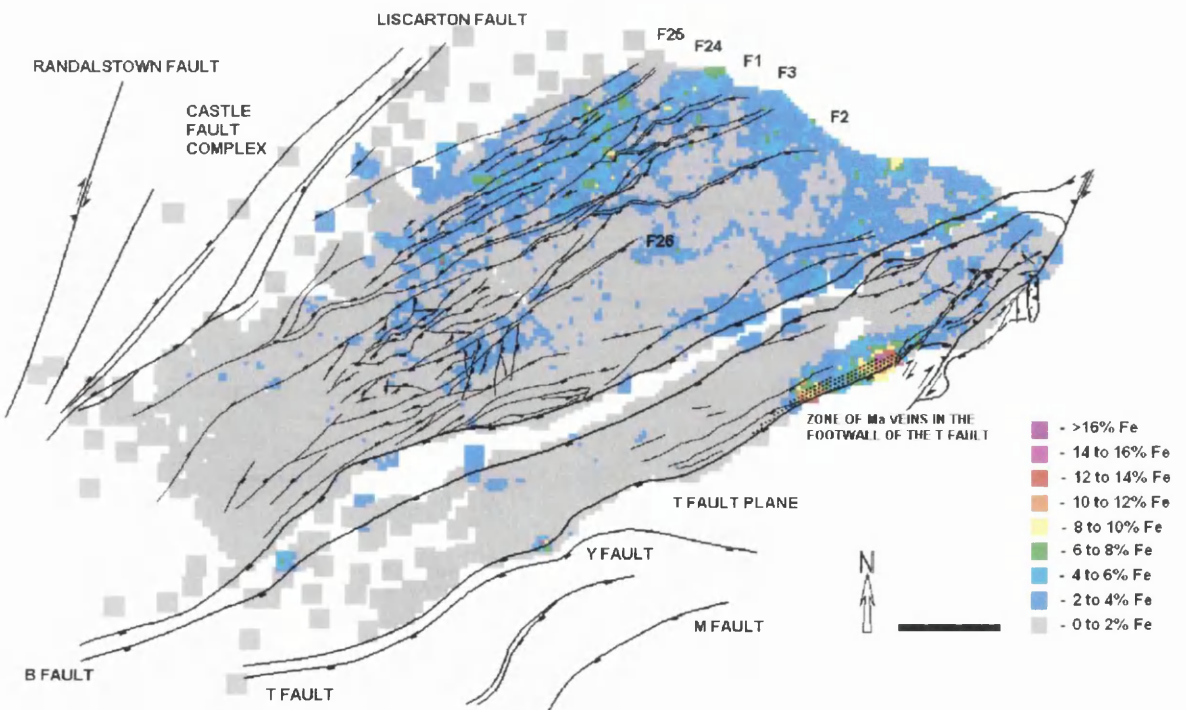


Figure 3-17 Distribution of %Fe in Slice 4 of the Navan deposit.

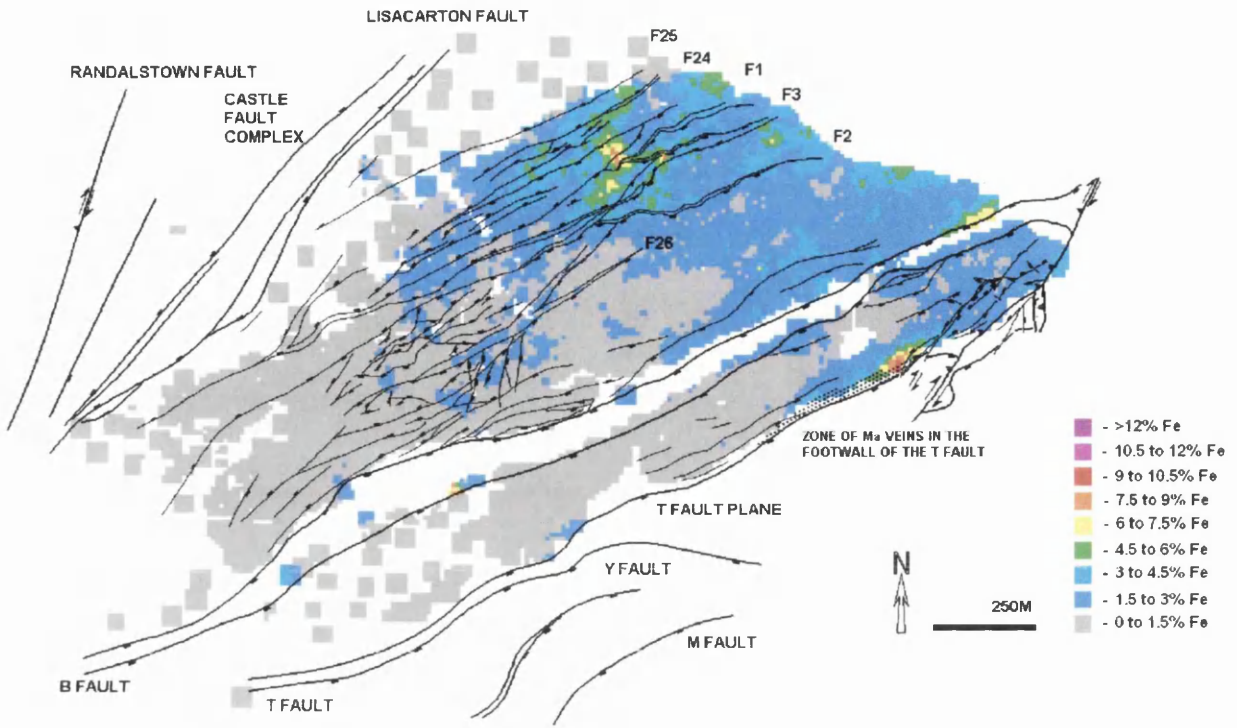


Figure 3-18 Distribution of %Fe within the lowermost 24m of 5 Lens (Slices 1 to 7) in the Navan deposit.

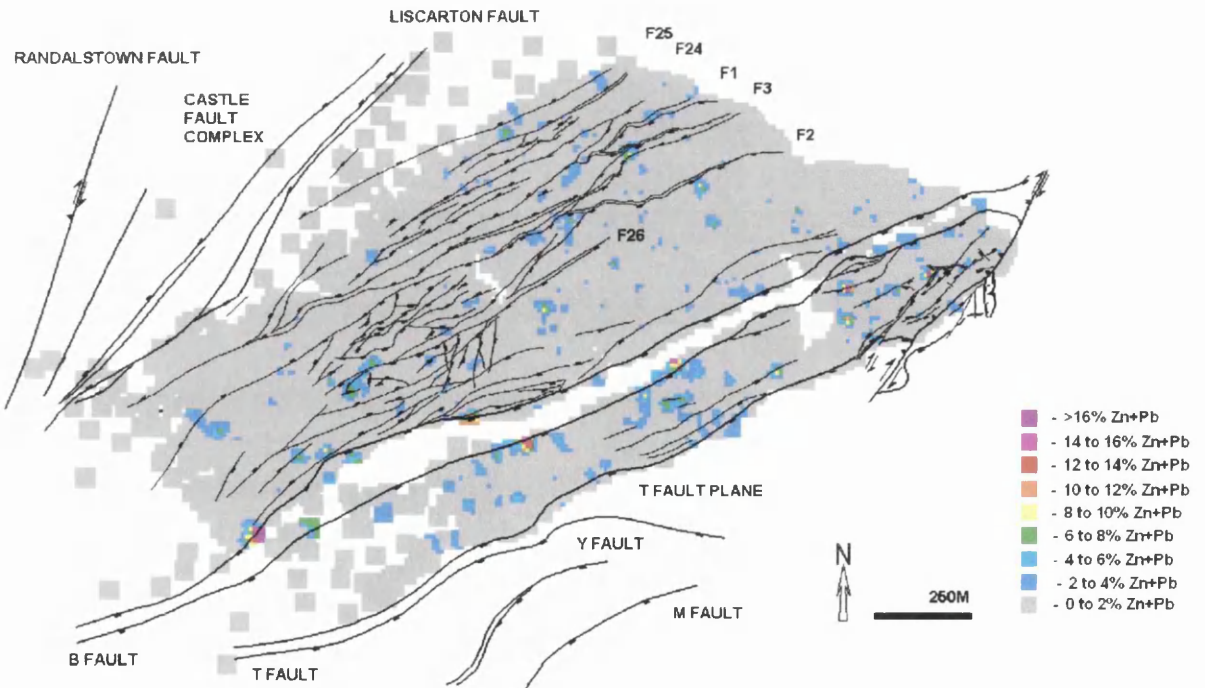


Figure 3-19 Distribution of %Zn+Pb in Slice 1 of the Navan deposit.

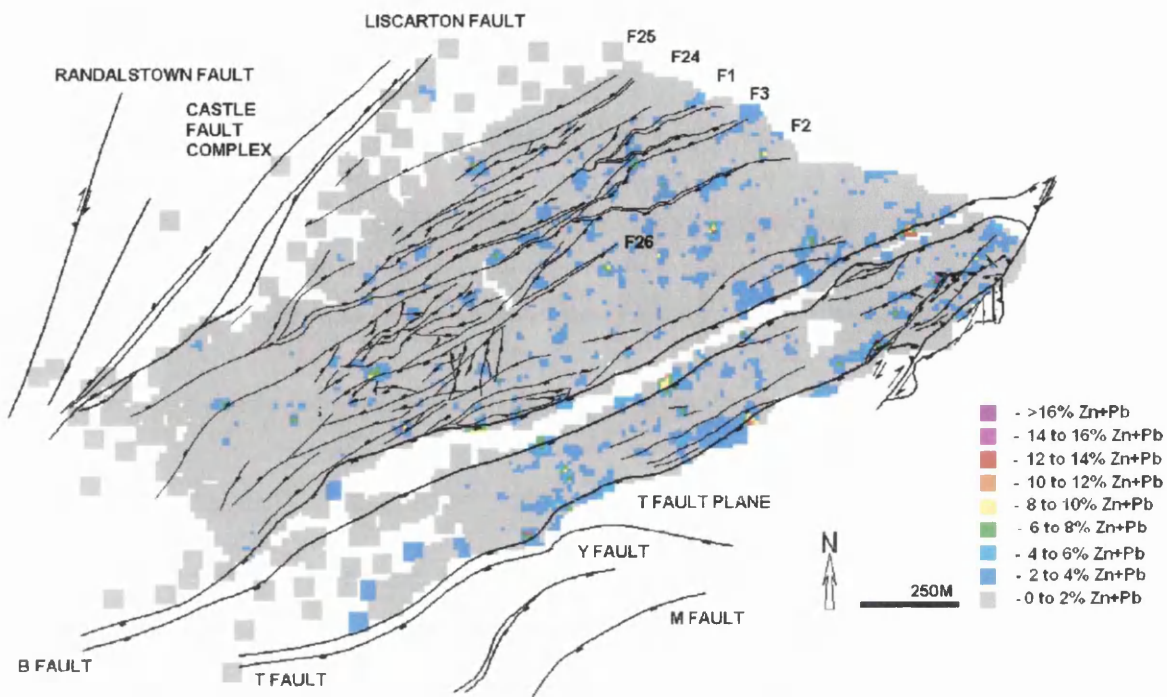


Figure 3-20 Distribution of %Zn+Pb in Slice 2 of the Navan deposit.

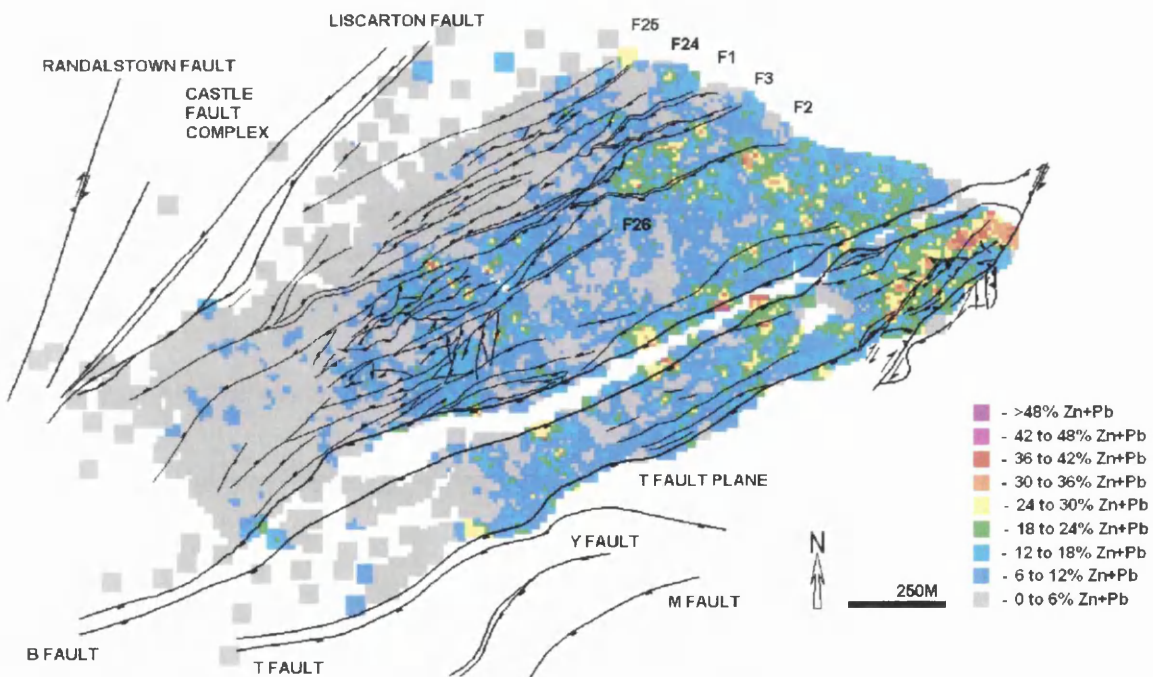


Figure 3-21 Distribution of %Zn+Pb in Slice 3 of the Navan deposit.

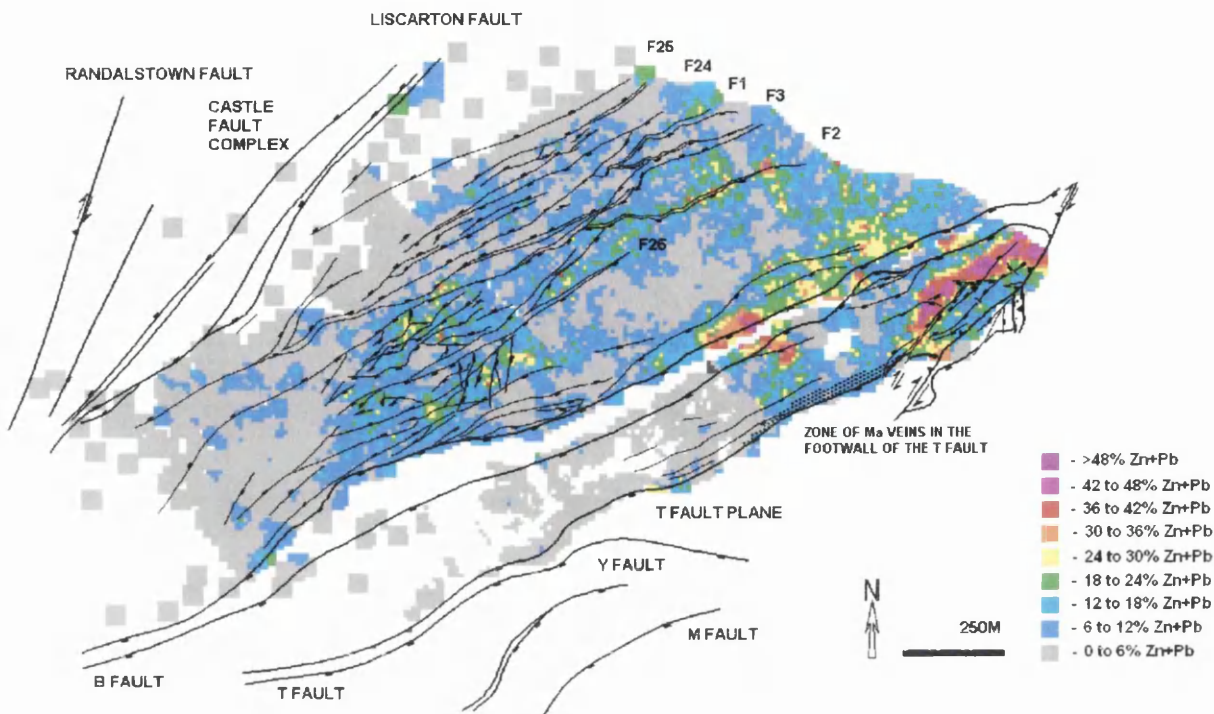


Figure 3-22 Distribution of %Zn+Pb in Slice 4 of the Navan deposit.

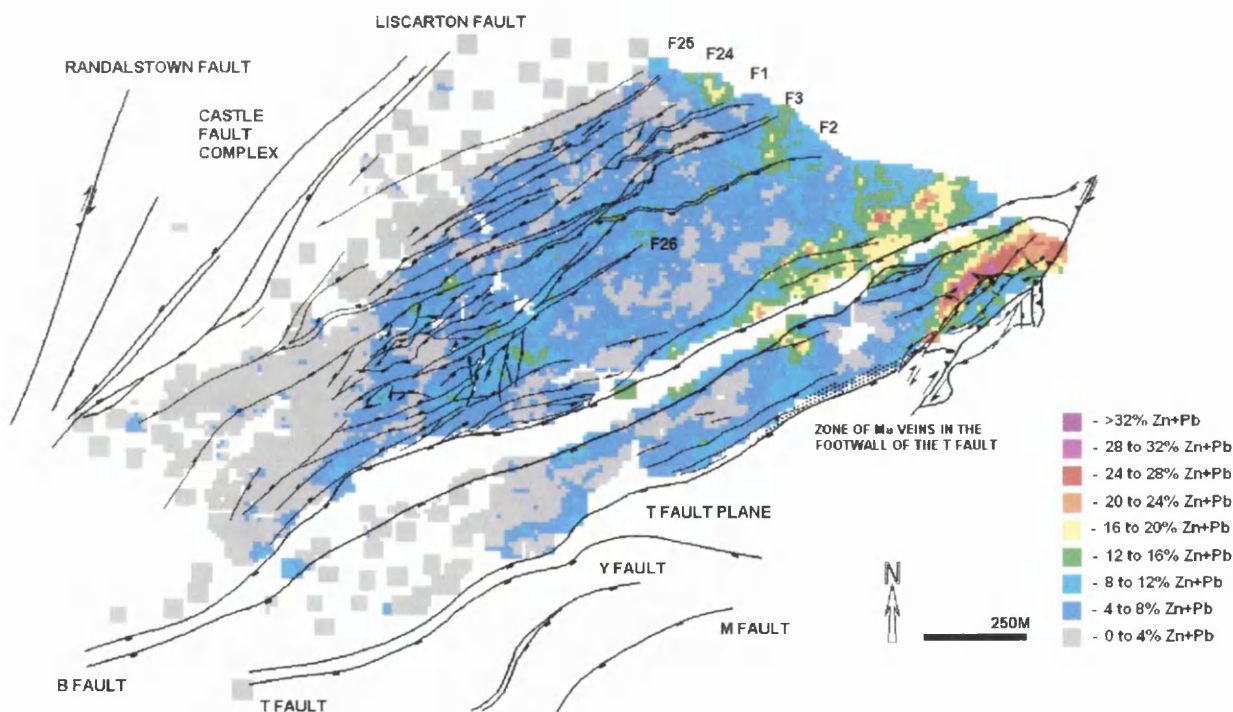


Figure 3-23 Distribution of %Zn+Pb within the lowermost 24m of 5 Lenses (Slices 1 to 7) in the Navan deposit.

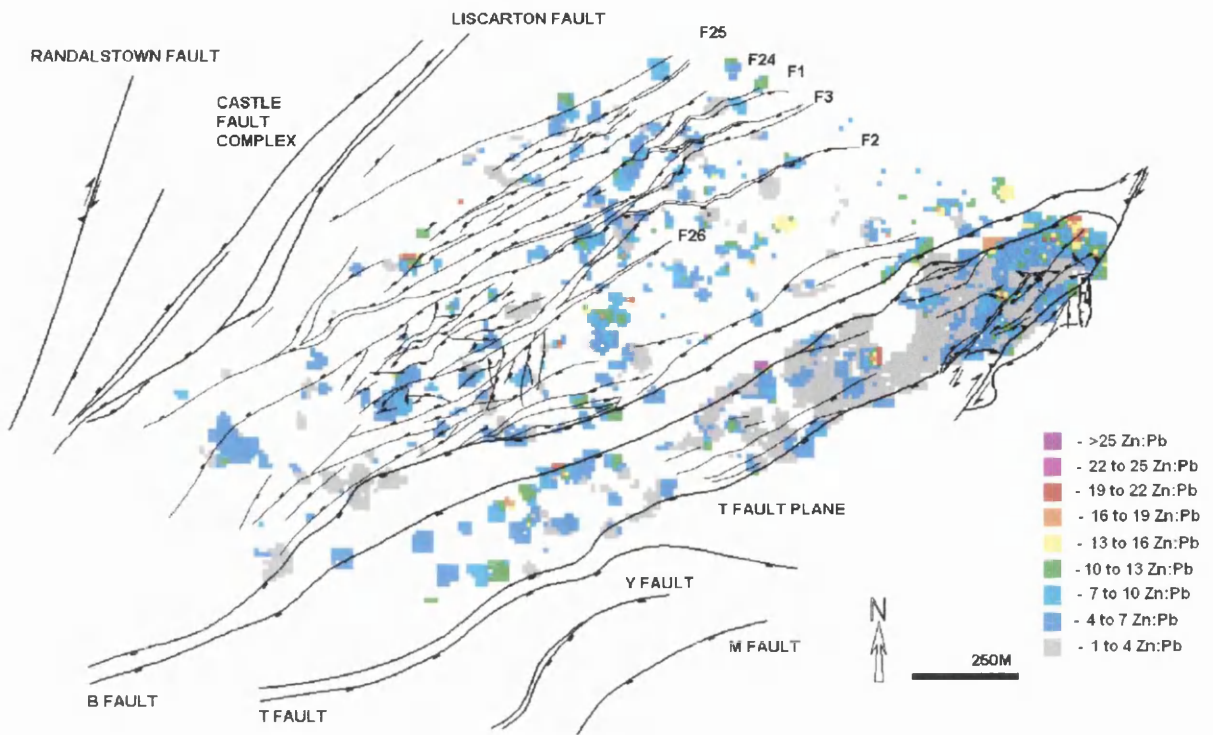


Figure 3-24 Distribution of Zn:Pb values in Slice 1 of the Navan deposit.

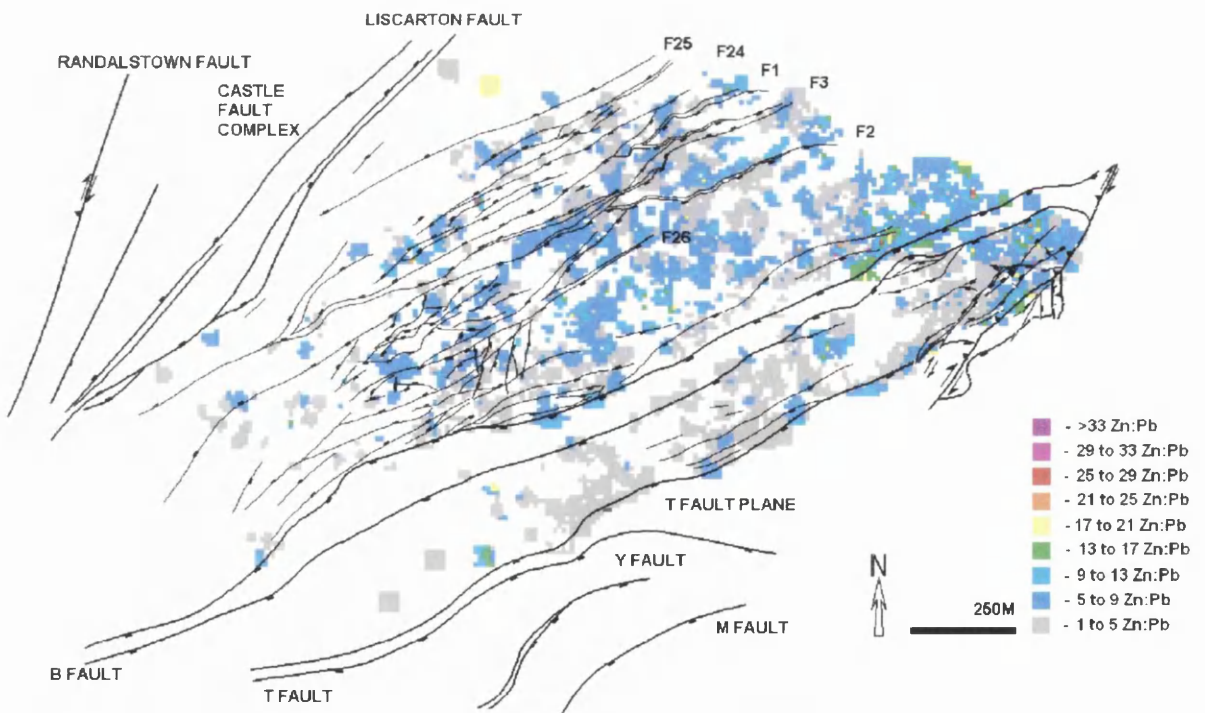


Figure 3-25 Distribution of Zn:Pb values in Slice 2 of the Navan deposit.

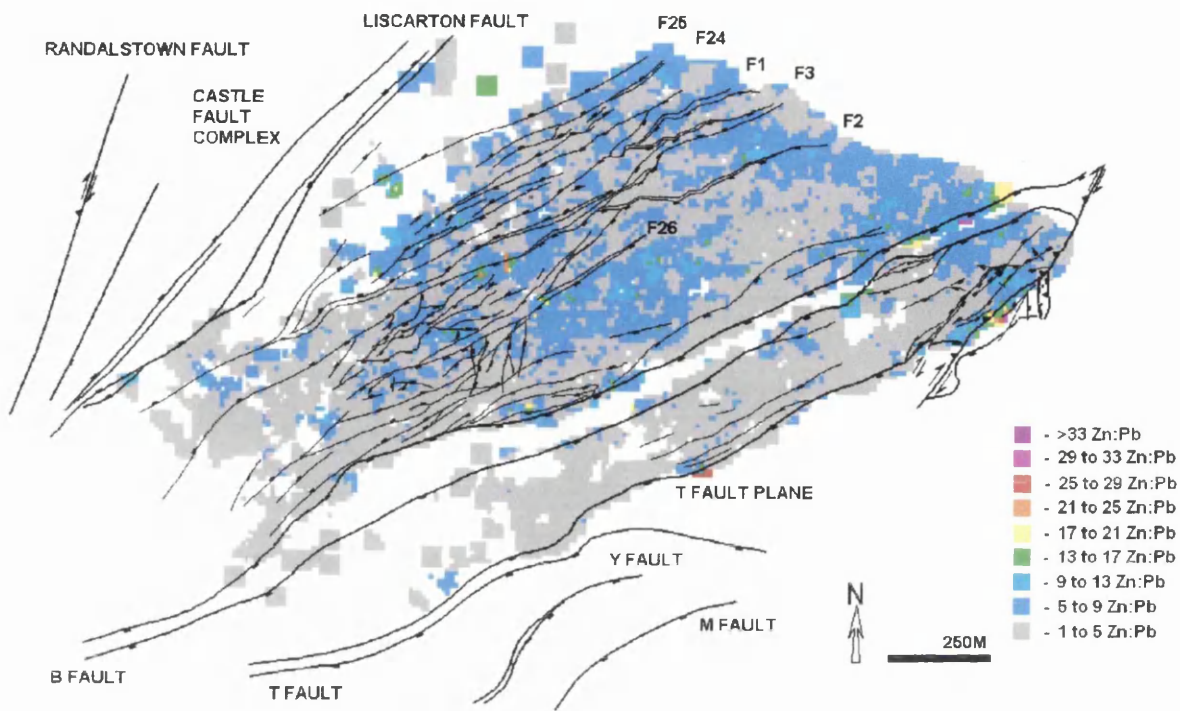


Figure 3-26 Distribution of Zn:Pb values in Slice 3 of the Navan deposit.

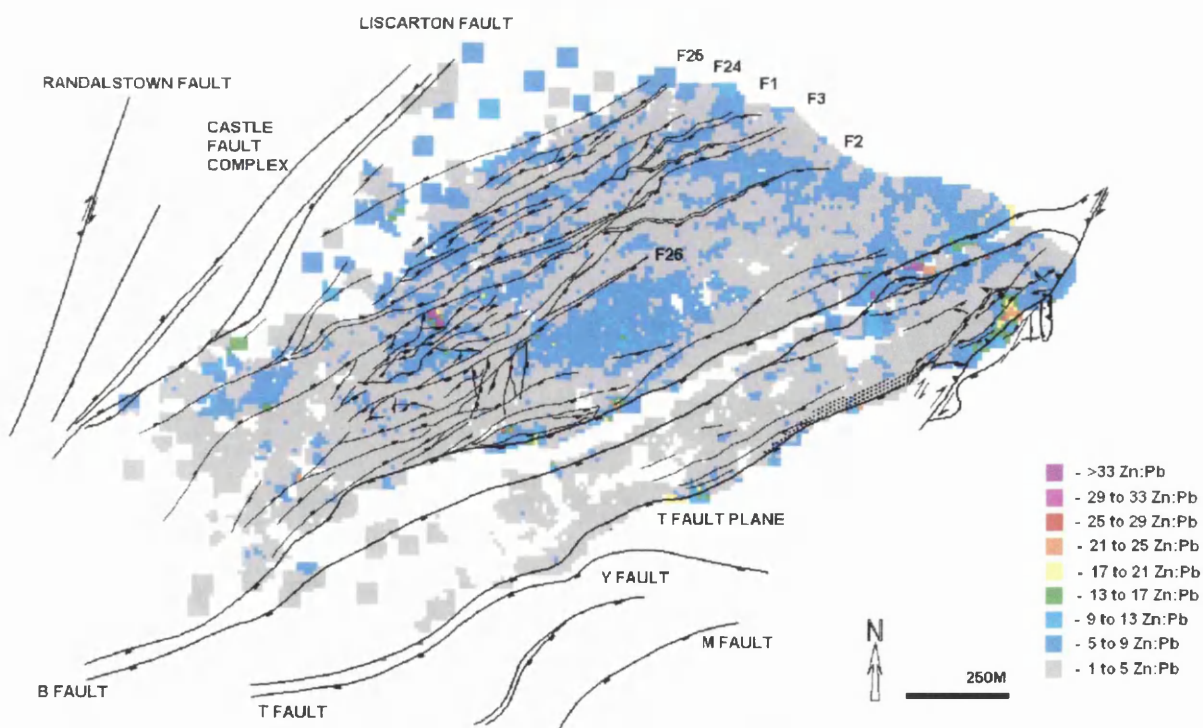


Figure 3-27 Distribution Zn+Pb values in Slice 4 of the Navan deposit.

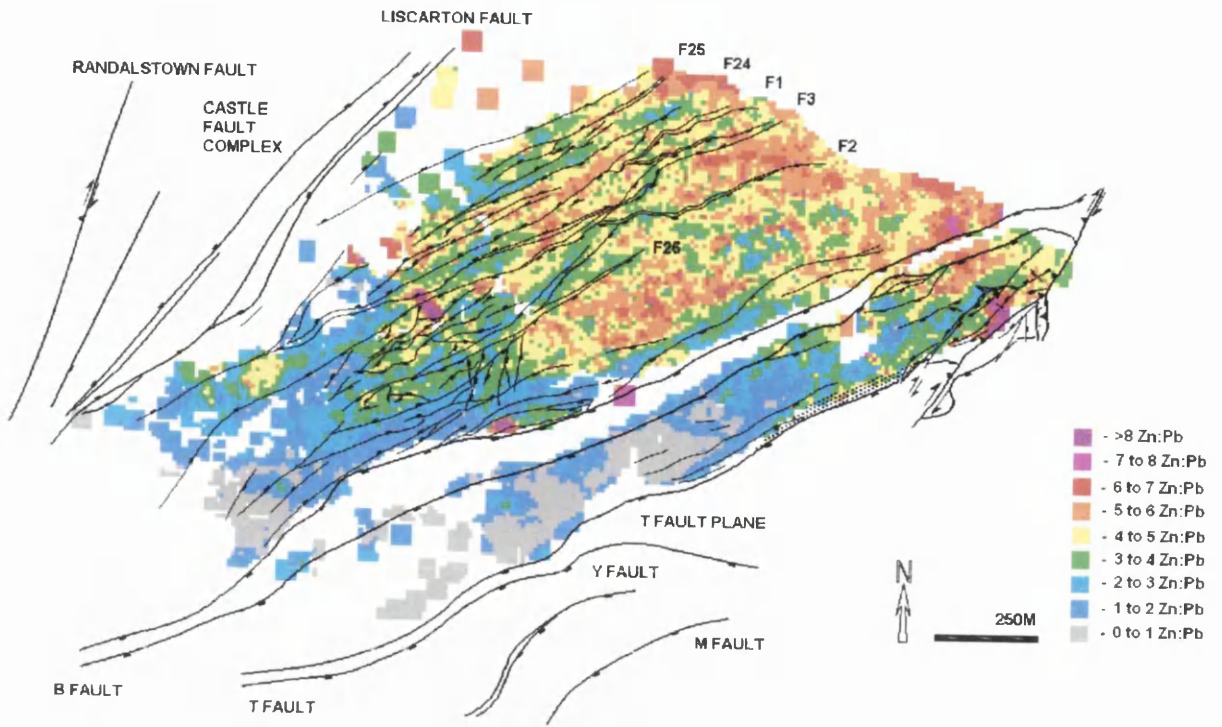


Figure 3-28 Distribution of Zn:Pb values within the lowermost 24m of 5 Lens (Slices 1 to 7) in the Navan deposit.

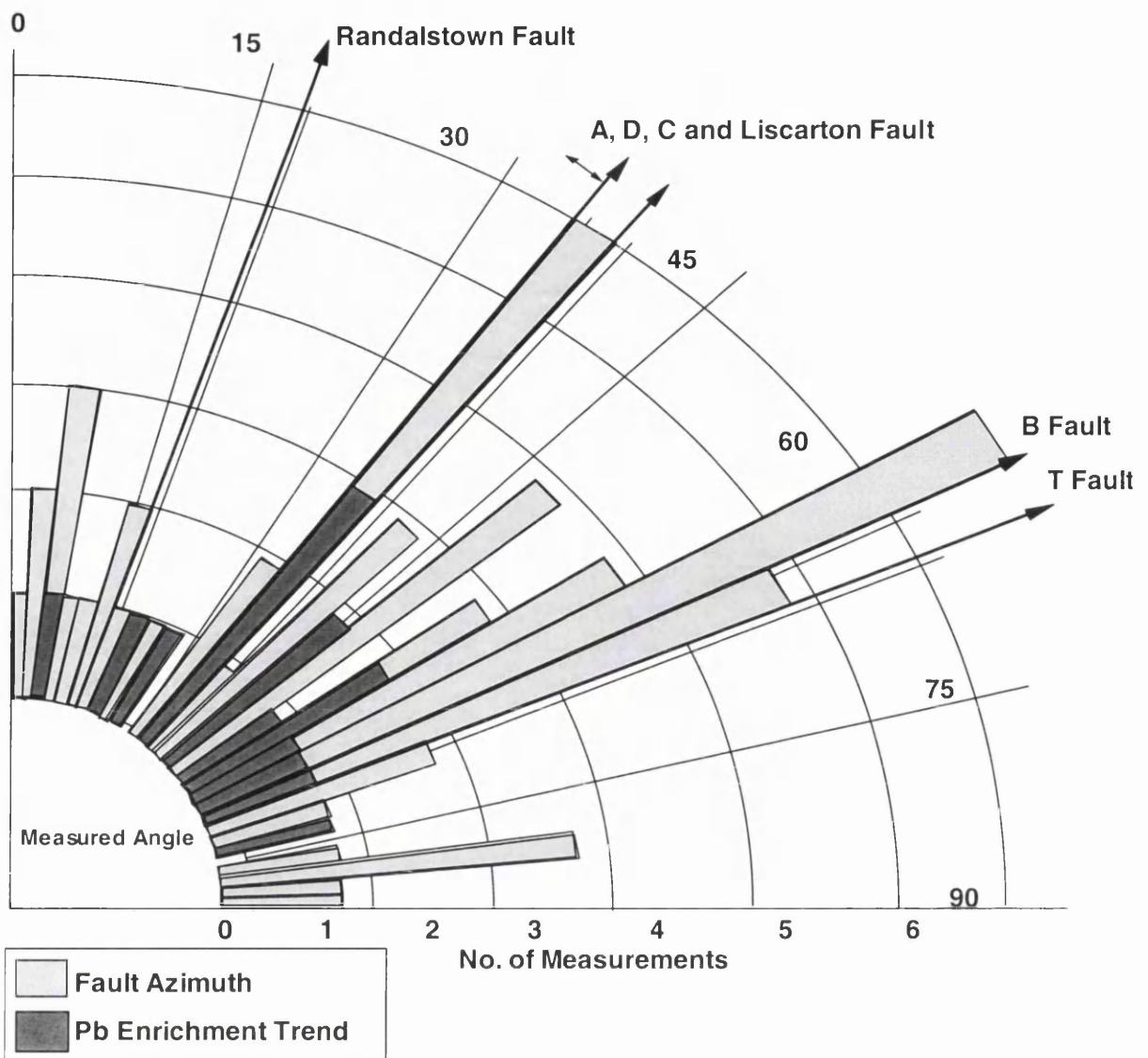


Figure 3-29 Diagram demonstrating the distribution of fault azimuths (based on 60 measurements) within the Navan deposit, compared to the trend directions of 15 recognisable Pb enhancements in 5 lens. In the event the Pb isochores most clearly show the relationship between metal enhancements and minor NNE to ENE minor faulting, rather than the ENE partly listric, locally major faults.

4. $\delta^{34}\text{S}$ variations with respect to possible feeder structures

4.1 Introduction

The basal 5 lens of the Navan Zn+Pb deposit contains ~70 % of the known tonnage of the ~90 Mt orebody and thus is the focus of this examination (for location of study area see Fig. 4-1). The study was centred on the lowest twenty-one meters of the basal 5 lens of the Navan deposit (Fig. 4-4). The lithological footwall of the orebody is delineated by a green shale recognizable throughout most of the deposit, and is located in the Micrite Unit (Fig. 3-2). The base of a dolomitic calc-arenite termed the 5 lens Dolomite (Fig. 3-3), which acts as an important control to ore localization in the western part of the deposit (Rizzi, 1993; Anderson et al., 1998), was chosen as the upper stratigraphic limit of the study.

Metal distribution patterns (particularly Pb), suggest that migration of metal-bearing fluids was principally directed up early to mid Lower Carboniferous, near vertical NNE, NE and ENE minor normal faults (see Chapter 3 and Fig. 3-29). These faults predate or are coeval with the major extensional, partly listric, ENE faults which now control the general disposition of the deposit (see Chapter 1 and 2). Only where these major ENE faults cross putative deep-seated, NE (Caledonoid) and NW structures are they associated with lead enrichments.

A systematic $\delta^{34}\text{S}$ survey in the 5 lens across five minor NNE through to ENE-trending faults associated with distinct lead enrichments and one ENE trending,

partly listric, major extensional fault adjacent to that trend, has been completed. This tested the hypothesis that the metal-bearing fluid (associated with positive $\delta^{34}\text{S}$ values), utilised the more minor (NNE to ENE) trending faults identified by the metal distribution isochores. Mineral sulfide petrography is used to contextualize the sampling and to give a qualitative indication of the degree of chemical disequilibrium of the system.

The contents of this chapter form parts of Blakeman et al., (in press) (Enc.).

4.2 Sulphur Isotopes

Anderson (1990) and Anderson et al. (1998) demonstrated that $\delta^{34}\text{S}$ within the Navan deposit has a bimodal distribution with some 80 percent of the sulfide having negative values (Fig. 4-2). They interpreted this pattern as a reflection of the mixing of a deep-seated, metal-bearing fluid possessing a low sulphur:metal ratio (positive $\delta^{34}\text{S}$ values), with a local fluid containing bacteriogenically-reduced sulfide (negative $\delta^{34}\text{S}$ values) derived ultimately from Lower Carboniferous seawater sulfate. Without this large mass of bacteriogenic sulfide, the Navan deposit would only have been about a fifth of the size (Anderson et al., 1998). Since then Fallick and his co-workers have demonstrated that 90% of the sulfide ore at Navan was precipitated with bacteriogenic sulfide and that only ~10% of the sulfide, that with the positive $\delta^{34}\text{S}$ values, was probably acquired from diagenetic sulfides remobilised by the deep-seated metal-bearing fluid within the underlying Lower Palaeozoic basement (Fallick et al., 2001). Anderson et al. (1998) also noted a correlation between $\delta^{34}\text{S}$ values and mineral textures and Paragenetic position (Fig. 4-13). Minerals precipitated later in the paragenetic sequence in hand specimen-scale samples exhibited values that are more negative.

Coarse bladed, zoned and granular textures exhibit relatively high $\delta^{34}\text{S}$ values from -1 to +15 per mil. Bedding-parallel replacement textures show a range of values from -23 to -15 per mil. Framboidal pyrite in the Conglomerate Group Ore and colloform pyrite/marcasite in the upper parts of the deposit have values ranging from -37 per mil to -28 per mil.

In order to test the hypothesis that the metal distribution patterns define the metal-bearing fluid conduits, the origin of the fluids in the palaeohydrological system operating at the time of mineralisation needs to be determined. This characterisation has been sought by completing a high-resolution $\delta^{34}\text{S}$ and ore mineral textural study systematically across five minor faults, associated with an enhanced Pb trend, and one adjacent major fault within the Navan 5 Lens (Figs. 4-5 and 4-6).

4.2.1 Hypotheses

Two end-member hypotheses to explain the Pb distribution patterns in the basal 5 Lens are considered:

1. That mineralisation occurred after the full development of the B and T Faults, these faults acting as the main conduits for the upwelling metal-bearing fluids (Fig. 4-3). This hypothesis could be thought of as a variant of the hypothesis generally used to explain “Mississippi Valley-Type” mineralisation.
2. That mineralisation occurred prior to/coeval with initial movements on the B and T Faults, but during/after the development of the early steeply dipping minor NNE, NE and ENE normal fault sets. All faults would have acted both as feeders

for the upwelling metal-bearing fluids, and loci for the downdrafts of bacteriogenic bearing-seawater-derived solutions (Fig. 4-4). This hypothesis has been adumbrated under the appellation, “Irish Type” mineralisation.

In the first hypothesis it is envisaged that rapid subsidence within the Dublin Basin lying to the south of Navan, allowed the development of major partly listric extensional faults, which tapped metal-rich fluids rising from depth, as described by Anderson et al. (1998). These hot mineralising fluids would have accessed the minor fault sets where they abutted against the major faults (Fig. 4-3). Down-flowing, locally derived, bacteriogenic bearing-bearing fluids used the minor fault sets to gain access to the host rocks. As these two fluids mixed, an increasingly negative $\delta^{34}\text{S}$ signature with distance from the B and T Faults would be apparent. In addition, bladed marcasite and galena signifying rapid precipitation/deposition (Anderson et al.1998) would only occur at and close to the major extensional faults.

In contrast, an expectation from the second model is that positive $\delta^{34}\text{S}$ signatures would be associated with both major and minor faults of all trends (Fig. 4-4). That is, these signatures would be found in sulfides in the major, partly listric, ENE, extensional faults, as well as in the earlier/coeval, NNE, NE and ENE fractures. Mineral textures indicating rapid precipitation/deposition (Anderson et al.1998), would also be expected to be associated with all the faults.

4.2.2 Scientific methods

4.2.2.1 Sampling, reflected light microscopy and isotopic technique.

Sampling: As the objective was to elucidate the sources of the sulphur and the relationship of ore depositional processes to faulting and thereby to assess the relative merits of the two hydrogeological hypotheses, a profile survey of $\delta^{34}\text{S}$ values across the various fault generations has been completed. A suite of samples were selected to cover material exhibiting all the ore textures and parageneses described in Anderson et al. (1998). The profile (Fig. 4-5 and 4-6) is located in the north-eastern section of the deposit (see Fig. 4-1). The study was concentrated in the lowermost 5 lens within the Micrite unit and beneath the 5 lens Dolomite (Fig 4-5). The profile intersects the B Fault (trending ENE) and five minor faults trending from NNE to ENE associated with a distinct lead enrichment trend (Fig. 4-6). Ninety-five samples were analysed from nineteen diamond drill-hole (DDH) cores taken along the profile length (~115 m). See Appendix 1.

Reflected light microscopy: Polished blocks have been examined in reflected light to ascertain mineral parageneses and to give an indication of the dynamism or otherwise of conditions at, and following, the time of mineral precipitation in an area singled out for this isotopic study (see profile in Fig. 4-5 and 4-6).

Isotope technique: *In situ* laser analyses of sulfide $\delta^{34}\text{S}$ in polished blocks, selected on the basis of the petrological study, were made using the established technique described by Kelley and Fallick (1990). The sulphur dioxide produced was analysed on-line by a VG SIRA 2 mass spectrometer. All sulphur isotope results are expressed in conventional delta ($\delta^{34}\text{S}$) notation, as per mil (‰)

deviations relative to Cañon Diablo troilite (CDT). Reproducibility based on complete duplicate analyses (including combustion) was better than 0.3 ‰.

4.3 Results

4.3.1 Mineral textures

Figure 4-7 illustrates the textures observed 0.5 meters into the footwall of a NE trending fault intersection (DDH U12477). Early comminuted marcasite blades are surrounded by paragenetically later coarse granular sphalerite. Figure 4-8 exemplifies the textures found in DDH U12473 located one meter into the footwall of a NE striking normal fault toward the NW end of the profile. Here resorbed cubic galenas that now show pseudo-dendritic (skeletal) textures, are surrounded by pyrite (including framboidal pyrite) with minor cubic crystalline centres. Sphalerite and dolomite enclose this assemblage. Figure 4-9 illustrates sample DDH U12472, located one meter into the hanging wall of a NE trending fault. Here, comminuted clasts of early sphalerite sit in a sea of minor barite and pyrite overgrown by colloform pyrite. Later galena predates a sphalerite 'honeyblende' matrix. The photomicrograph of sample DDH U12493 from the NW end of the profile, ~5 m into the footwall of a NNE trending early minor fault, displays early galena surrounded by framboidal pyrite which is in turn cut by later sphalerite (Fig. 4-10). DDH U12478 is located 15 m away from any observed fault (Fig. 4-11). Here sphalerite is intergrown with dolomite and minor pyrite.

To generalize in the area of study, it appears that early comminuted bladed marcasite predates bladed galena and granular sphalerite. Then resorbed cubic galenas predate framboidal pyrite. Sphalerite and dolomite follow. Galena is also surrounded by framboidal pyrite, which in turn is cut by later sphalerite. Yet early sphalerite (some with truncated colloform textures) is enclosed by minor barite and pyrite; the ensemble overgrown by colloform pyrite. Later galena predates a sphalerite 'honeyblende' matrix. Elsewhere sphalerite is intergrown with dolomite and minor pyrite. This chaotic paragenesis is indicative of deposition in far-from-equilibrium conditions, conditions implied too by the colloform, rhythmically banded sphalerite of Anderson et al. (1998) as well of the rapidly fluctuating sulphur isotopes seen in a composite galena blade (Kelley and Fallick, 1990; Anderson et al., 1998 (figures 13B and 24) and see Letnikov, 1997).

4.3.2 Isotope results

The sulphur isotope results are listed in Appendices 2 and 3, and illustrated in Figures 4-7 to 4-12, and Figures 4-14 and 4-15. Half a meter into the footwall of a NE trending fault intersection (DDH U12477) the $\delta^{34}\text{S}$ values of all the sulfides are positive. Early comminuted marcasite blades have an average $\delta^{34}\text{S}$ of +17.1‰. The surrounding coarse granular sphalerite averages +5.8‰ and the bladed galena averages +10.9‰ (Fig. 4-7). Values of $\delta^{34}\text{S}$ in minerals in DDH U12473 located one meter into the footwall of a NE striking normal fault are more varied. Pseudo-dendritic galenas have an average $\delta^{34}\text{S}$ of -7.4‰; the surrounding framboidal pyrite averages -16.5‰, whereas the later sphalerite returns to the heavier value of +4.3‰ (Fig. 4-8).

One meter into the hanging wall of a NE trending fault, sulfides in sample DDH U12472 range to appreciably light values. For example, $\delta^{34}\text{S}$ in comminuted clasts of early sphalerite ranges from -1.4‰ to -17.4‰, and colloform pyrite overgrowths have an average $\delta^{34}\text{S}$ of -28.9‰. Also later galenas have average $\delta^{34}\text{S}$ of -17.2‰, and the later sphalerite 'honeyblende' matrix has $\delta^{34}\text{S}$ ranging from -7.7‰ to -22.1‰ (Fig. 4-9). Low $\delta^{34}\text{S}$ values are also a feature of sample DDH U12493 collected from ~5 m into the footwall of a NNE trending early minor fault. Galena averages -11.4‰, framboidal pyrite -29.9‰, and later sphalerite averages -13.2‰ (Fig. 4-10). Values of $\delta^{34}\text{S}$ continue to be low 15 m away from any observed fault, as in the sphalerite in DDH U12478 that averages -9.7‰ and minor pyrite, which returns an average $\delta^{34}\text{S}$ of -25.3‰ (Fig. 4-11).

Were the sulfides to have been precipitated in isotopic equilibrium pyrite should always have the highest $\delta^{34}\text{S}$, with sphalerite next highest, and galena the lowest $\delta^{34}\text{S}$ (Ohmoto and Goldhaber, 1997). At the likely highest temperature of hydrothermal ore deposition at Navan (i.e. 200°C; Everett and Wilkinson, 2000), the isotopic differences should be around the following: $\delta^{34}\text{S}_{\text{py-sp}} = 1.3‰$; $\delta^{34}\text{S}_{\text{py-ga}} = 4.5‰$; $\delta^{34}\text{S}_{\text{sp-ga}} = 3.3‰$ (Ohmoto and Goldhaber, 1997). In all of the specimens analysed, isotope relationships indicate disequilibria. The $\delta^{34}\text{S}$ values in sphalerite are lower than those in the associated galena, and the pyrite has lower $\delta^{34}\text{S}$ values still than either sphalerite or galena. Plots of the frequency distribution of $\delta^{34}\text{S}$ values in sulfide phases are given in Figure 4-14. The observed patterns bear favourable comparison with the findings of Anderson et al., (1998) for the Navan deposit as a whole, and Anderson (1990) for 5 lens in particular (see Fig. 4-2).

Figure 4-15 shows the distribution of $\delta^{34}\text{S}$ values with respect to distance from the nearest fault, and its location in either the footwall or hanging wall. Bladed marcasite (Fig. 4-15c), which only occurs within 3 m of a fault, has the most positive $\delta^{34}\text{S}$ (+9.6‰ to +17.5‰) (see also Anderson et al., 1998). Galenas (Fig. 4-15b) similarly show positive $\delta^{34}\text{S}$ close to faults (+9.3‰ to +15.8‰), whereas away from faults only negative values are encountered (-5.9‰ to -26.4‰). Sphalerite (Fig. 4-15a) behaves as galena, more positive $\delta^{34}\text{S}$ values being dominant within ~3 m of the nearest fault (+0.8‰ to +10.0‰) and only negative $\delta^{34}\text{S}$ (-1.4‰ to -22.1‰) values occur in more distal samples. On the other hand, pyrite $\delta^{34}\text{S}$ values display a different pattern (Fig. 4-15c). The apparent background is constant at a $\delta^{34}\text{S}$ value of ~-30‰. A positive shift occurs only within 3 m of the fault, in both the footwall and hanging wall, although there is a strong negative shift close to the fault plane itself (see also Fig. 4-12).

4.4 Interpretation of sulphur isotope analyses and mineral textures

Precipitation of sulfides with positive $\delta^{34}\text{S}$ values took place directly from cooling, and therefore increasingly super-saturated, decreasingly buoyant, metal-bearing fluids. These fluids not only invaded the faults, they also initially displaced the dense bacteriogenic bearing-bearing fluids from a zone in the footwall host rock up to 3 meters across (Fig. 4-15) (c.f., Rizzi, 1992). To explain this disposition of the isotope values it may be speculated that hydrostatic pressure may have been lower in the footwall, perhaps a result of gravitation of the ambient brine to depth during tectonism, so encouraging the development of secondary convection cells in and paralleling the minor faults (Sibson et al., 1975).

According to Anderson et al. (1998) the sulphur to metal ratio present in the hydrothermal fluid was low. Experimental work by Bischoff et al. (1981) also illustrated that the sulfur-bearing capacity of the hydrothermal ore fluids feeding the Irish deposits was low. Thus, the additional bacteriogenic sulfide source is essential to achieve high tonnage. Fallick et al. (2001) illustrate that at Navan more than 90% of ore grade sulfide was bacteriogenic. The observation that negative $\delta^{34}\text{S}$ values reflect the dominance of bacteriogenic sulfide away from the feeder faults is in concert with their results. The positive $\delta^{34}\text{S}$ values in galena and sphalerite samples correlate with high lead concentrations. Thus while the minor NNE, NE and ENE faults, as well as the B fault, acted as conduits for the metal-bearing fluids, the conclusion is forced that the earlier near vertical set was the more exploited (Fig. 4-15a and 4-15b). It follows that the second of the two

alternative hypotheses, i.e., the syn-diagenetic mesothermal or Irish Type model, depicted in Figure 4-4, is the more consistent with the mineralogical and isotopic constraints.

The Irish Type model is also favoured by the further observations discussed below. The distribution, textures and $\delta^{34}\text{S}$ values shown by marcasite and pyrite contrast with those of galena and sphalerite. Marcasite occurs only within ~3 m of a fault plane and displays high positive $\delta^{34}\text{S}$ values (Figs. 1-14c and 4-15c). Conversely, pyrite reflects a somewhat similar pattern to galena and sphalerite with a positive shift in $\delta^{34}\text{S}$ within ~3 meters of the faults (Fig 4-15a, b and c). However, sample DDH U12498 (Fig. 4-12), located within one meter of a NE trending minor fault, returned strongly negative $\delta^{34}\text{S}$ values. This result is interpreted as reflecting the gravitation of bearing-bearing saline seawater containing highly fractionated bacteriogenically-reduced sulfide from above, into the feeder conduits on at least one occasion.

It is important to note here that pyrite $\delta^{34}\text{S}$ is always substantially lower than the base-metal sulfide $\delta^{34}\text{S}$, i.e. the extent of bacteriogenic fractionation is greater leading up to pyrite deposition, than that operating during Zn+Pb sulfide deposition. This is highlighted by sample DDH U12472. Here the extremely low $\delta^{34}\text{S}$ pyrite deposition occurs before and after base-metal sulfide precipitation, indicating that a change in the sulfidation (the bacteriogenic sulfide producing system) takes place before and after mineralisation pulses. It may be that this excursion and reversion reflects a bacterial consortium operating in more oxidising conditions during periods of quiescence (pyrite deposition), allowing increased disproportionation cycles during dissimilatory bacterial reduction of sulfate, likely involving intermediate, largely bacterially-mediated reactions with thiosulfate, sulphite and sulphur (Jørgensen, 1990; Thamdrup et al., 1993; Canfield and Thamdrup, 1994; Finster, et al., 1998; Cypionka et al., 1998). A

corollary of this observation is that the sulfide in pyrite cannot be the source of base-metal sulfide, as remobilised pyrite sulfide would simply retain its original $\delta^{34}\text{S}$ signature (see also Boyce et al., 1983b, and Anderson et al., 1989).

Furthermore, the extent of bacteriogenic fractionation (on average in the base-metal sulfides $\delta^{34}\text{S}_{\text{sulfate-sulfide}} = 36\text{‰}$; greater for pyrite) in all sulfides indicates a dominance of open system reduction of sulfate. Thus, whilst it is clear from these observations that bacteriogenic sulfide penetrated beneath the seafloor, the seawater sulfate reservoir was accessed throughout the main mineralising event.

Evidence of oscillations in the mixing front between the predominantly metal-bearing hydrothermal solutions and bacteriogenically reduced sulfide bearing fluids can be gleaned from sample DDH U12473 (Fig. 4-8). Here early galena is partially resorbed and overgrown by later pyrite with a bacteriogenic signature. But still later sphalerite overgrowths show a strong positive shift in their $\delta^{34}\text{S}$ signatures, indicating deposition from later hydrothermal, positive $\delta^{34}\text{S}$ -rich solutions.

Whether pyrite or marcasite are precipitated from low to medium temperature hydrothermal solutions depends on pH (Murowchick and Barnes, 1986; Schoonen and Barnes, 1991). In this study, marcasite is seen to be precipitated paragenetically early in an environment dominated by deep-seated, metal-bearing fluids with positive $\delta^{34}\text{S}$ values. The conditions of the hydrothermal fluids prevailing during the very earliest phase of sulfide deposition (prior to reaction with the micrite units) are likely to be acidic (Bischoff et al., 1981). Thus marcasite precipitation is favoured. Moreover the marcasite is bladed, a morphology to be expected where precipitation was rapid under relatively low pH

conditions. It is also comminuted (samples DDH U12477 and U12472; Figs 4-7 and 4-9 respectively), a texture indicative of early post-depositional fault related and/or hydraulic/chemical brecciation (Sawkins, 1969). It is reiterated that marcasite is only found in or near faults and always carries a positive $\delta^{34}\text{S}$ value and bladed texture, indicating that the incoming hydrothermal fluid was acidic.

4.5 Conclusions

A profile located within the basal 5 lens which represents ~70 percent of the known tonnage of the Navan orebody was subjected to a detailed $\delta^{34}\text{S}$ survey, based on a careful petrographic, structural and metal distribution study. The profile traverses both minor NNE, NE and ENE fractures each associated with distinct lead enrichments, and one partly listric, major ENE fault, the B fault, with occasional lead enrichment. Sulfides with relatively high $\delta^{34}\text{S}$ (0 to +17‰) are, without exception, found within 3 meters of both the minor, steeply dipping NNE, NE and ENE normal faults, as well as the B fault. Combined with the lead distribution patterns, this sulphur isotope pattern points to the role of the minor, steeply dipping, normal structures as hydrothermal feeders. The partly listric B fault, although accommodating metal-bearing fluid flow, played a secondary role in the genesis of 5 lens. Bacteriogenic sulfide ($\delta^{34}\text{S} \leq -5‰$) dominates away from these faults (and throughout the deposit in general: Anderson et al., 1998; Fallick et al., 2001).

The presence of negative $\delta^{34}\text{S}$ values associated with pyrite close to these fractures shows that, at times, the locally derived cooler bacteriogenic bearing-bearing saline seawater-derived fluid also gained access to these faults. The fact that where observed in drill-core and underground exposure, the minor faults along the investigated profile are infilled by carbonate, also indicates that fluids were capable of moving freely within these fractures, allowing simultaneous access to hydrothermal solutions from below as well as to seawater-derived brine from above. These observations are not consonant with fault-trapping, and are inconsistent with the expectations of the MVT model of mineralisation for Navan.

The textural observations reported here indicate that active faulting took place during the earliest part of the mineralising process. These active faults allowed pulses of the deep-seated hydrothermal metal-bearing fluid to periodically displace the locally derived bacteriogenic bearing-bearing fluid. The chemical and physical disequilibria between these two fluids is reflected in the mineral phase boundaries and the disordered $\delta^{34}\text{S}$ values recorded for adjoining sphalerite, galena and pyrite (Figs. 4-7-4-11; Appendix 1).

No evidence can be discerned on the minor NNE, NE and ENE faults on the profile, which anyway are confined to early to mid Lower Carboniferous lithologies, to demonstrate movements during late Carboniferous tectonism. Therefore, the onset of metallogenesis at Navan must be placed early in the rifting history of the Irish Midlands, i.e. during the early to mid Lower Carboniferous. This conclusion is in agreement with the arguments of Ashton et al., (1992), and Anderson et al., (1998). It is also in concert with observations at the Silvermines and Tynagh SEDEX deposits (e.g. Russell, 1975; Taylor and Andrew, 1978; Boyce et al., 1983b, 1999; Banks, 1985).

The conclusion that a deep-seated Caledonoid structure (or suite of structures), was one of the controls of mineralisation at Navan, and that metal-bearing fluids flowed through the basement, is consistent with the findings of Anderson et al. (1989) and Boyce et al. (1983b) that diagenetic sulfides within the basement lithologies were the source of positive $\delta^{34}\text{S}$ values associated with the metal-bearing fluid. Such a deep hydrological system is also compatible with fluid

inclusion, isotopic, and halogen studies conducted elsewhere in the Irish orefield (Boyce et al., 1983b; Samson and Russell, 1987; Banks and Russell, 1992; Everett et al., 1999a and b; Gleeson et al., 1999).

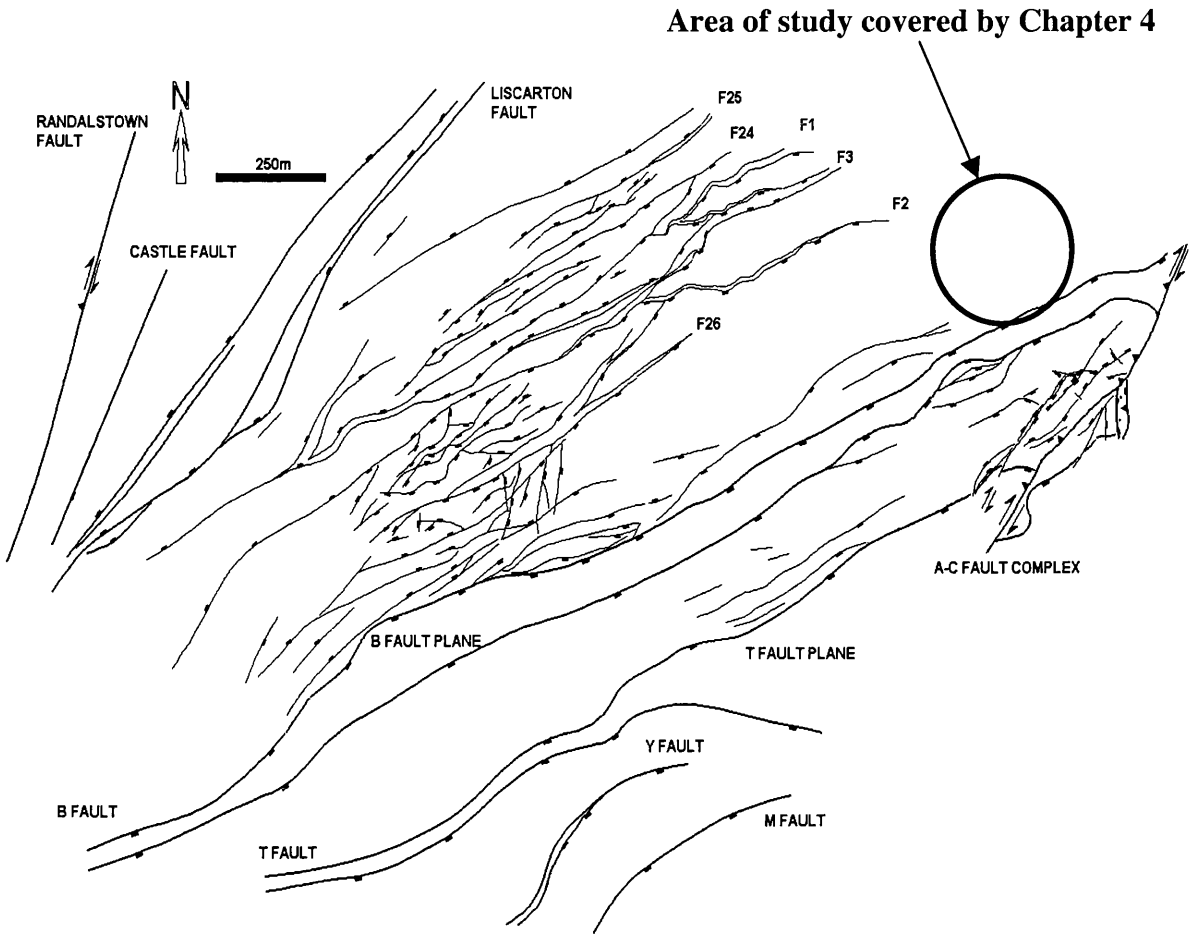


Figure 4-1 Structural plan of the Navan deposit showing the study area covered by Chapter 4. (See also Figs. 4-5 and 4-6).

5 Lens Data Only (Comprises ~70% of Known Ore Tonnage)

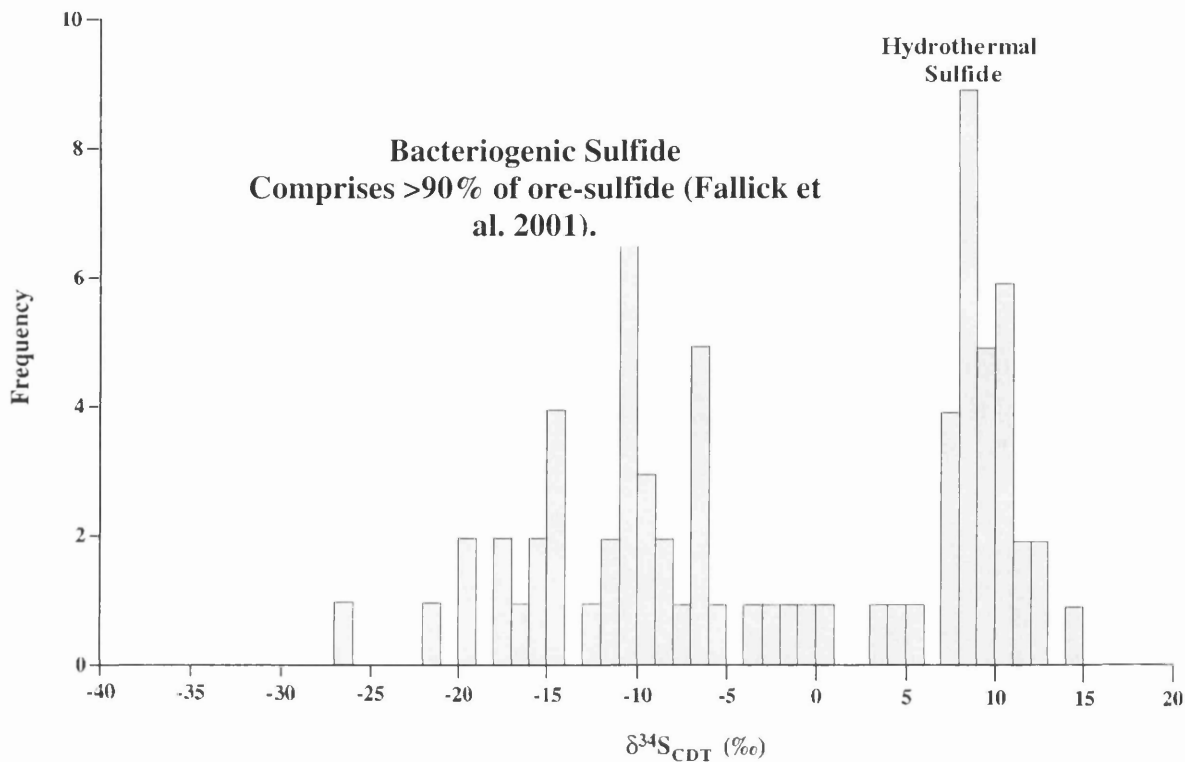


Figure 4-2 Histogram showing the known distribution of sulfur isotope results within 5 lens (extracted from Anderson, 1990).

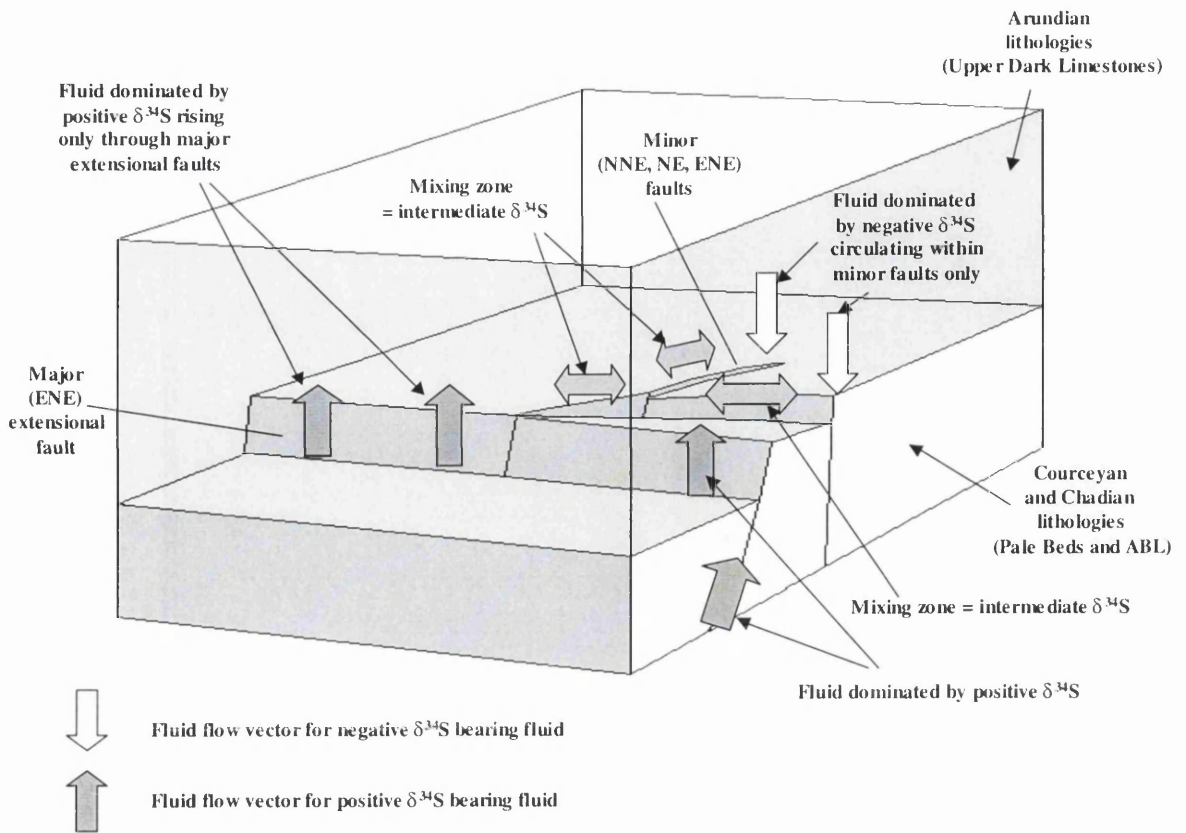


Figure 4-3 Cartoon model illustrating mineralisation supposedly post-dating the full development of the B and T Faults, i.e., these faults acted as the main conduits for the metal-bearing fluids (the MVT paleohydrological model).

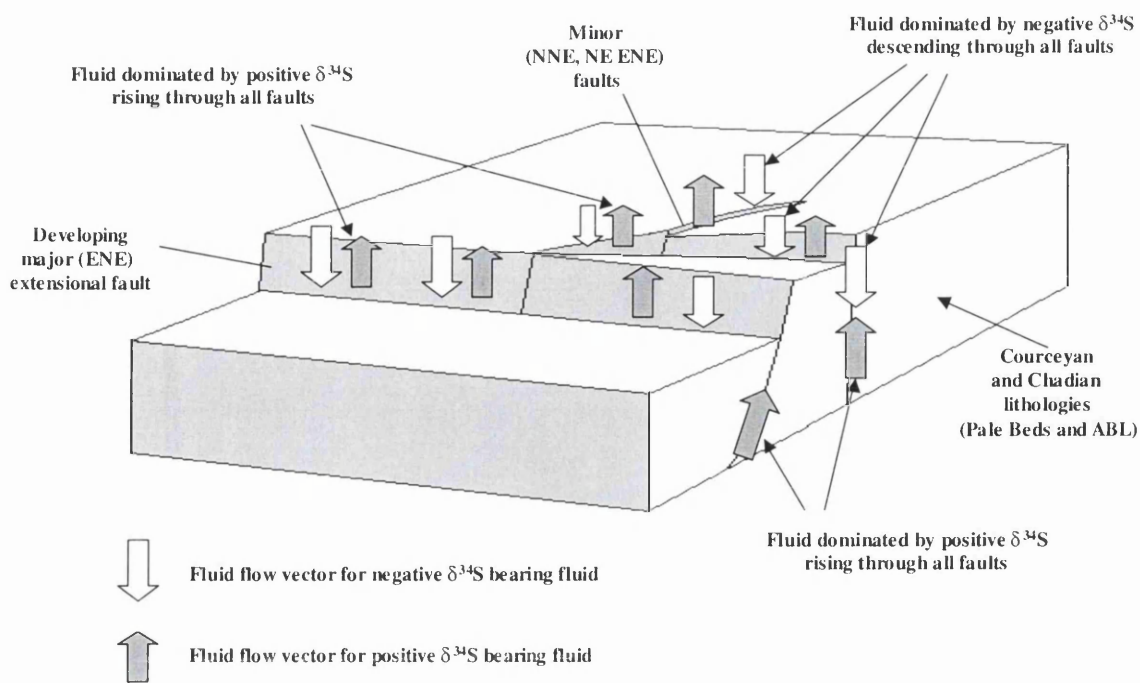


Figure 4-4 Cartoon model illustrating the occurrence of mineralisation during/after the development of the early steeply dipping minor NNE, NE and ENE normal fault sets, but in the main, prior to movements on the B and T Faults (Syn-depositional mesothermal or Irish Type model). The minor NNE, NE and ENE normal faults carry the bulk of the upwelling hot metal-bearing fluids but are also the loci for the downdrafts of bacteriogenic sulfide-bearing seawater-derived solutions. In the event, this model is favoured by the analyses presented here.

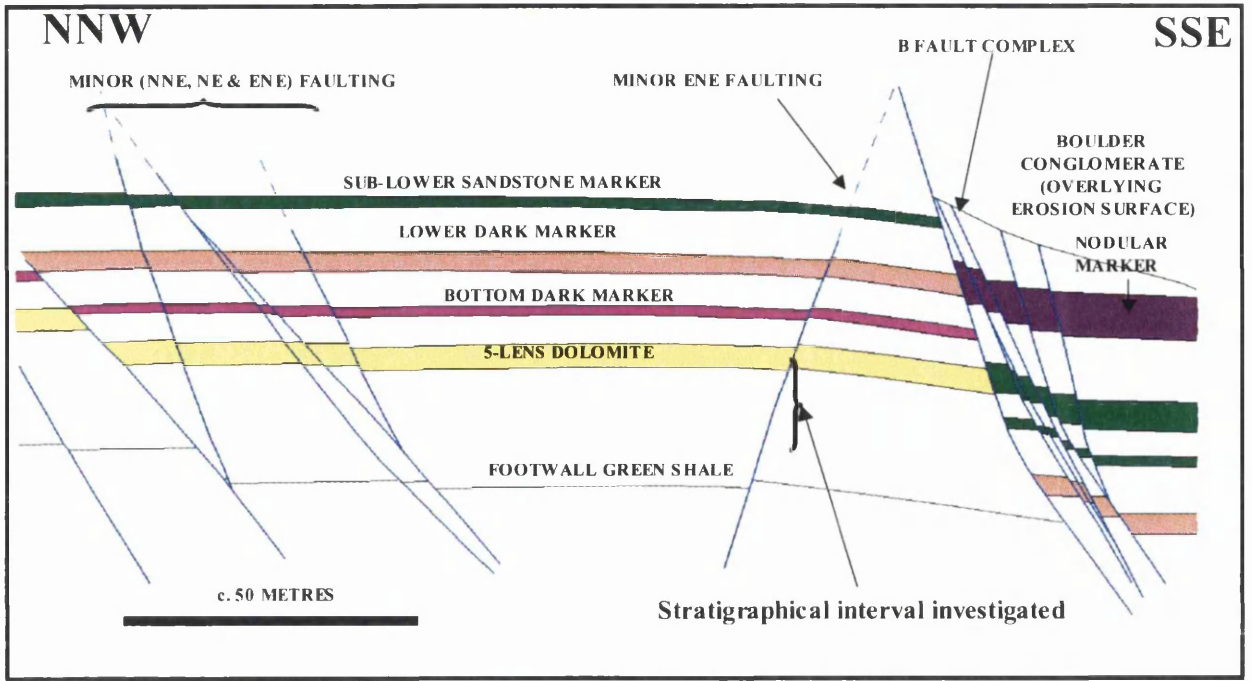


Figure 4-5 Stratigraphic cross-section of profile showing location of lithologies and structures discussed in text.

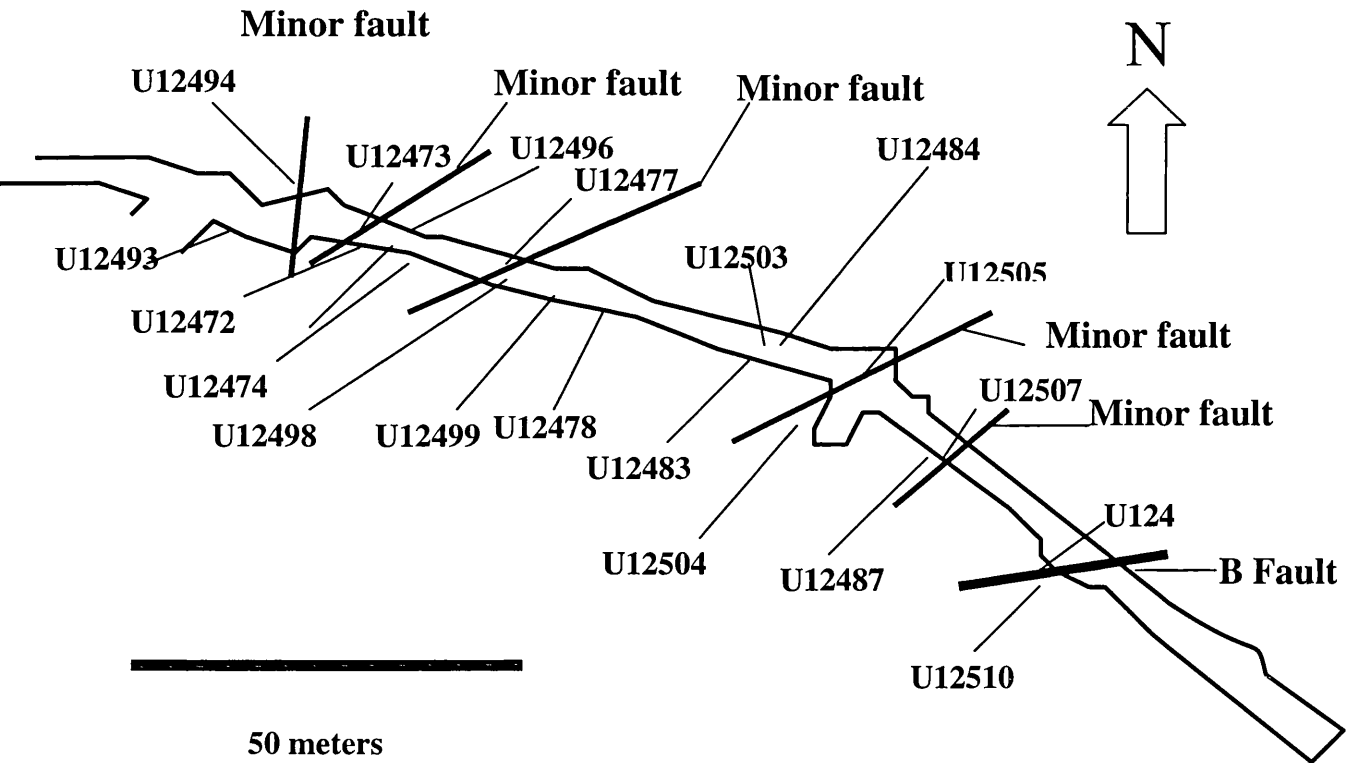


Figure 4-6 Plan of profile discussed in text (numbers refer to diamond drill hole samples).

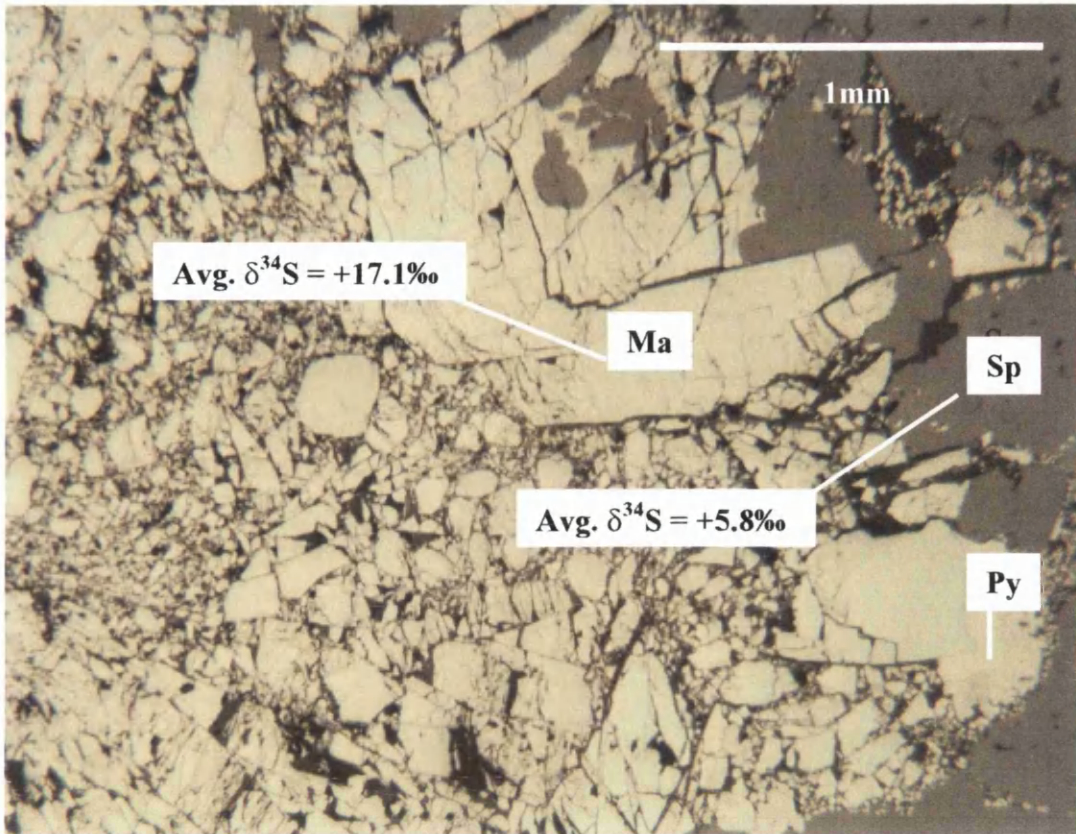


Figure 4-7 Photomicrograph of DDH U12477 located 0.5m into the footwall of a minor NE trending fault. Note comminuted early marcasite (Ma), collomorphic pyrite overgrowths (Py), and late course-grained sphalerite (Sp).

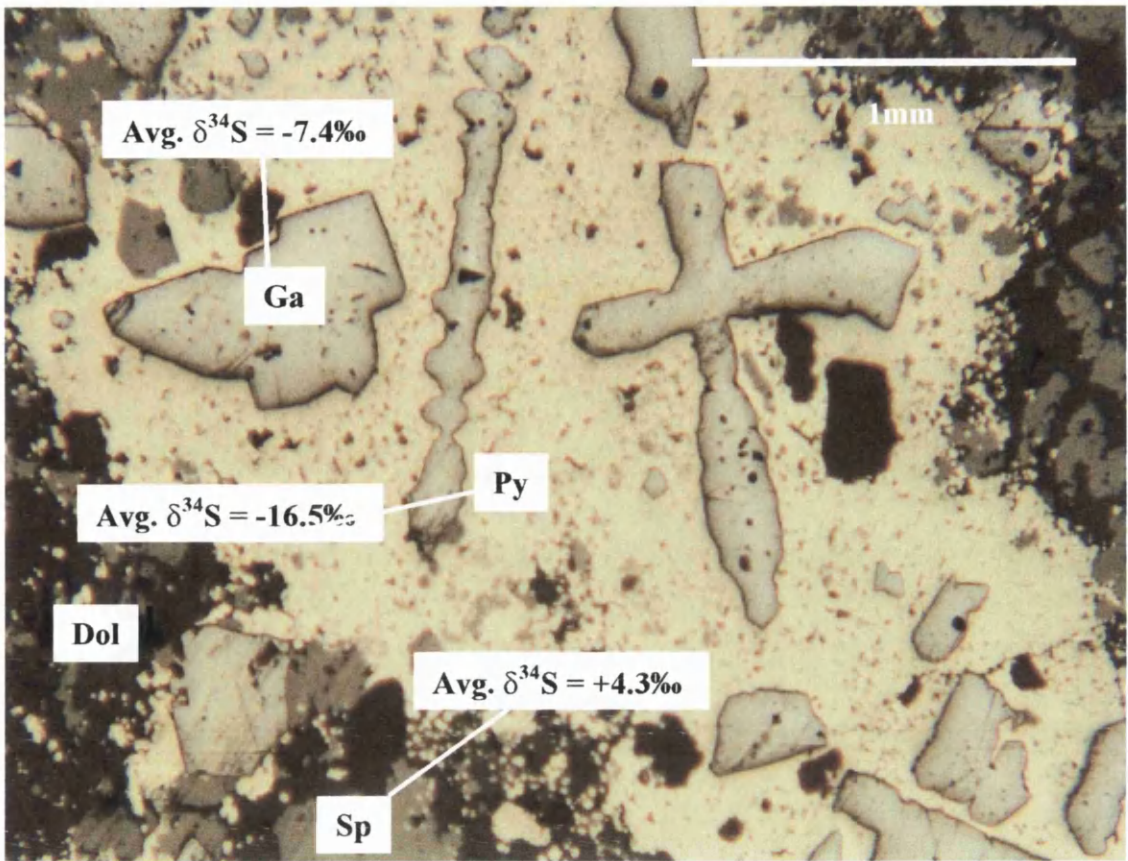


Figure 4-8 Photomicrograph of DDH U12473 located 1m into the footwall of a minor NE trending fault, showing highly resorbed (pseudo-dendritic) galena (Ga), later framboidal pyrite (Py), and finally course grained sphalerite (Sp), and dolomite (Dol).

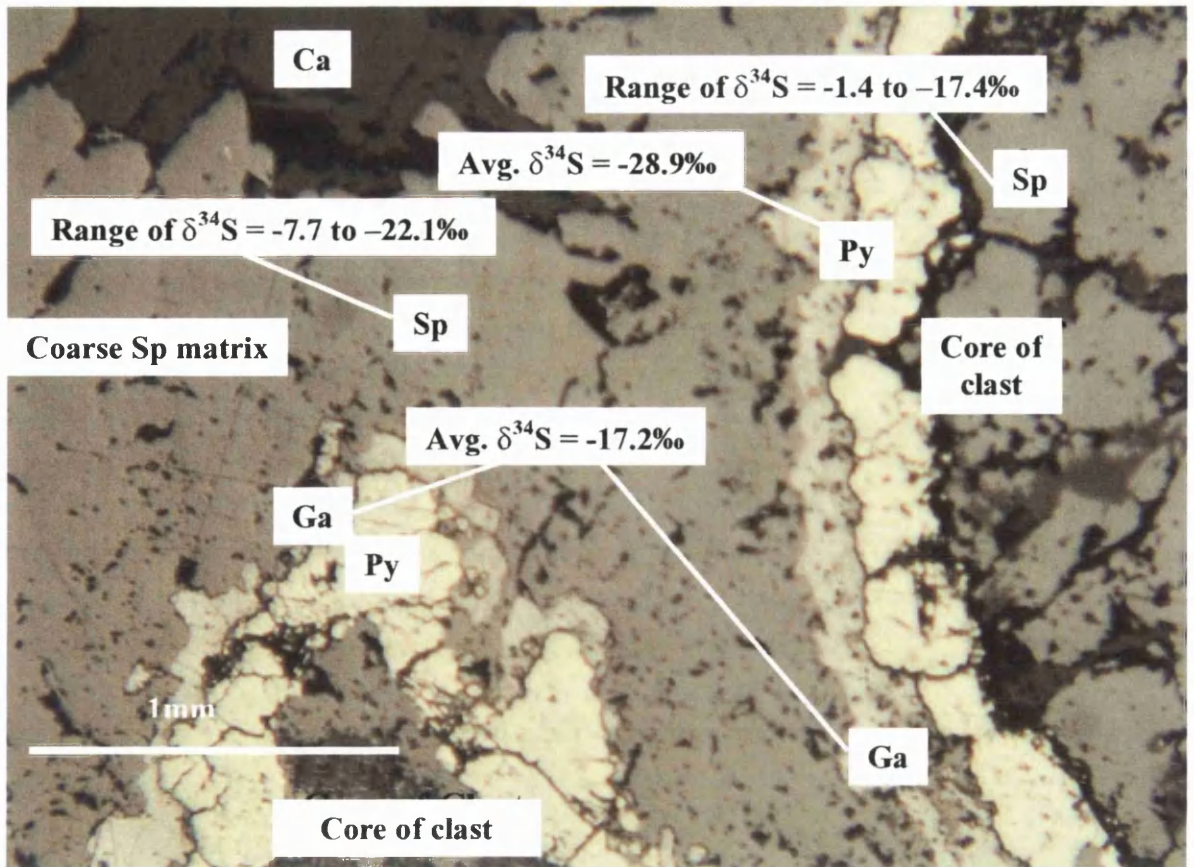


Figure 4-9 Photomicrograph of DDH U12472 located less than 1m into the hanging wall of a minor NE trending fault, showing clasts of comminuted sphalerite (Sp) (with minor pyrite and barite), overgrown by collomorphic pyrite (Py) and galena (Ga), and a subsequent infilling matrix of fine- to course-grained 'honeyblende' sphalerite (Sp). Ca is calcite.

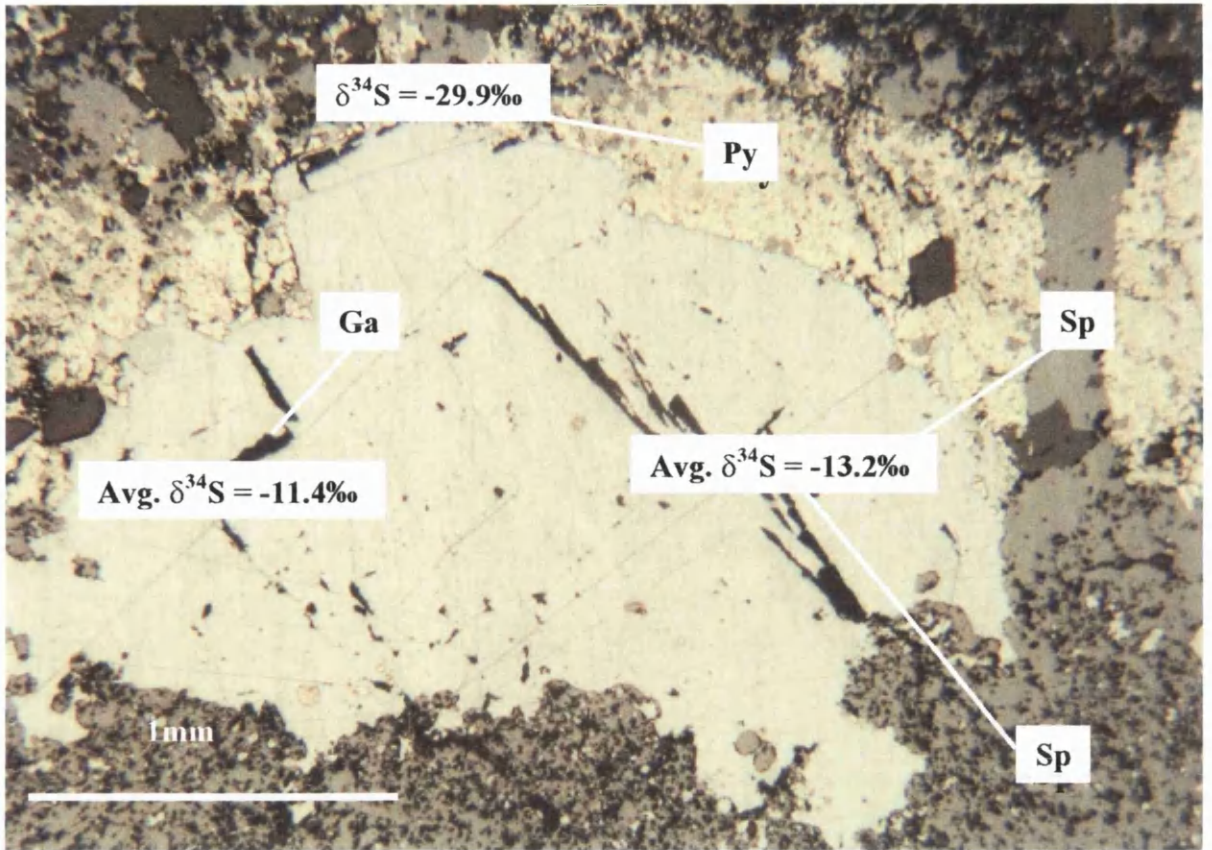


Figure 4-10 Photomicrograph of DDH U12493 located ~5m into the footwall of a minor NNE trending fault, showing early galena (Ga), later framboidal pyrite (Py), with fine- to coarse-grained cross-cutting sphalerite (Sp).

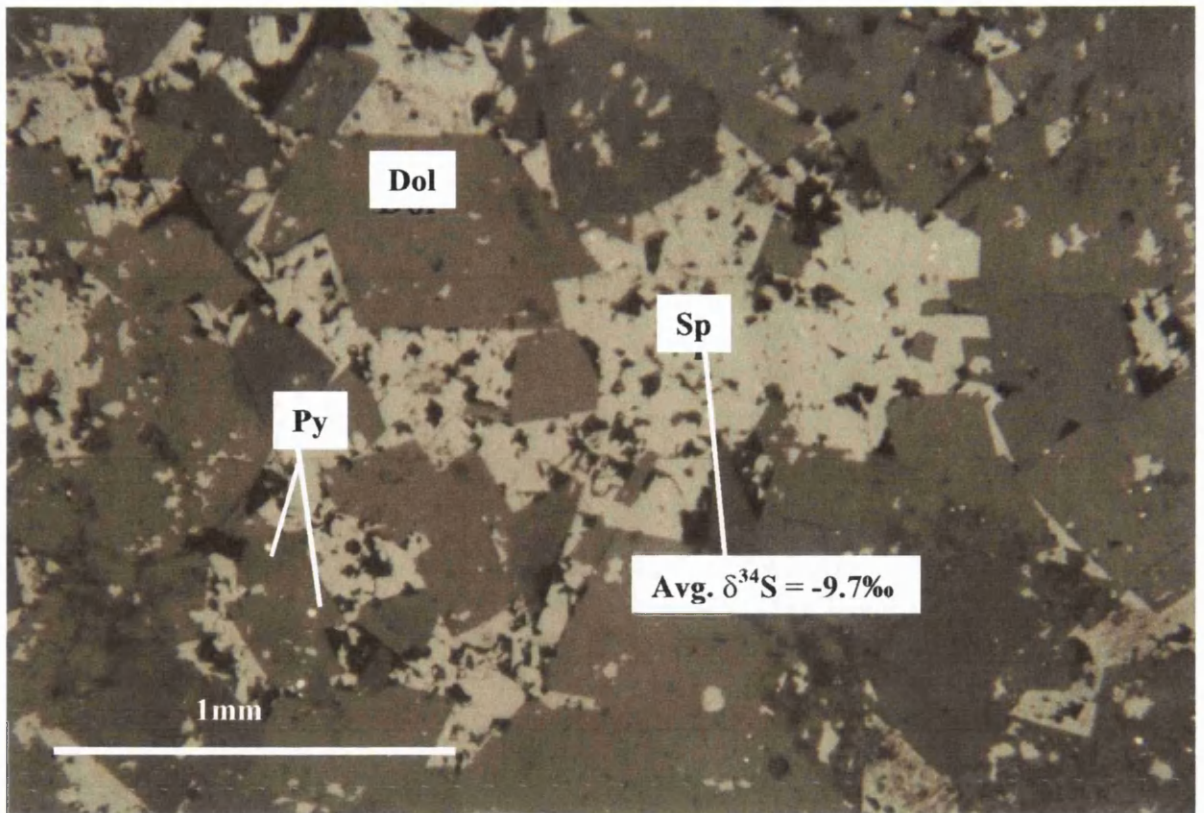


Figure 4-11 Photomicrograph of DDH U12478 located 15m away from any observed fault. Note intergrowths of fine-grained sphalerite (Sp) and dolomite (Dol).

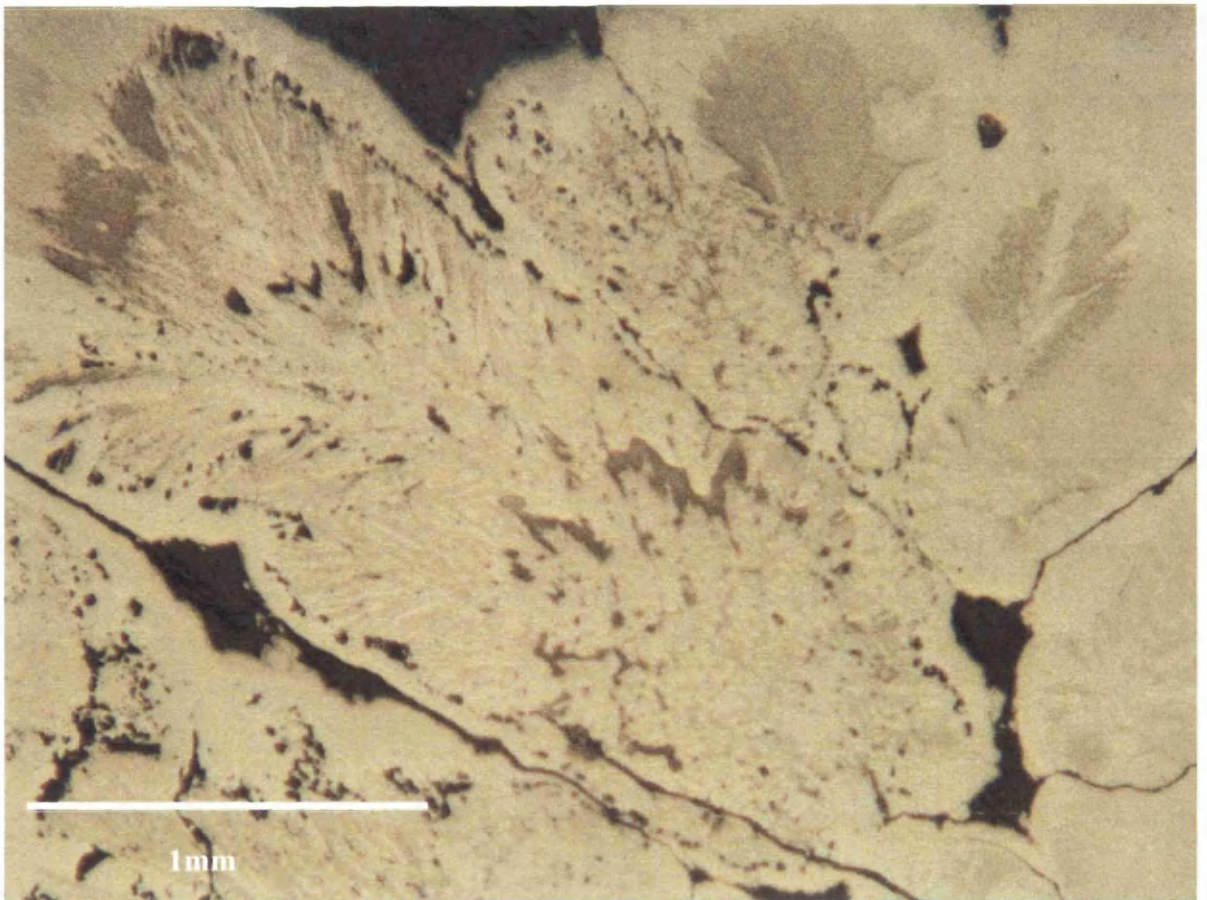


Figure 4-12 Photomicrograph of U14298 showing plumose-framboidal pyrite (average $\delta^{34}\text{S} = -33.5$ per mil.), from within 1m of a fault plane.

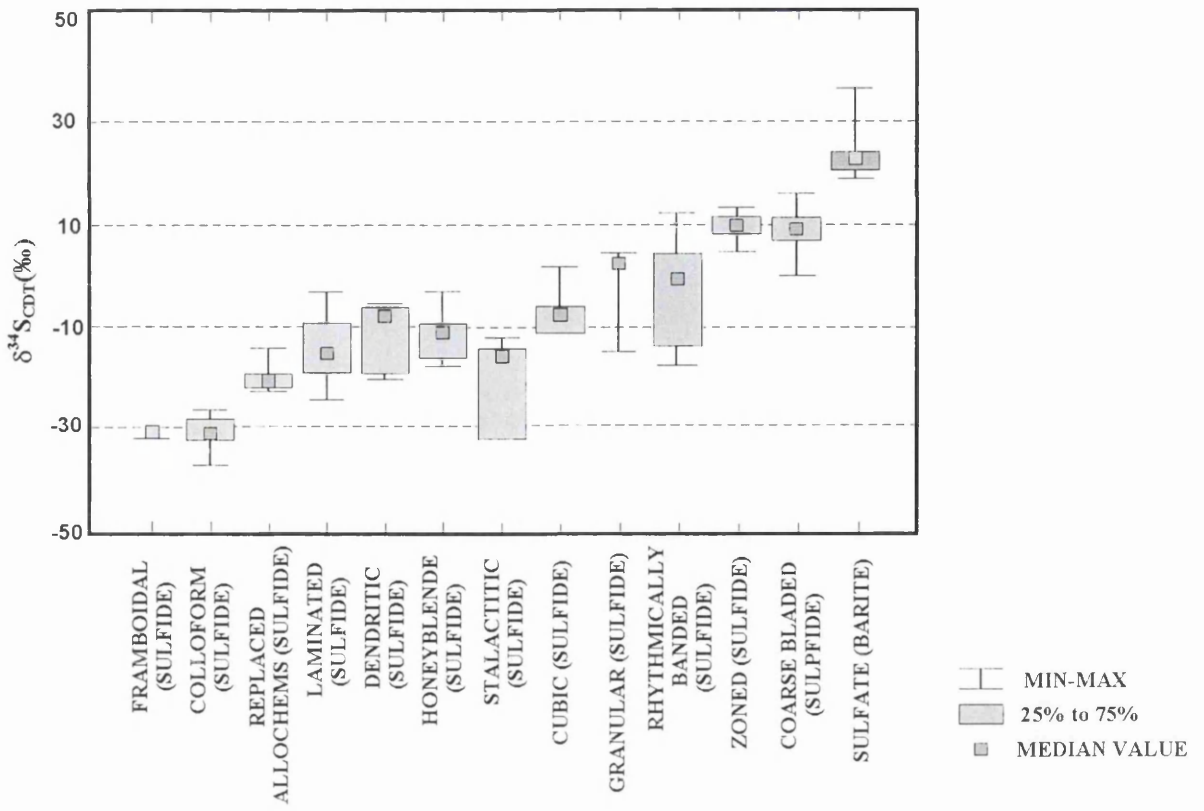


Figure 4-13 Summary of the ranges of sulfur isotope results from different minerals and textures (extracted from Anderson et al., 1998).

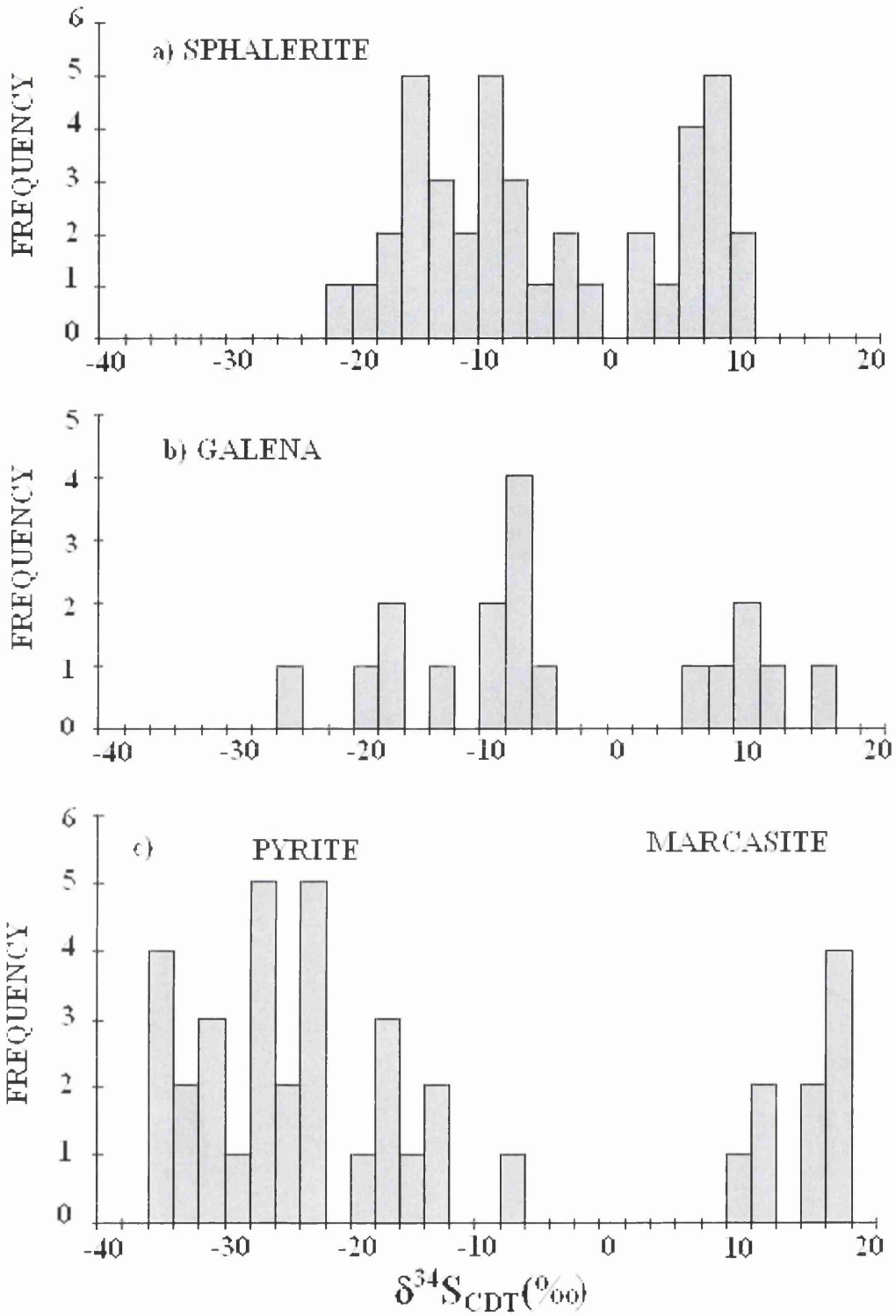


Figure 4-14 Frequency distribution of $\delta^{34}\text{S}$ values per sulfide phase revealed by this study. Compare with Fig. 4-2.

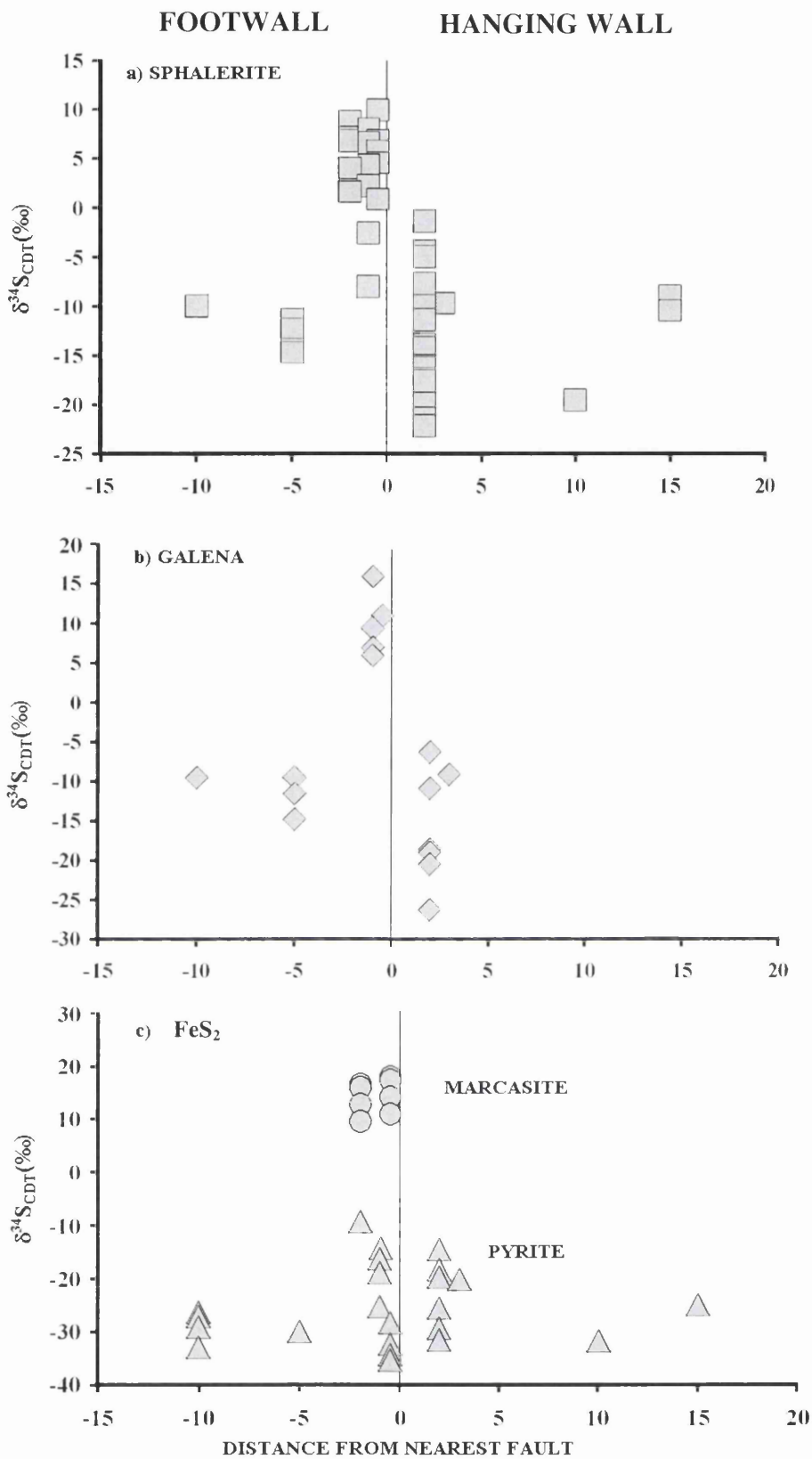


Figure 4-15 Diagrammatic summary of the distribution of $\delta^{34}\text{S}$ values (sphalerite, galena, marcasite and pyrite) with respect to the nearest fault, and whether the sample was located in either the footwall or the hanging wall.

5. A Genetic Model for the Navan Deposit.

5.1 Introduction.

This study has highlighted evidence that places the onset of metallogenesis at Navan early in the Lower Carboniferous. Mineralisation occurred during the phases of tectonic extension that would lead ultimately to the development of horst and graben topography within the North Dublin Basin by the late Chadian. Only the genetic model of Russell (1978 and 1986), developed for the whole Irish Base-Metal Orefield, can accommodate mineralisation at that time. Thus what follows fine-tunes the hypothesis of Russell (1978 and 1986) with particular reference to the Navan deposit.

The model developed here suggests that Irish Style Mineralisation is an integral part of developing extensional shallow marine carbonate marginal environments since the start of the Carboniferous; thereby potentially widening the theatre of exploration outside the bounds of the Irish Midlands. It describes, in temporal progression, the development of the conduits used by both the metal-bearing and the bacteriogenically reduced sulfide-bearing fluid. Chemical and physical observations are highlighted where appropriate.

5.2 Genetic model.

5.2.1 Onset of extension and marine transgression.

Early NNW-SSE extension within the Dublin Basin reactivated Caledonoid faults. Thus basement structure control led to an array of faults within the overlying Courceyan rocks which trend slightly west of north to north-east. This fault complex is bounded by the Randlestown and the D (Slane/Boundary) Faults. These larger, bounding faults accommodated the major proportion of lateral movement at this time.

The northward marine transgression during the early Courceyan coincided with basement-controlled faulting. The seawater was highly saline, a result of evaporation within a sabkha located in the Navan area. Thus early Carboniferous seawater gained access to the basement through active, near vertical faults (Fig. 5-1). The formation waters occupying fractures within the Lower Palaeozoic rocks were thereby, continually recharged as in the Russell model (Russell, 1968; Russell 1978). The extension-related fracturing allowed the initiation of an open hydrothermal convective system. The major conduits for the down flowing dense seawater were the larger Caledonide faults (Fig. 5-1). Of all the faults in the Navan area it was only those of Caledonian age that were in existence at the onset of the marine transgression. Yet these major structures were not utilised in accommodating the rising solutions. We know this because the zinc and lead grades fall off dramatically as these structures are approached. This seeming contradiction may hold the clue to the siting of the convective updraft. Recall that

the Navan orebody is a by-product of the dissipation of thermal energy by mass transfer. In general natural (as opposed to forced) open convective structures are organised from the surface rather than the base (e.g. Pearson, 1958; Anderson, 2001). As the surface tension of aqueous fluids at 200°C is nearly an order of magnitude less than cold waters, it follows that the former are able to exploit lower permeabilities. Thus gravitation to depth of a dense brine of surface derivation was facilitated by existing fractures and the momentum of flow was maintained by an increase in permeability consequent to extensional tectonics. The now heated water, still pressurised from above, could migrate, less hindered by viscosity, into less fractured basement, and rise buoyantly to the surface in “less obvious” structures (Fig. 5-2). Thus, the two corridors of relatively unmineralised ground that follow the trace of both the Randlestown and D faults can be explained.

5.2.2 Continued extension and development of the ‘Dolomite Plume’.

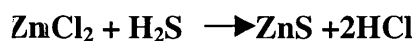
Continued extension within the Dublin Basin resulted in the earlier faults within the early to mid Lower Carboniferous lithologies being obliquely aligned to the principal axes of extension (NNW-SSE). They were therefore incapable of accommodating the movement required. Thus a major ENE trending fault system developed to accommodate this phase of extension. This fault system was open to both early Lower Carboniferous seawater from above and fractures within the basement acting as conduits for the upwelling metal-bearing fluid.

It may also be predicted from this scenario that the majority of dolomites at Navan prove to be of marine origin and not hydrothermal as postulated by Braithwaite and Rizzi (1996) and supposed by Peace (2000). After all, empirical analyses of submarine springs (e.g. Von Damm, 1990) as well as the specific rock water studies of Bischoff et al. (1981), show concentrations of magnesium in hydrothermal solutions to be vanishingly small. Downward flowing marine waters would have passed through the Lower Carboniferous sediments both prior to entering the basement or replacing the original interstitial fluids, giving an opportunity to precipitate dolomite within the carbonate succession (Figs. 5-2 and 5-3). Supporting this hypothesis is the data of Rizzi (1993). Analyses of carbonate isotopic compositions ($\delta^{18}\text{O} = -6.6\text{‰}$ to -10.4‰ and $\delta^{13}\text{C} = -0.2\text{‰}$ to $+2.5\text{‰}$) within dolomites at Navan are indicative of a depositional fluid similar in composition to that of Carboniferous seawater (Braithwaite and Rizzi, 1997).

5.2.3 Updraughts established within the developing horst and the mixing of fluids.

Convective circulation resulted in thermal up-draughts located away from the larger faults, within the developing horst blocks. As the horst blocks matured further, the regional faults, i.e. Randallstown and D, remained within graben structures. With basin geometries thus, the overlying cold dense water column was capable of overpowering any initially weak thermal updraughts. Metal-bearing fluids were thus focused into the host lithologies along relatively minor extensional faults active from the very outset of extension. The relationship between this generation of faulting and the metal-bearing fluid is highlighted by

this study. Metal-bearing fluids, having precipitated some metals along with all of the available sulfide, rapidly attained a more acidic, and therefore corrosive, character – notionally:



An acidic metal-bearing fluid now existed that was highly efficient at corroding further fluid pathways horizontally through the more reactive members of the carbonate host. As this fluid progressed it utilised the existing porosity to access dissolved bacteriogenically reduced seawater sulfate present within the residual pore waters. Thus permeability was enhanced by the corrosive nature of the metal-bearing fluid allowing further volumes of metal-bearing fluid to enter the system.

By now extensive mineralisation within the Pale Beds hosts of the Navan deposit was ongoing, fed by the regionally minor fault arrays (Figs. 5-2 and 5-3). This was achieved on a deposit scale by two distinct, but interacting processes (Fig. 5-4).

i) Down flow of bacteriogenic sulfide enriched seawater within the minor fault arrays that had penetrated within at least tens of metres of the seafloor. Thereby allowing access to fluids enriched in sulfide produced by an extensive surficial sulfuretum to mix with the metal-bearing fluid.

ii) Replacement of reactive sequences within the host rocks (e.g. 5 Lens Micrites) that already contained interstitial waters enriched in bacteriogenically reduced

sulfide. This extensive replacement of the host took place by repeated pulses of acidic metal-bearing fluid corroding the more reactive hosts and releasing bacteriogenic sulfide to form metal sulfides.

Anderson et al., (1998) and Fallick et al., (2001) in particular, have pointed to the importance of the presence of bacteriogenic sulfide at Navan. Further to their findings this Thesis presents data in concert with that of Anderson (1990) and Anderson et al. (1998) demonstrating that individual sulfide phases are associated with a specific $\delta^{34}\text{S}$ signature. For example mean values of $\delta^{34}\text{S}_{(\text{ZnS})} = -12.7$ per mil and $\delta^{34}\text{S}_{(\text{PbS})} = -13.9$ per mil have been reported by Fallick et al. (2001). These values are considerably higher than the values reported for $\delta^{34}\text{S}_{(\text{pyrite})}$ of ~ -30 per mil (Anderson 1990 and this study). Any remote, or historic, sulferetum could only produce a homogenous $\delta^{34}\text{S}$ signature across the respective sulfide phases. Fractionation of ^{34}S therefore, must have been ongoing during metal sulfide deposition involving an active sulferetum predominantly located in the surficial environment at, and immediately above the developing orebody. Further understanding of this process is achieved by a comparing the Navan deposit with the Tatestown/Scallenstown satellite (Andrew and Proustie, 1986) to the north-west. At Tatestown/Scallenstown (3.6mt) $\delta^{34}\text{S}$ values between -4 and $+13$ per mil dominate the ZnS and PbS phases (Caulfield et al., 1986). However, $\delta^{34}\text{S}_{(\text{pyrite})}$ values are centred around -20 per mil (Caulfield et al., 1986) indicating that bacteriogenic processes must have ongoing during mineralisation. The epigenetic Tatestown/Scallenstown satellite (Andrew and Proustie, 1986), is hosted exclusively by 5 Lens equivalent lithologies. It follows that either a buried sulferetum was operating or reactivated at the time of metallogenesis, or that

downdrafts of seawater enriched in sulfate reducing bacteria were capable of mixing with the metal-bearing fluid within the ore-depositional horizons themselves. A similar situation would have pertained at Navan, and this process would account for the very low values found in 5 Lens pyrites away from the feeder conduits. This process is further supported by the occurrence of barite throughout the Navan deposit (including 5 Lens), with a $\delta^{34}\text{S}$ signature of $\sim+20$ per mil (Anderson, 1990; Anderson et al., 1998). This strongly suggests that Lower Carboniferous seawater had access to the ore-bearing horizons at the time of mineralisation (Figs. 5-4 and 5-5).

5.2.4 Full extension and the role of the Boulder Conglomerate as a host.

The later stages of extension resulted in gravitational instability and catastrophic footwall collapse affected the larger structures. Erosive debris flows dissected the flanks of the horst block eroding and redistributing previously mineralised Pale Beds.

By the time full development of the major listric, extensional faults had occurred sequences of predominantly argillaceous material were being deposited within the grabens (the Tober Colleen Mudstone of McConnell et al., 2001) (Fig. 5-6). This combination of reduced seismic activity and deposition of mudstone ultimately resulted in the damming of the down-draught zones thereby starving the hydrothermal cell of fresh fluids. Meanwhile waning updraughts continued within the horst centred fault zones, leading to replacive mineralisation of the Boulder

Conglomerate (Conglomerate Group Ore) and in places possible exhalation on to the sea floor (Figs. 5-7 to 5-10, and 5-12 to 5-14).

5.2.5 A change of environment and the waning of mineralising activity.

The Upper Dark Limestones represent an environment dominated by turbidite deposition. Erosive turbidites ultimately led to the destruction of the environment supporting the surficial sulfidation thereby denying any remaining rising metal-bearing fluid access to a ready sulfide reservoir. Thereby, the replenishment of sulphate-reducing bacteria to the ore-depositional horizons was ended. The toxic metal bearing fluid eventually poisoned any surviving sulfidation at depth.

Thus an environment now pertained that was not conducive to Irish Style mineralisation. The source of the metal-bearing fluid (Lower Carboniferous seawater) was denied access to the basement, and the predominant source of the sulfide required to permit precipitation of the metals was removed. It is not envisaged that this was a sudden process as minor iron-rich bedding-parallel pyritic mineralisation pertains within the lower-most parts of the Thinly Bedded Unit (Fig. 5-11).

5.2.6 Summary

The above model accounts for why the Navan deposit formed where and when it did. The source of the metal-bearing fluid and the pathways taken to access the Lower Palaeozoic basement were available from the very outset of extension during the lower Courceyan. Developing stable horst blocks fractured by regionally minor extensional faulting allowed rising metal-bearing fluids to access the reactive hosts of the Navan deposit and precipitate metals as they mixed with a locally produced bacteriogenic sulfide-bearing fluid. The bacteriogenic sulfide was produced by a sulfuretum that was intimate, and partly fed by, the mineralising process, at times utilising metals (especially iron) from the metal-bearing fluid to achieve greater fractionations during periods of low metal-bearing fluid ingress.

This situation pertained until the end of the Chadian/early Arundian when accelerated extension within the Dublin Basin led to the collapse and erosion of the horst margins. A predominance of mudstone deposition coupled with the end of extension resulted in the ultimate choking of the downdraft zones, followed by the development of an erosive turbidite environment that eventually removed the sulfide-producing factory. A period therefore, of roughly 10 million years (from the start of the Courceyan to the end of the Chadian/early Arundian) accommodated the complete mineralising process.

An intimacy of the mineralising process with extensional tectonism and (in Ireland) carbonate margins is inferred. An added essential factor is the presence of a co-existing sulfuretum (Fallick et al., 2001) to produce the large volume of sulfide required (at Navan, around 5 million tonnes of sulfur). Therefore, it follows that any exploration model for Irish Style mineralisation must take into

account the factors that control the development and distribution of large, highly active sulfureta as well as areas of suitable structural geometries, within hosts of early Lower Carboniferous age.

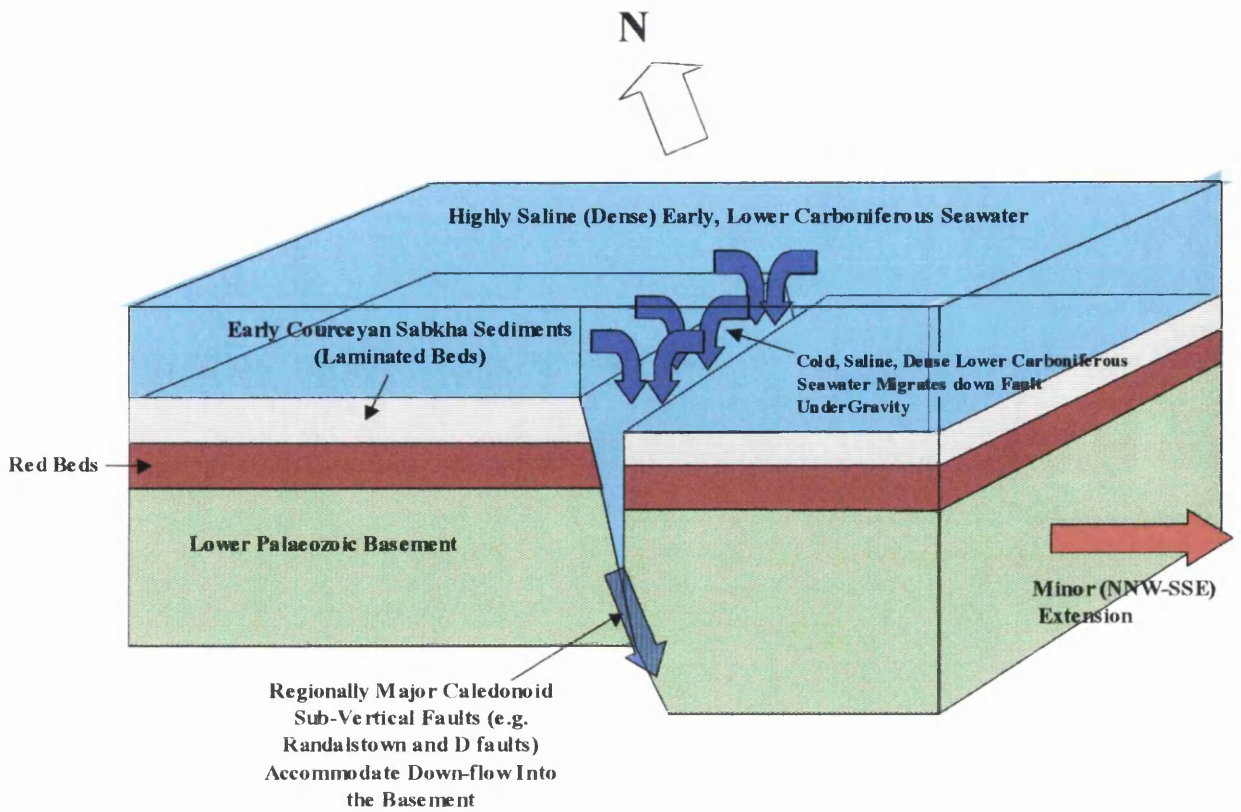


Figure 5-1 Schematic diagram illustrating the conditions pertaining during the lowermost Courceyan. Cold, dense, highly saline Lower Carboniferous seawater gains access to the Lower Palaeozoic basement via regionally major Caledonoid faults in and around the Navan area that are under extension.

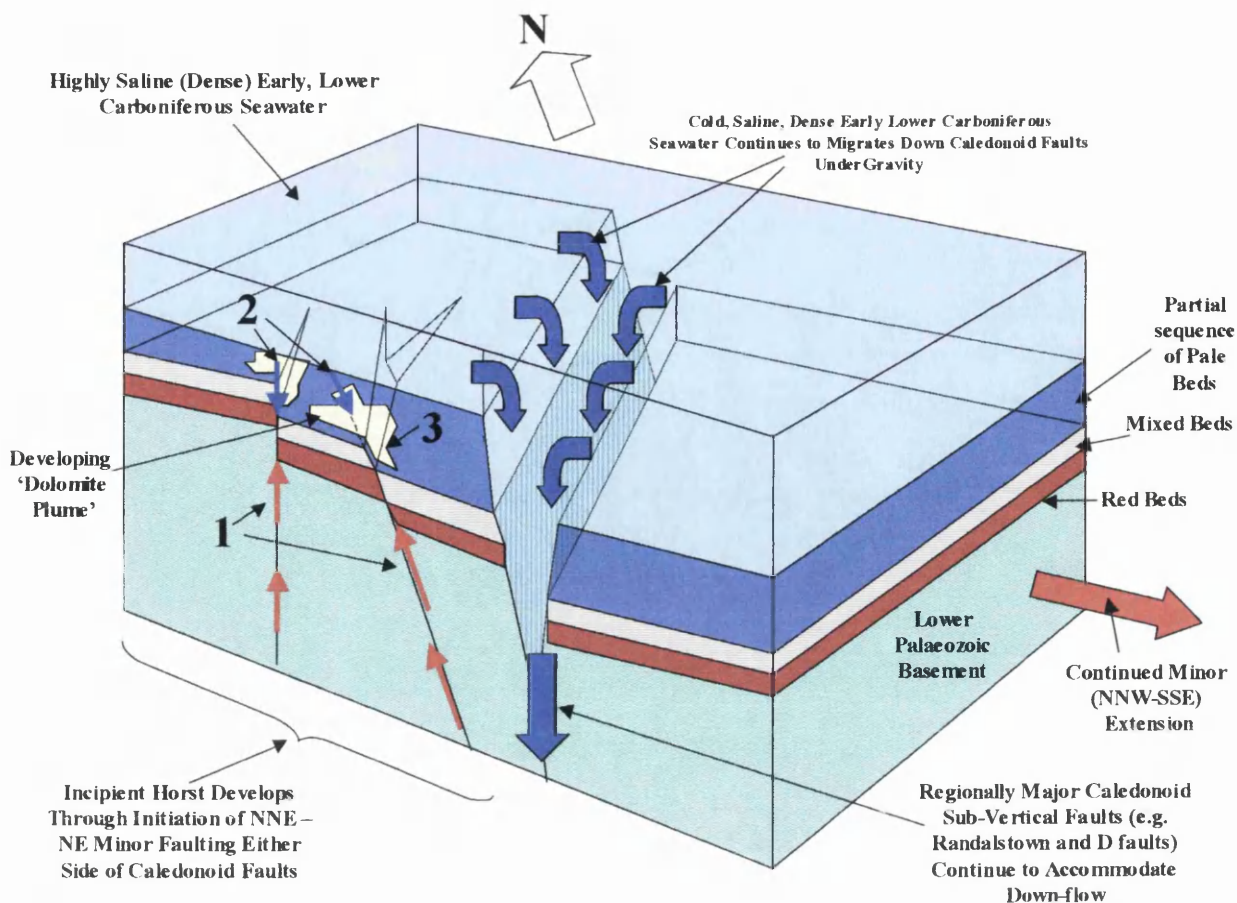


Figure 5-2 Schematic diagram showing continued NNW-SSE extension leading to development of incipient horsts with minor NNE-NE faulting (Note that the regionally major Caledonoid faults remain within the developing grabens). (Mid-Courceyan).

1 = Initially weak pulses of hot (buoyant), metal-bearing solutions are concentrated into the developing horsts along the NNE-NE fault arrays.

2 = Down-flowing cold seawater (enriched in bacteriogenic H_2S and sulfate reducing bacteria) circulates within the same structures, leading to the precipitation of dolomite, and ultimately mixing with the metal-bearing fluid to precipitate metal sulfides.

3 = Developing 'Dolomite Plume' precipitated from down-flowing Lower Carboniferous seawater (see Braithwaite and Rizzi, 1997), (also enriched in bacteriogenic H_2S and sulfate reducing bacteria). Vasconcelas et al., (1995) and Vasconcelas and McKenzie, (2000) report the intimacy of sulfate-reducing bacteria with dolomite producing systems.

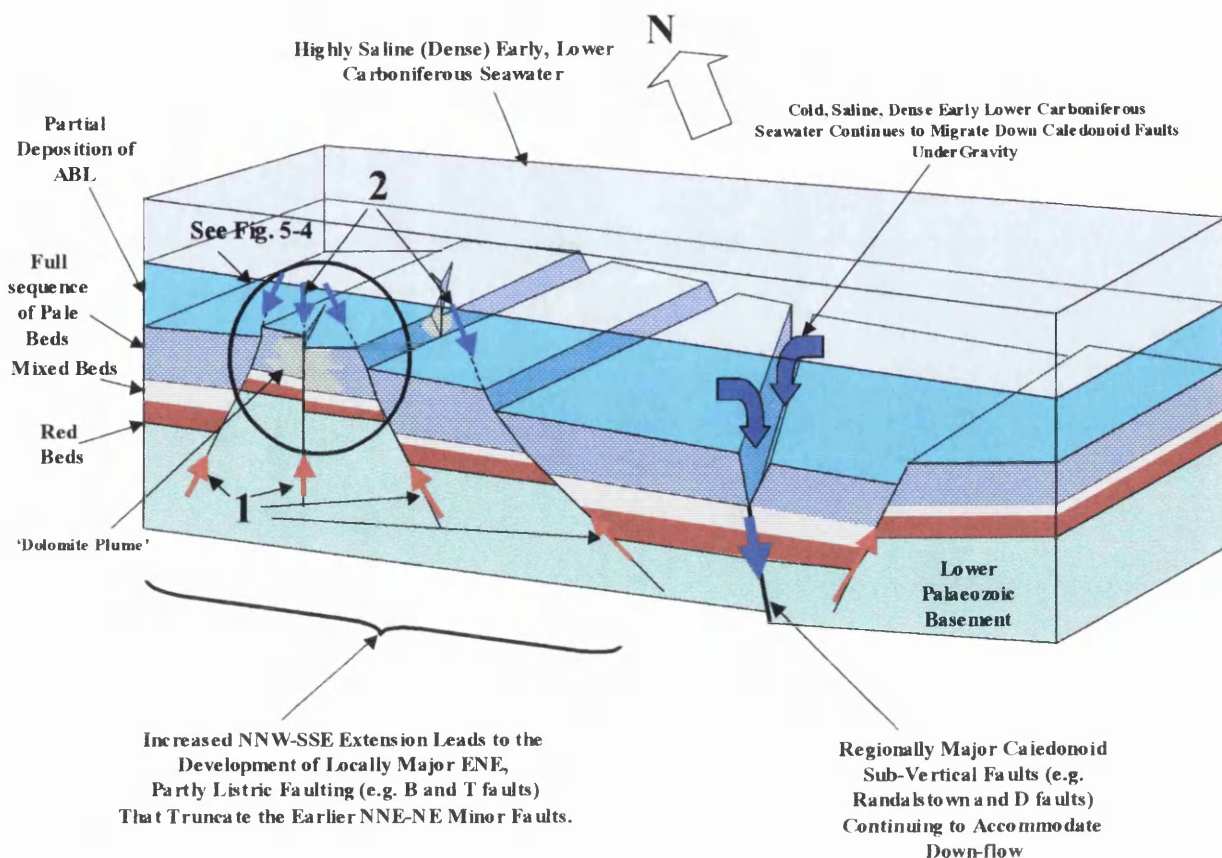


Figure 5-3 Schematic diagram illustrating the development of locally major ENE trending partly listric faults that truncate the earlier NNE-NE faulting within the horsts. (Late Courceyan – Early Chadian). ABL = Argillaceous Bioclastic Limestone.

1 = Rising, hot (buoyant), metal-bearing solutions continue to be concentrated into the developing horsts along the more minor fault arrays, as well as the now developing ENE partly listric faults where those faults intersect basement structures at depth.

2 = Down-flowing cold seawater (enriched in bacteriogenic H_2S and sulfate reducing bacteria) continues to circulate within the minor NNE-NE faults and now also the partly listric ENE faults, ultimately mixing with the metal-bearing fluid to precipitate metal sulfides. Precipitation of dolomite continues.

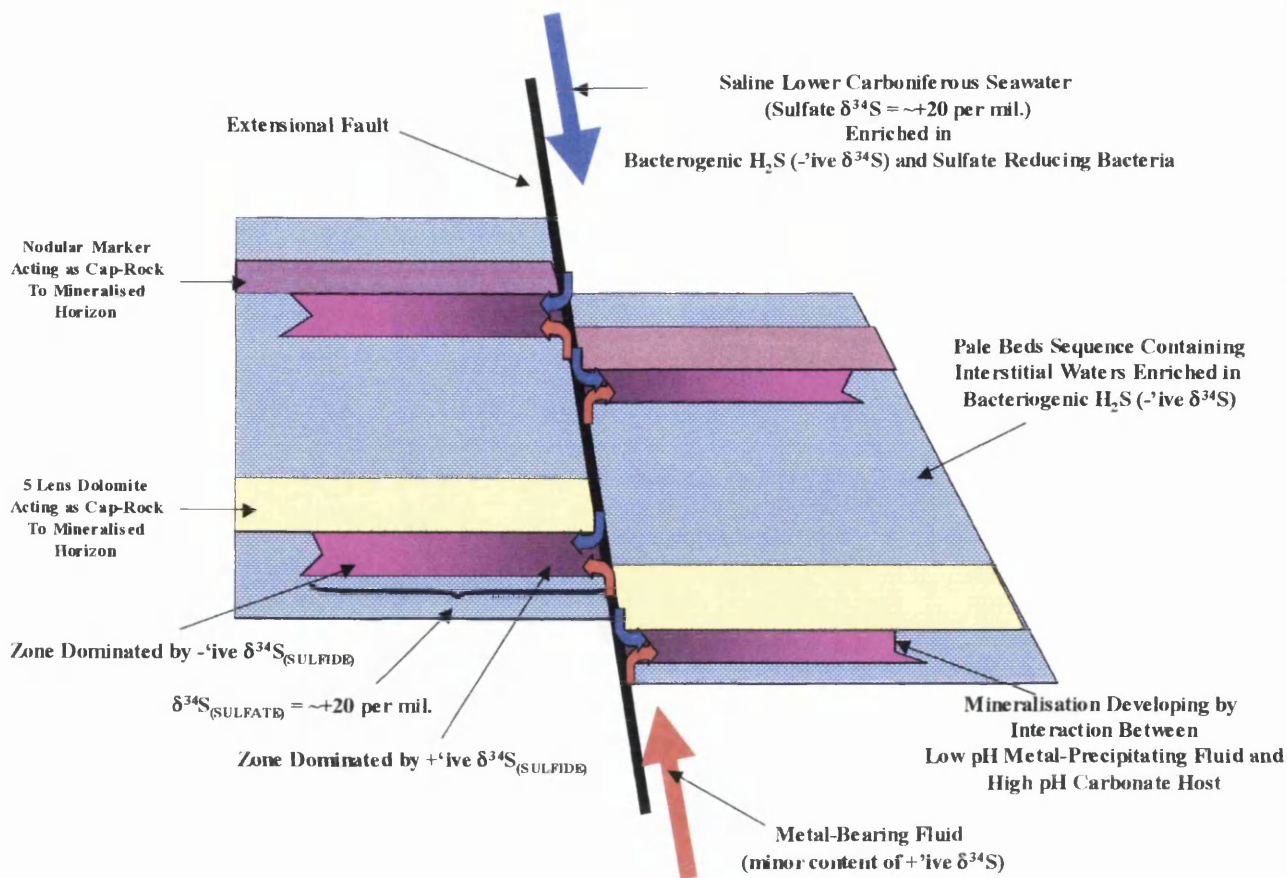


Figure 5-4 Schematic diagram demonstrating the details of metal-sulfide and sulfate precipitation.

Active faulting during mineralisation (see Chapters 2 and 4) allows pulses of buoyant, metal-bearing fluid to enter the feeder fault arrays, and mix with the supernatant brine enriched in bacteriogenic H_2S , and sulfate reducing bacteria (see Chapter 4). Metal precipitation is concentrated beneath dolomitised or more argillaceous members within the Pale Beds sequence (as per Anderson, 1990; Anderson et al., 1998). Interstitial waters (enriched in bacteriogenic H_2S), within the Pale Beds are released to the developing system by the interaction of acidic metal-precipitating fluids and the carbonate-rich host. Thus metal-sulfides proximal to the feeder faults are dominated by positive $\delta^{34}S$ values (metal-bearing fluid signature), while more distal mineralisation acquires the negative signatures associated with bacteriogenic sulfide (see Chapter 4). Metal-sulfates (dominated by barite – see Fig 5-5) retain the $\delta^{34}S$ value of Lower Carboniferous seawater ($\sim +20 \delta^{34}S$ per mil.) throughout.



Figure 5-5 Exposure of barite mineralisation in 5 Lens (white lathes), ($\delta^{34}\text{S} = \sim +20$ per mil., Anderson, 1990; Anderson et al., 1998), surrounded by massive sphalerite mineralisation. (Locality = 1075 2636F). Width of view = 1 metre.

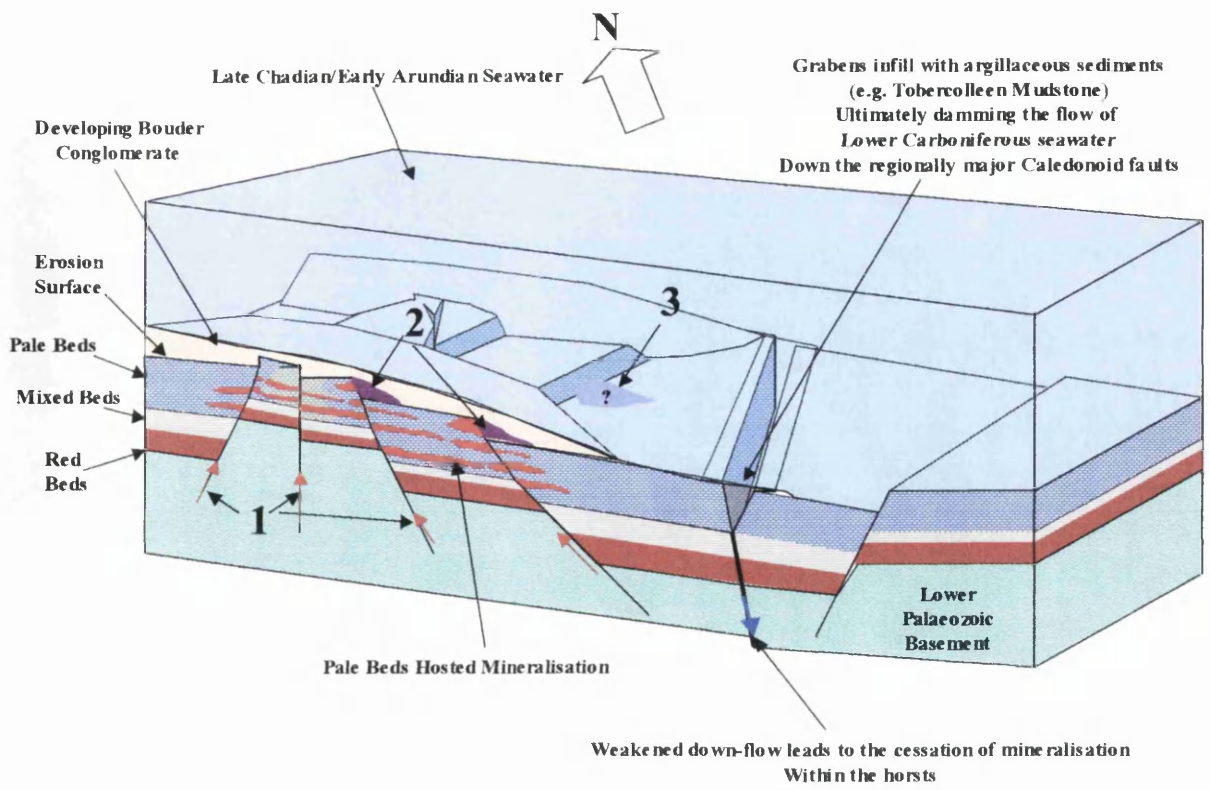


Figure 5-6 The development of the Boulder Conglomerate (late Chadian) above the Erosion Surface. Deposition of argillaceous units (e.g. the Tobercolleen Mudstone) within the grabens ultimately dams the downdraught part of the convection cell, leading in turn to the ultimate cessation of mineralising activity in the horsts.

1 = Much reduced flow of metal-bearing solutions from depth as the feed waters to the Cell are gradually diminished.

2 = Developments of minor replacive mineralisation (pyrite-rich), within the Boulder Conglomerate (Conglomerate Group Ore), (Ford, 1996), proximal to feeder faults.

3 = Possible development of exhalites (pyrite-rich) on the late Chadian/early Arundian sea-floor (See Figs. 5-7 to 5-10, and 5-12 to 5-14).

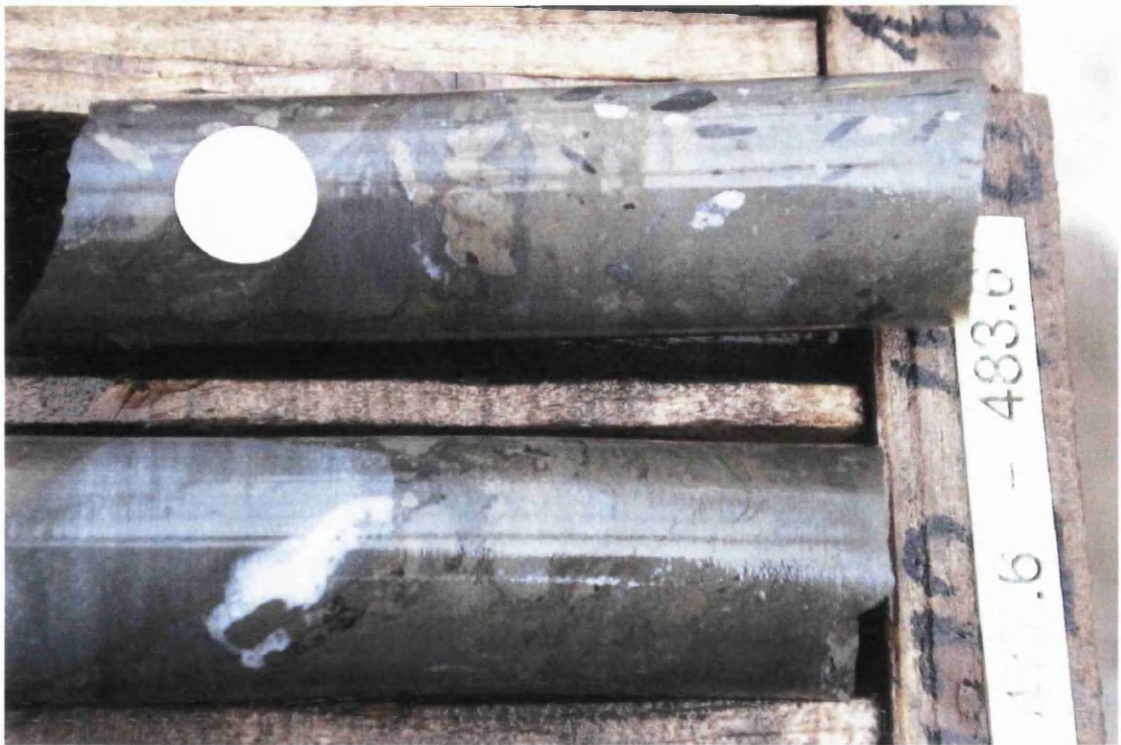


Figure 5-7 Surficial depositional processes of sulfides within the Conglomerate Group Ore? Pyrite rich debris flow within the Conglomerate Group Ore. Note the inclusion of carbonate and shale rip-up clasts. Ten pence coin for scale (N01604 @ 482.1m)



Figure 5-8 Exhalative processes? Shale-sulfide-carbonate rhythmites (N010627 @ 430 metres). Two pence coin for scale.



Figure 5-9 Exhalative processes? Close-up of Shale-Sulfide-carbonate rhythmites (N01062 @ 428 metres) Two pence coin for scale.



Figure 5-10 Exhalative processes? Flaser-bedded pyrite-shales within the Conglomerate Group Ore (N01627 @ 415 metres). Two pence coin for scale.

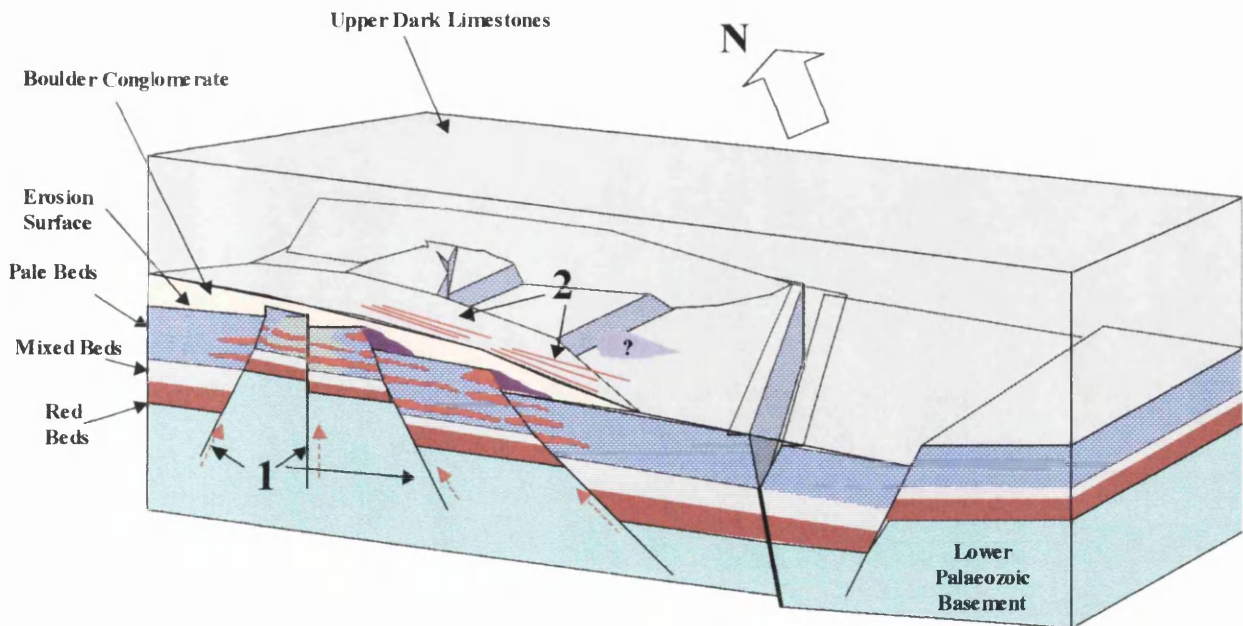


Figure 5-11 Early Arundian times. The deposition of the basal unit of the Upper Dark Limestones (Thinly Bedded Unit) buries the horst and graben topography of the late Chadian, thereby finally sealing off local feeders to the convective cell. However, more distal regionally major Caledonoid structures may continue to feed the system before they too are blocked.

1 = Much reduced upward flow of metal-bearing fluids (due to reduced flow in the down-draught zones) continues to feed minor mineralising activity within the Pale Beds and the Boulder Conglomerate.

2 = Occasionally iron-rich fluids seep onto the seafloor proximal to areas of underlying Conglomerate Group Ore during the earliest deposition of the Thinly Bedded Unit, leading to pyrite-rich bedding parallel mineralisation within the lowermost parts of this lithology (see Figs. 5-12 to 5-14).



Figure 5-12 Exhalative processes? Bedding parallel, framboidal pyrite-rich mineralisation within the basal parts of the Thinly Bedded Unit containing shale rip-up clasts. Note also the suggestion of an infilled depression. (Locality = 14355 221) Width of view = 4 metres.



Figure 5-13 Exhalative processes? Distorted (roll-over structure) bedding parallel pyrite mineralisation in the base of the Thinly Bedded Unit. (Locality = 1465 202). Pen-knife for scale.



Figure 5-14 Exhalative processes? Detail of bedding parallel pyrite mineralisation within the base of the Thinly Bedded Unit (Locality = 1465 202). Note pyrite rip-up clasts within shale members, and bedding within the pyrite truncated by the base of the mudstone. Pen-knife for scale.

6. Conclusions.

Arguments in favour of a deep-seated Caledonoid control of the mineralisation at Navan are reinforced by this study. Moreover, the conclusion that metal-bearing fluids flowed through the basement is consistent with the findings of Anderson et al. (1989) that diagenetic sulfides within the basement lithologies were the source of positive $\delta^{34}\text{S}$ values associated with the metal-bearing fluid. Such a deep hydrological system is compatible with fluid inclusion, isotopic, and halogen studies conducted elsewhere in the Irish orefield (Everett et al., 1999; Gleeson et al., 1999).

Detailed observations of the relationships between early to mid Lower Carboniferous extensional faulting, putative Upper Carboniferous faulting representative of a compressional tectonic regime, and sulfide mineralisation has revealed that the mineralising event occurred concurrently with active extensional faulting during the early to mid Lower Carboniferous.

A distinct correlation between positive $\delta^{34}\text{S}$ values and high lead enrichments associated with early to mid Lower Carboniferous faults has also been revealed, and indicates that the minor, steeply dipping normal NNE, NE and ENE trending faults at Navan acted as foci for the metal-bearing solutions. The presence of negative $\delta^{34}\text{S}$ values associated with pyrite samples close to these fractures shows that, at times, the locally derived bacteriogenic-sulfide bearing fluids also circulated within the faults. Micro-textural observations indicate that active faulting took place during the earliest part of the mineralising process, which may also have allowed pulses of the hydrothermal, deep-seated metal-bearing fluid to displace the locally derived bacteriogenic sulfur-bearing fluid. No evidence has

been discerned on the minor NNE, NE and ENE faults observed during this study, which anyway are confined to early to mid Lower Carboniferous lithologies, to demonstrate movements during late Carboniferous tectonism. Therefore, placing metallogenesis at Navan early in the rifting history of the Irish Midlands, i.e. during the early to mid Lower Carboniferous, is forced by the observations made during this study. This conclusion is consistent both with the arguments of Ashton et al. (1992), and Anderson et al. (1998), on Navan, as well as with observations elsewhere in the Irish Orefield, notably the Silvermines and Tynagh deposits (e.g. Taylor and Andrew 1978; Boyce et al. 1983b, 1999; Banks 1985).

There is now overwhelming evidence that metallogenesis in the Irish Midlands took place during the early to mid Lower Carboniferous. It involved syndiagenetic replacement and in places exhalative deposition. For example, the discovery of fossilised vent structures (Larter et al., 1981) and fauna (Boyce et al., 1983b; Banks, 1985; and Boyce et al., 1999), demonstrates seafloor exhalative activity at both Silvermines and Tynagh around 355Ma. Consistent with these findings is the fact that about 98 percent of the total tonnage of base metals (economic and non-economic) within the Irish ore-field occurs within early to mid Lower Carboniferous strata (and see Andrew 1986; Johnson 1999), a pattern of significance in mineral exploration. Only about 2 percent of the mineralisation occurs within supra-Chadian lithologies. These are tightly clustered into the Kildare District in the eastern Irish Midlands (Hitzman and Beaty, 1996). The results reported here reinforce recognition within the Irish base-metal ore-field of the significance of bacteriogenic sulfide to overall tonnage (Boast et al., 1981; Boyce et al., 1983b; Anderson et al., 1998; Fallick et al. 2001.). When this evidence is combined with the findings of this study (active extensional faulting

during mineralisation), it becomes apparent that the major metallogenic event in the Irish Midlands occurred between 355Ma and 345Ma.

Of the current published models for the genesis of the Irish base metal ore-field only that of Russell (1978; 1986), invoking circulation of seawater derived metal-bearing fluids through the Lower Palaeozoic basement, at temperatures $\geq 200^{\circ}\text{C}$, leading to epigenetic and syndiagenetic replacive mineralisation, and in some deposits, syngenetic exhalation onto the sea floor, is consistent with the findings of this thesis: that is, mineralisation took place during active faulting, including the reactivation of basement structures, in the early to mid Lower Carboniferous.

7. Bibliography:

Alkindi, G.A.S.A., 1979. Trace element aureoles around some base-metal mineralisation in Ireland. Unpublished PhD Thesis, University of Strathclyde.

Anderson, D.L., 2001. Top-down tectonics? *Science* 293, 2016-2018.

Anderson, I.K., 1990. Ore depositional processes in the formation of the Navan zinc-lead deposit, Co. Meath, Ireland. Unpublished PhD Thesis, University of Strathclyde.

Anderson, I.K., Andrew, C.J., Ashton, J.H., Boyce, A.J., Caulfield, J.B.D., Fallick, A.E., Russell, M.J., 1989. Preliminary sulphur isotope data of diagenetic and vein sulfides in the Lower Palaeozoic strata of Ireland and Southern Scotland: implications for Zn+Pb+Ba mineralisation. *Journal of the Geological Society*, London, 146, 715-720.

Anderson, I. K., Ashton, J. H., Boyce, A. J., Fallick A. E., Russell, M.J., 1998. Ore depositional processes in the Navan Zn-Pb Deposit, Ireland. *Bulletin of the Society of Economic Geologists*, 93, No, 5, 535-563.

Andrew, C.J., 1986a. A diagrammatic representation of the Courceyan stratigraphy of the Irish Midlands. In Andrew, C.J., Crowe, R.W.A., Finlay, S.,

Pennell, W.M., Pyne, J.F., (eds.). Geology and genesis of mineral deposits in Ireland. Irish Association for Economic Geology Special Publication.

Andrew, C.J., 1986b. The tectono-stratigraphic controls to mineralisation in the Silvermines area, County Tipperary, Ireland. In Andrew, C.J., Crowe, R.W.A., Finlay, S., Pennell, W.M., Pyne, J.F., (eds.). Geology and genesis of mineral deposits in Ireland. Irish Association for Economic Geology Special Publication.

Andrew, C.J., 1992. Basin development chronology of the lowermost Carboniferous strata in the Irish north-Central Midlands. In Bowden, A.A., Earls, G., O'Conner, P.G., Pyne, J.F., (eds.). The Irish Minerals Industry 1980 - 1990. Irish Association for Economic Geology Special Publication.

Andrew, C.J., 1993. Mineralisation in the Irish Midlands. In Patrick, R.A.D., and Poyla, D.A., 1993. Mineralisation in the British Isles. Chapman and Hall, London.

Andrew, C.J., 1995. The Silvermines District, Co. Tipperary, Ireland. In Anderson, I.K., Ashton, J., Earls, G., Hitzman, M., Tear, S., (eds.). 1995. Irish carbonate-hosted Zn-Pb deposits. SEG Guidebook Series, 21.

Andrew, C.J., Ashton, J.H., 1985. Regional setting, geology and metal distribution patterns of Navan orebody, Ireland. Transactions of the Institution of Mining and Metallurgy, Section B: Applied earth Science, 94, B66-B93.

Andrew, C.J., Proustie, A., 1986. Syndiagenetic or epigenetic mineralisation - the evidence from the Tatestown zinc-lead prospect, Co. Meath. In Andrew, C.J.,

Crowe, R.W.A., Finlay, S., Pennell, W.M., Pyne, J.F., (eds.). Irish Association for Economic Geology Special Publication. Geology and genesis of mineral deposits in Ireland.

Ashton, J.H., 1995. Guide to the geology of the Navan orebody. In Anderson, I.K., Ashton, J.H., Earls, G., Hitzman, M., Tear, S., (Eds.). 1995. Irish Carbonate-hosted Zn-Pb deposits. SEG Guidebook Series, 21.

Ashton, J.H. and Harte, G., 1989, Technical Computerization at Tara Mines Ltd., Navan, Ireland: Transactions of the Institution of Mining and Metallurgy, 98A, 85-97.

Ashton, J.H., Black, A., Geraghty, J., Holdstock, M., Hyland, E., 1992. The geological setting and metal distribution patterns of Zn-Pb-Fe mineralisation in the Navan Boulder Conglomerate. In Bowden, A.A., Earls, G., O'Conner, P.G., Pyne, J.F., (eds.). The Irish Minerals Industry 1980-1990. Irish Association for Economic Geology Special Publication.

Ashton, J.H., Downing, D.T., Finlay, S., 1986. The geology of the Navan Zn-Pb orebody. In Andrew, C.J., Crowe, R.W.A., Finlay, S., Pennell, W.M., Pyne, J.F., (eds.). Geology and genesis of mineral deposits in Ireland. Irish Association for Economic Geology Special Publication.

Ashton, J. H., Geraghty, J. F., Holdstock, M., Martinez, N., O'Keefe, W.G., Peace, W. and Philcox M.E. In Press. The Navan orebody, discovery and

geology of the South West Extension. In, Europe's major base-metal deposits. Irish Association for Economic Geology Special Publication.

Banks, D.A., 1985, A Fossil worm assemblage from the Tynagh lead-zinc deposit in Ireland: *Nature*, 313, 128-131.

Banks, D.A. 1986. Hydrothermal chimneys and fossil worms from the Tynagh Pb-Zn deposit, Ireland. In Andrew, C.J., Crowe, R.W.A., Finlay, S., Pennell, W.M., Pyne, J.F., (eds.). *Geology and genesis of mineral deposits in Ireland*. Irish Association for Economic Geology Special Publication.

Banks, D.A., 1987. On the origin of the Tynagh lead+zinc+copper deposit, Ireland. Unpublished PhD Thesis, University of Strathclyde.

Banks, D.A. and Russell, M.J., 1992. Fluid mixing during ore deposition at the Tynagh base-metal deposit, Ireland. *European Journal of Mineralogy*. 4, 921-931.

Binney, W.P., 1987. A sedimentological investigation of Maclean chanel transported sulphide ores: Geological Survey of Canada Paper 86-24, 107-147.

Bischoff, J.L., Radtke, A.S., Rosenbaur, R.J., 1981. Hydrothermal alteration of greywacke by brine and seawater: roles of alteration and chloride complexing on metal solubilisation at 200° and 350°C. *Economic Geology*, 76, 659-675.

Boast, A.M., 1979. A textural and isotopic study of Irish base metal mineralisation of Lower Carboniferous age, with specific reference to the Tynagh deposit. Unpublished PhD Thesis, Imperial College of Science and Technology, London.

Boast, A.M., Swainbank, I.G., Coleman, M.L., Halss, C., 1981. Lead isotope variation in the Tynagh, Silvermines and Navan base-metal deposits, Ireland. *Trans. Instn Min. Metall. (Section B: App l. earth sci.)*, 90.

Boland, M., 1995. Silvermines stratigraphy and mineralisation - representative drillholes. In Anderson, I.K., Ashton, J., Earls, G., Hitzman, M., Tear, S., (eds.). 1995. Irish carbonate-hosted Zn-Pb deposits. *SEG Guidebook Series, Vol. 21.*

Boyce, A.J., Anderton, R., Russell, M.J., 1983a. Rapid subsidence and early Carboniferous base-metal mineralisation in Ireland. *Trans. Instn Min. Metall. (Section B: App l. earth sci.)*, 92.

Boyce, A.J., Coleman, M.L., and Russell, M.J., 1983b. Formation of fossil hydrothermal chimneys and mounds from Silvermines, Ireland: *Nature*, 306, 545-550.

Boyce, A.J., Fletcher, T.J., Fallick, A.E., Ashton, J., Russell, M.J., 1993. Petrographic and $\delta^{34}\text{S}$ study of Lower Palaeozoic rocks under the Navan Zn+Pb deposits: a source of hydrothermal sulphur. In Fenoll Hach-Ali, Torres-Ruiz and

Gervilla (Eds.), Current research in geology applied to ore-deposits; Proceedings of the second biennial SGA meeting, Granada, ISBN 84-338-1772-8, 53-56.

Boyce, A.J., Fallick, A.E., Little, C.T.S., Wilkinson, J.J., and Everett, C.E., 1999. A hydrothermal vent tube worm in the Ballynoe barite deposit, Silvermines, Ireland: Implications for timing and ore genesis: In Stanley et al. (eds.), Mineral Deposits: Processes to Processing, Proceedings of the fifth biennial SGA meeting and the tenth quadrennial IAGOD symposium, London. 825-827.

Braithwaite, C.J.R., Rizzi, G., 1997. The geometry and petrogenesis of hydrothermal dolomites at Navan, Ireland. *Sedimentology*. 44. 421-440.

Canfield, D.E. and Thamdrup, B., 1994. The production of ^{34}S -depleted sulfide during bacterial disproportionation of elemental sulfur. *Science*, 266, 1973-1975.

Caulfield, J.B.D., LeHuray, A.P., Rye, D.M., 1986. A review of lead and sulphur isotope investigations of Irish sediment-hosted base metal deposits, with new data from the Keel, Ballinalack, Moyvoughly and Tatestown deposits. In Andrew, C.J., Crowe, R.W.A., Finlay, S., Pennell, W.M., Pyne, J.F., (eds.). *Geology and genesis of mineral deposits in Ireland*. Irish Association for Economic Geology Special Publication.

Chadwick, R. A., Evans, D.J., Holliday, D.W., 1993. The Maryport Fault: the post-Caledonian tectonic history of southern Britain in microcosm. *Journal of the geological Society of London*, 150. 247-250.

Claypool, J.B., Holser, W.T., Sakai, I.R., Zak, I., 1980. The age curves for sulfur and oxygen isotopes in marine sulfate and their mutual interpretation. *Chemical Geology*, 28, 199-260.

Coomer, P.G., and Robinson, B.W., 1976, Sulphur and sulphate-oxygen isotopes and the origin of the Silvermines deposits, Ireland: *Mineralium Deposita*, 11, 155-169.

Corfield, S.M., Gawthorpe, R.L., Gage, M., Fraser, A.J., Besley., 1996. Inversion tectonics of the Variscan foreland of the British Isles. *Journal of the Geological Society of London*, 153. 17-32.

Cypionka, H., Smock, A.M., and Böttcher, M.E., 1998, A combined pathway of sulfur compound disproportionation in *Desulfovibrio desulfuricans*. *FEMS Microbiology Letters*, 166, 181-186.

Derry, D.R., Clark, G.R., Gillatt, N., 1965. The Northgate base-metal deposit at Tynagh, County Galway, Ireland. *Economic Geology*. 60. 1218-1237.

Dixon, P. R., LeHuray, A.P., Rye, D.M., 1990. Basement geology and tectonic evolution of Ireland as deduced from Pb isotopes. *Journal of the Geological Society of London*,. 147. 121-132.

Everett, C.E., Rye, D.M., Wilkinson, J.J., Boyce, A.J., Ellam, R.M., and Fallick, A.E., 1999a. The genesis of Irish-type Zn-Pb deposits: Characterization and origin of the principal ore fluid, *in* Stanley et al., eds, Mineral Deposits: Processes to Processing, Proceedings of the fifth biennial SGA meeting and the tenth quadrennial IAGOD symposium, London. 845-848.

Everett, C.E., Wilkinson, J.J., and Rye, D.M., 1999b. Fracture-controlled fluid flow in the Lower Palaeozoic rocks of Ireland: implications for the genesis of Irish-type Zn-Pb deposits, *in* McCaffrey, K.J.W., Lonergan, L. and Wilkinson, J.J. eds, Fractures, Fluid Flow and Mineralisation. Geological Society, London, Special publications, 155, 247-276.

Everett, C.E. and Wilkinson, J.J., 2000, What makes an orebody? A comparison of fluid inclusion and sulfur isotope data from prospects and deposits in the Irish Zn-Pb orefield. GSA Abstracts with Programs, 32, A-282.

Fallick, A.E., Ashton, J.H., Boyce, A.J., Ellam, R.M., and Russell, M.J., 2001, Bacteria were responsible for the magnitude of the world-class hydrothermal base-metal orebody at Navan, Ireland. Economic Geology, 96, 883-888.

Finster, K., Liesack, W. and Thamdrup, B.,1998, Elemental sulfur and thiosulfate disproportionation by *Desulfocapsa sulfoexigens* sp. nov., a new anaerobic bacterium isolated from marine surface sediment: Applied Environmental Microbiology, 64, 119-125.

Ford, C.V., 1996, The integration of petrologic and isotopic data from the Boulder Conglomerate to determine the age of the Navan orebody, Ireland: Unpublished Ph.D. thesis, University of Glasgow, p. 176.

Freeman, B., Klemperer, S.L., Hobbs, R.W., 1988. The deep structure of Northern England and the Iapetus Suture Zone from BIRPS deep seismic reflection profiles. *Journal of the Geological Society of London*, 145. 727-740.

Gardiner, P.R.R., Pyne, J.F., McArdle, 1982. Mineral exploration in Ireland. *Mining Magazine*, 147. No. 5.

Geraghty, M., McConnell, B., 1999. Bedrock Geology, 1:100,000 Scale Map Series, Sheet 13, Meath, Geological Survey of Ireland.

Gleeson, S.A., Banks, D.A., Everett, C.E., Wilkinson, J.J., Samson, I.M., and Boyce, A.J., 1999. Origin of mineralising fluids in Irish-type deposits: Constraints from Halogens, *in* Stanley et al., eds, *Mineral Deposits: Processes to Processing*, Proceedings of the fifth biennial SGA meeting and the tenth quadrennial IAGOD symposium, London. 857-860.

Habicht, K.S., Canfield, D.E., 1997. Sulphur isotope fractionation during bacterial sulfate reduction in organic-rich sediments. *Geochimica et Cosmochimica Acta*. 61, No, 24. 5351-5361.

Halliday, A.N., Mitchell, J.G., 1983. K-Ar ages of clay concentrates from Irish orebodies and their bearing on the timing of mineralisation. Transactions of the Royal Society of Edinburgh: Earth Sciences, 74. 1-14.

Hitzman, M.W., 1995. Mineralisation in the Irish Zn-Pb-(Ba-Ag) orefield. In Anderson, I.K., Ashton, J., Earls, G., Hitzman, M., Tear, S., (eds.), 1995. Irish carbonate-hosted Zn-Pb deposits. SEG Guidebook Series. 21.

Hitzman, M.W., Large, D., 1986. A review and classification of the Irish carbonate-hosted base metal deposits. In Andrew, C.J., Crowe, R.W.A., Finlay, S., Pennell, W.M., Pyne, J.F., (eds.). Geology and genesis of mineral deposits in Ireland. Irish Association for Economic Geology Special Publication.

Hitzman, M.W., and Beaty, D.W., 1996. The Irish Zn-Pb-(Ba) orefield. In: Sangster, D.F. (ed.) Society of Economic Geologists Special Publication No. 4, 112-143.

Johnston, J.D., 1992. The fractal geometry of vein systems: the potential for ore reserve calculation. In Bowden, A.A., Earls, G., O'Conner, P.G., Pyne, J.F., (eds.). The Irish Minerals Industry 1980-1990. Irish Association for Economic Geology Special Publication.

Johnston, J.D., 1995. Variscan deformation in Ireland. In Anderson, I.K., Ashton, J., Earls, G., Hitzman, M., Tear, S., (eds.). 1995. Irish carbonate-hosted Zn-Pb deposits. SEG Guidebook Series, 21.

Johnston, J.D., 1999. Regional fluid flow and the genesis of Irish Carboniferous base metal deposits: *Mineralium Deposita*, v. 34, p. 571-598.

Jorgensen, B.B., 1990. A thiosulfate shunt in the sulfur cycle of marine-sediments, *Science*, v. 249, p. 152-154.

Kelley, S.P., Fallick, A.E., 1990. High precision spatially resolved analysis of ^{34}S in sulfides using a laser extraction technique. *Geochemica et Cosmochemica Acta*. 54. (3).

Kneller, B.C., 1991. A foreland basin on the southern margin of Iapetus. *Journal of the Geological Society of London*, 148. 207-210.

Lee, M.K., Pharaoh, T.C., Soper, N.J., 1990. Structural trends in central Britain from images of gravity and aeromagnetic fields. *Journal of the Geological Society of London*. 147. 241-258.

Leeder, M.R., 1982. Upper Palaeozoic basins of the British Isles - Caledonide inheritance versus Hercynian plate margin processes. *J. geol. Soc London*. 139, 479-491.

LeHuray, A.P., Caulfield, J.B.D., Rye, D.M., Dixon, P.R., 1987. Basement controls on sediment-hosted Zn-Pb deposits: A Pb isotope study of

Carboniferous mineralisation in Central Ireland. *Economic Geology*, 82, 1695-1709.

Lenz, A.C., Vaughan, A.P.M., 1994. A late Ordovician to Middle Wenlockian graptolite sequence from a borehole within the Rathkenny Tract, eastern Ireland, and its relation to the palaeogeography of the Iapetus Ocean. *Can. J. Earth Sci.* 31. 608-616.

Letnikov, F.A., 1997. Self-organisation of formation of magmatic and hydrothermal ore deposits. *Geology of Ore Deposits*. 39, No. 4.

Libby, D.J., Downing, D.T., Ashton, J.H., Oram, R.A., O'Murchú, D., Dallas, W.G., Maybury, M., 1985. The Tara Mines story. *Transactions of the Institution of Mining and Metallurgy*, 94A, 1-41.

Mallon, A.J., 1997, Petrological and mineralogical characteristics of the Old Red Sandstone Facies rocks beneath base-metal deposits as a guide to the setting of mineralisation in the Irish Midlands: Unpublished Ph.D. Thesis, University College Cork.

McArdle, P., 1990. A review of carbonate-hosted base metal-barite deposits in the Lower Carboniferous rocks of Ireland. *Chronique de La Recherche Minière*, No 500.

McConnell, B., Philcox, M., Geraghty, M., 2001. Geology of Meath: A geological description to accompany the Bedrock Geology 1:100,000 Scale Map Series, Sheet 13, Meath. With contributions from J. Morris, W. Cox, G. Wright and R. Meehan. Geological Survey of Ireland.

McNestry, A., and Rees, J.G., 1992. Environments and palynofacies of a Dinantian (Carboniferous) littoral sequence: The basal part of the Navan Group, Navan, County Meath, Ireland. *Palaeogeography, Palaeoclimatology, Palaeoecology* 96, 175-193

Mills, H., Halliday, A.N., Ashton, J.H., Anderson, I.K., Russell, M.J., 1987. Origin of a giant orebody at Navan, Ireland. *Nature*. 327. 6119. 223-226.

Murowchick, J.B., 1992. Marcasite inversion and the petrographic determination of pyrite ancestry. *Economic Geology*, 87, 1141-1152.

Murowchick, J.B., and Barnes, H.L., 1986. Marcasite precipitation from hydrothermal solutions: *Geochimica et Cosmochimica Acta*, 50, 2615-2629.

Murphy, F.C., Anderson, T.B., Daly, J.S., Gallagher, V., Graham, J.R., Haroer, D.A.T., Johnston, J.D., Kennan, P.S., Kennedy, M.J., Long, C.B., Morris, J.H., O'Keefe, W.G., Parkes, M., Ryan, P.D., Sloan, R.J., Stillman, C.J., Tietzch-Tyler, D., Todd, S.P., Wrafter, J.P., 1991. An appraisal of Caledonian suspect terranes in Ireland. *Irish Journal of Earth Sciences*, 11, 11-41.

O'Brien, M.V., 1966. Review of mining activities in the Republic of Ireland. Extract from the Transactions/Section A of the Institution of Mining and Metallurgy, 75. A70-84.

Ohmoto, H., and Goldhaber, M., 1997. Sulfur and carbon isotopes, *in* Barnes, H.L., ed, *Geochemistry of Hydrothermal Ore Deposits*, John Wiley, New York, 517-611.

O'Keefe, W.G., 1986. Age and postulated source rocks for mineralisation in central Ireland, as indicated by lead isotopes. In Andrew, C.J., Crowe, R.W.A., Finlay, S., Pennell, W.M., Pyne, J.F., (eds.). *Geology and genesis of mineral deposits in Ireland*. Irish Association for Economic Geology Special Publication.

Owen, A.W., Harper, D.A.T., Romano, M., 1992. The Ordovician biogeography of the Grangegeeth terrane and the Iapetus suture zone in eastern Ireland. *Journal of the Geological Society of London*, 149. 3-6.

Patrick, R.A.D., Coleman, M.L., Russell, M.J., 1983. Sulphur isotopic investigation of vein lead-zinc mineralisation at Tyndrum, Scotland. *Mineral. Deposita*. 18. 477-485.

Patrick, R.A.D., Russell, M.J., 1989. Sulphur isotope investigation of Lower Carboniferous vein deposits of the British Isles. *Mineral. Deposita*, 24. 148-153.

Peace, W.M., 1999, Carbonate-hosted Zn-Pb mineralisation, upper Pale Beds, Navan, Ireland. Unpublished PhD Thesis, University of Melbourne.

Peace, W.M., Wallace, M.W., 2000, Timing of mineralisation at the Navan Zn-Pb deposit: A post Arundian age for Irish Mineralisation. *Geology*, 28, 8, 711-714.

Philcox, M.E., 1984. Lower Carboniferous lithostratigraphy of the Irish Midlands. Irish Association for Economic Geology. 89 pages.

Philcox, M.E., 1989. The mid-Dinantian unconformity at Navan, Ireland. In: The role of tectonics in Devonian and Carboniferous sedimentation in the British Isles (eds Arthurton, R.S., Gutteridge, P. and Nolan, S.C.) Yorkshire Geological Society Occasional Publication 6, 67-81.

Philcox, M.E, Jones, G.L., Somerville, I.D., Strogon, P., 1995. The Carboniferous limestone of the North Dublin Coast and Feltrim Hill. In Anderson, I.K., Ashton, J., Earls, G., Hitzman, M., Tear, S., (eds.). 1995. Irish carbonate-hosted Zn-Pb deposits. SEG Guidebook Series, 21.

Phillips, W.E.A., Stillman, C.J., Murphy, T., 1976. A Caledonian plate tectonic model. *Journal of the Geological Society of London*, 32, 579-609.

Phillips, W.E.A., and Sevastopulo, G.D., 1986, The stratigraphic and structural setting of Irish mineral deposits, *in* Andrew, C.J., Crowe, R.W.A., Finlay, S.,

Pennell, W.M., Pyne, J.F., eds, *Geology and genesis of mineral deposits in Ireland*, Irish Association For Economic Geology, 1-30.

Platt, J.W., 1980. Review of Irish Caledonian stratabound sulfides. *Geol. Surv. Irl. Special Paper No. 5.* 25-28.

Readman, P.W., O'Reilly, B.M., Murphy, T., 1997. Gravity gradients and upper-crustal tectonic fabrics, Ireland. *Journal of the Geological Society of London*, 154. 817-828.

Rees, J.R., 1987. The Carboniferous geology of the Boyne Valley area, Ireland. Unpublished PhD Thesis, University of Dublin.

Rhoden, H.N. 1958, Structure and economic mineralisation of the Silvermines district, Co. Tipperary, Ireland: *Transactions of the Institution of Mining and Metallurgy*, 68, 67-94.

Rizzi, G., 1993. The sedimentology and petrography of Lower Carboniferous limestones and dolomites; host rocks to the Navan zinc-lead deposit, Ireland. Unpublished PhD Thesis. University of Glasgow.

Rizzi, G., Braithwaite, C.J.R., 1996. Cyclic emersion surfaces and channels within Dinantian limestones hosting the giant Navan Zn-Pb deposit, Ireland. In Strogon, P, Somerville, I.D., Jones, G.L.I., (eds.). 1996. *Recent advances in Lower Carboniferous geology.* Geological Society Special Publication No. 107, 207-219.

Romano, M., 1980. The stratigraphy of the Ordovician rocks between Slane (County Meath) and Collon (County Louth), Eastern Ireland. *J Earth Sci. Dubl. Soc.* 3. pp 53-79.

Russell, M.J., 1971. North-South geofractures in Scotland and Ireland. *Scott. J. Geol.* 8(1), 75-84, 1971.

Russell, M.J., 1972. The geological environment of post-Caledonian base-metal mineralisation in Ireland. Unpublished PhD Thesis, University of Durham.

Russell, M.J. 1975. Lithogeochemical environment of the Tynagh base-metal deposit, Ireland, and its bearing on ore deposition: *Transactions of the Institution of Mining and Metallurgy*, 84B, 128-133.

Russell, M.J., 1978. Downward excavating hydrothermal cells and Irish Type ore deposits: importance of an underlying thick Caledonian prism. *Transactions of the Institution of Mining and Metallurgy*. 87B: 168-171.

Russell, M.J., 1986. Extension and convection: a genetic model for the Irish Carboniferous base metal and barite deposits. In Andrew, C.J., Crowe, R.W.A., Finlay, S., Pennell, W.M., Pyne, J.F., (eds.). *Geology and genesis of mineral deposits in Ireland*. Irish Association for Economic Geology Special Publication.

Russell, M.J., Solomon, M., Walshe, J.L., 1981. The genesis of sediment-hosted, exhalative zinc and lead deposits. *Mineral. Deposita*, 16. 113-127.

Russell, M.J., Skauli, H., 1991. A history of theoretical development in carbonate-hosted base-metal deposits, and a new tri-level enthalpy classification. In Hutchinson, R.W., Grauch, R.I., (eds.). Monograph 8, Economic Geology. 96-116.

Russell, M.J., Hazeldine, R.S., 1992. Accounting for geofractures. In Bowden, A.A., Earls, G., O'Conner, P.G., Pyne, J.F., (eds.). The Irish Minerals Industry 1980 - 1990. Irish Association for Economic Geology Special Publication.

Samson, I.M., Russell, M.J., 1987. Genesis of the Silvermines Zinc-Lead-Barite deposit, Ireland: Fluid inclusion and stable isotope evidence. *Economic Geology*. 82. 371-394.

Schoonen, M.A.A., Barnes, H.L., 1991a. Reactions forming pyrite and marcasite from solution: I. Nucleation of FeS₂ below 100°C. *Geochemica et Cosmochemica Acta*. 55. 1495-1504.

Schoonen, M.A.A., Barnes, H.L., 1991b. Reactions forming pyrite and marcasite from solution: II. Via FeS precursors below 100°C. *Geochemica et Cosmochemica Acta*. 55. 1505-1514.

Schoonen, M.A.A., Barnes, H.L., 1991c. Reactions forming pyrite and marcasite from solution: III. Hydrothermal processes. *Geochemica et Cosmochemica Acta*. 55. 3491-3504.

Schultz, R.W., 1968. The geology of the primary sulphide-barite deposits of Tynagh, Co. Galway, Ireland Unpublished PhD thesis, University of Dublin.

Shinn, E.A., 1983. Birdeyes, fenestrae, shrinkage pores and loferites: a re-evaluation. *Journal of sedimentary petrology*, 53, 619-629.

Sibson, R.H., McMoore, J. and Rankin, R.H., 1975, Siesmic pumping – a hydrothermal fluid transport mechanism: *Journal of the Geological Society of London*, 131, 653-659.

Singer, S.B., 1995. World class base and precious metal deposits – a quantitative analysis. *Economic Geology*, 90, 88-104.

Strogen, P., Jones, G.Ll., Somerville, I.D., 1990. Stratigraphy and sedimentology of Lower Carboniferous (Dinantian) boreholes from West Co. Meath, Ireland. *Geological Journal*. 25. 103-137.

Symmons, D.T.A., Smethurst, M.T., Ashton, J.H., (in press). Paleomagnetism of the Navan Zn-Pd deposit, Ireland. *Economic Geology*.

Taylor, S., 1984, Structural and palaeotopographic controls of lead-zinc mineralisation in the Silvermines orebodies, Ireland: *Economic Geology*. 79, 529-548.

Taylor, S., and Andrew, C.J., 1978, Silvermines orebodies, Co. Tipperary, Ireland: Transactions of the Institution of Mining and Metallurgy, 87B, 111-124.

Thamdrup, B., Finster, K., Hansen, J.W. and Bak, F., 1993, Bacterial disproportionation of elemental sulfur coupled to chemical reduction of iron or manganese: Applied Environmental Microbiology, 59, 101-108.

Todd, S.P., Murphy, F.C., Kennan, P.S., 1991. On the trace of the Iapetus Suture in Ireland and Britain. Journal of the Geological Society of London. 148. 869-880.

Varga, R.J., Gee, J.S., Bettison-Varga, L., Anderson, R.S., Johnson, C.L., 1999. Early establishment of seafloor hydrothermal systems during structural extension: paeomagnetic evidence from the Troodos ophiolite, Cyprus. Earth and Planetary Science Letters, 171, 221-235.

Vasconcelos, C., McKenzie, J.A., Bernasconi, S., Grujic, D., 1995. Microbial mediation as a possible mechanism for natural dolomite formation at low temperatures. Nature, 377, 220-222.

Vasconcelos, C., and McKenzie, J.A., 2000. Sulfate reducers – dominant players in a low-oxygen world? Science, 290, 1711-1712.

Vaughan A.P.M. 1991. The Lower Palaeozoic geology of the Iapetus Suture Zone in eastern Ireland. Unpublished PhD Thesis, University of Dublin.

Vaughan, A.P.M., Johnston, J.D., 1992. Structural constraints on the closure geometry across the Iapetus suture in eastern Ireland. *Journal of the Geological Society of London*, 149, 65-74.

Von Damm, K.L., 1990. Sea floor hydrothermal activity: Black smoker chemistry and chimneys. *Annual review of Earth and Planetary sciences*, 18, 173-204.

8. APPENDICES

APPENDIX 1

Table of structural data presented in Chapter 2.

North east trending mineralised fractures (sulfide rich).

1. 015/85S, at junction of 1330 13LHWA/1330 13LHXR (see p67 and fig. 2-2).
2. 010/78S, at junction of 1330 13LHWA/1330 13LHXR (see p67 and fig. 2-2).

North west trending mineralised fractures (sulfide rich).

1. 310/80S, at junction of 1330 13LHWA/1330 13LHXR (see p67 and fig. 2-2).
2. 305/75S, at junction of 1330 13LHWA/1330 13LHXR (see p67 and fig. 2-2).
3. 345/68S, at junction of 1330 13LHWA/1330 13LHXR (see p67 and fig. 2-2).
4. 350/75S, at far west of 1330 13LHWA (see p67 and fig. 2-2).
5. 365/85S, at far west of 1330 13LHWA (see p67 and fig. 2-2).

East, north east trending mineralised fractures (carbonate rich).

1. 078/75S, at far west of 1330 13LHWA (see p67 and fig. 2-2).
2. 080/80S, at far west of 1330 13LHWA (see p67 and fig. 2-2).
3. 080/75S, at far west of 1330 13LHWA (see p67 and fig. 2-2).
4. 075/78S, at far west of 1330 13LHWA (see p67 and fig. 2-2).
5. 075/75S, at far west of 1330 13LHWA (see p67 and fig. 2-2).
6. 077/80S, at far west of 1330 13LHWA (see p67 and fig. 2-2).

B Fault system.

B Fault.

1. 267/45S, at far west of 1330 13LHWA (see p68 and fig. 2-2).

B Fault branches.

1. 245/50S, 1330 13LHXL (see p68 and fig. 2-2).
2. 250/45S, 1330 13LHXL (see p68 and fig. 2-2).
3. 252/50S, 1330 13LHXL (see p68 and fig. 2-2).
4. 248/32S, 1330 13LHXR (see p68 and fig. 2-2).
5. 240/40S, 1330 13LHWA (see p68 and fig. 2-2).
6. 238/40S, 1330 13LHWA (see p68 and fig. 2-2).
7. 245/55S, 1330 13LHWA (see p68 and fig. 2-2).
8. 230/70S, 1330 13LHWA (see p68 and fig. 2-2).
9. 230/60S, 1330 13LHWA (see p68 and fig. 2-2).
10. 228/50S, 1330 13LHWA (see p68 and fig. 2-2).

APPENDIX 1 (cont.)

Table of structural data presented in Chapter 2.

B Fault accommodation structure.

1. 069/44N, 1330 13LHXR (see p68 and fig. 2-2).

Dextral reverse strike slip assemblage.

1. 260/90, 1330 13LHXL (see p69 and fig. 2-2).
2. 250/88N, 1330 13HXR (see p69 and fig. 2-2).
3. 255/90, 1330 13LHWA (see p69 and fig. 2-2).
4. 255/90, 1330 13LHWA (see p69 and fig. 2-2).
5. 258/90, 1330 13LHWA (see p69 and fig. 2-2).
6. 260/90, 1330 13LHWA (see p69 and fig. 2-2).
7. 267/85, 1330 13LHWA (see p69 and fig. 2-2).
8. 256/90, 1330 13LHWA (see p69 and fig. 2-2).

Slicken-crysts in dextral reverse strike slip assemblage.

1. 076/20, 1330 13LHWA (see p69 and fig. 2-2).

APPENDIX 2

Table of sulfur isotope data from the profile (see Chapter 4).

Sample #	Mineral	Texture	$\delta^{34}\text{S}_{\text{CDT}}(\text{‰})$	Distance from fault	Figure
U12477-1	Sp	Granular	+6.8	<1m into footwall	Figure 4-7
U12477-3	Ma	Bladed	+16.7	<1m into footwall	
U12477-4	Sp	Granular	+5.6	<1m into footwall	
U12477-5	Ma	Bladed	+17.5	<1m into footwall	
U12473-1	Ga	Cubic	-5.9	1-2m into footwall	
U12473-3	Sp	Honeyblende	-8.0	1-2m into footwall	Figure 4-8
U12473-4	Ga	Cubic	-9.4	1-2m into footwall	
U12473-5	Py	Framboidal	-18.8	1-2m into footwall	
U12473-6	Sp	Granular	+2.2	1-2m into footwall	
U12473-7	Py	Framboidal	-16.3	1-2m into footwall	
U12473-9	Sp	Granular	+4.3	1-2m into footwall	
U12473-11	Py	Framboidal	-14.4	1-2m into footwall	
U12472-2	Sp	Core ¹ Banded	-11.4	1 to 2m into hanging wall	Figure 4-9
U12472-8	Sp	Core ¹ Granular	-1.4	1 to 2m into hanging wall	
U12472-12	Sp	Core ¹ Honeyblende	-4.4	1 to 2m into hanging wall	
U12472-16	Sp	Core ¹ Honeyblende	-17.4	1 to 2m into hanging wall	
U12472-22	Sp	Core ¹ Honeyblende	-5.0	1 to 2m into hanging wall	
U12472-3	Py	o-g ² Collomorphic	-31.4	1 to 2m into hanging wall	
U12472-7	Py	o-g ² Collomorphic	-29.5	1 to 2m into hanging wall	
U12472-11	Py	o-g ² Collomorphic	-29.2	1 to 2m into hanging wall	
U12472-15	Py	o-g ² Collomorphic	-25.6	1 to 2m into hanging wall	
U12472-1	Ga	o-g ³ Collomorphic	-10.9	1 to 2m into hanging wall	
U12472-6	Ga	o-g ³ Collomorphic	-19.0	1 to 2m into hanging wall	
U12472-10	Ga	o-g ³ Collomorphic	-20.4	1 to 2m into hanging wall	
U12472-23	Ga	o-g ³ Collomorphic	-18.6	1 to 2m into hanging wall	
U12472-4	Sp	Late ⁴ Honeyblende	-19.8	1 to 2m into hanging wall	
U12472-5	Sp	Late ⁴ Honeyblende	-10.0	1 to 2m into hanging wall	
U12472-9	Sp	Late ⁴ Honeyblende	-17.6	1 to 2m into hanging wall	
U12474-13	Sp	Late ⁴ Honeyblende	-14.2	1 to 2m into hanging wall	
U12472-17	Sp	Late ⁴ Honeyblende	-17.6	1 to 2m into hanging wall	
U12472-18	Sp	Late ⁴ Honeyblende	-7.7	1 to 2m into hanging wall	
U12472-20	Sp	Late ⁴ Honeyblende	-22.1	1 to 2m into hanging wall	
U12472-19	Sp	Late ⁴ Honeyblende	-16.0	1 to 2m into hanging wall	
U12472-24	Sp	Late ⁴ Honeyblende	-13.9	1 to 2m into hanging wall	
U12493-1	Ga	Cubic	-11.6	5m into footwall	Figure 4-10
U12493-2	Ga	Cubic	-9.6	5m into footwall	
U12493-3	Ga	Cubic	-14.8	5m into footwall	
U12493-4	Sp	Honeyblende	-14.6	5m into footwall	
U12493-5	Sp	Honeyblende	-11.4	5m into footwall	
U12493-6	Ga	Cubic	-9.5	5m into footwall	
U12493-7	Sp	Honeyblende	-14.5	5m into footwall	
U12493-8	Py	Framboidal	-29.9	5m into footwall	
U12493-9	Sp	Honeyblende	-12.4	5m into footwall	
U12478-1	Py	Framboidal	-25.1	15m into hanging wall	Figure 4-11
U12478-2	Py	Framboidal	-25.4	15m into hanging wall	
U12478-3	Sp	Honeyblende	-10.4	15m into hanging wall	
U12478-4	Py	Framboidal	-25.2	15m into hanging wall	
U12478-5	Sp	Honeyblende	-9.0	15m into hanging wall	
U12473-12	Sp	Granular	+6.5	1-2m into footwall	
U12484-1	Ga	Cubic	-9.5	10m into footwall	
U12484-2	Py	Collomorphic	-29.2	10m into footwall	
U12484-3	Py	Collomorphic	-10.0	10m into footwall	
U12483-1	Py	Framboidal	-26.6	10m into footwall	

APPENDIX 2(Cont.)

Table of sulfur isotope data from the profile (see Chapter 4).

Sample #	Mineral	Texture	$\delta^{34}\text{S}_{\text{CDT}}(\text{‰})$	Distance from fault	Figure
U12503-3	Py	Framboidal	-33.2	10m into footwall	
U12487-1	Ma	Bladed	+15.7	2-3m into footwall	
U12487-2	Sp	Granular	+4.0	2-3m into footwall	
U12487-3	Sp	Granular	+8.7	2-3m into footwall	
U12487-4	Sp	Granular	+7.1	2-3m into footwall	
U12487-5	Ma	Bladed	+12.7	2-3m into footwall	
U12487-6	Ma	Bladed	+16.3	2-3m into footwall	
U12487-7	Sp	Granular	+6.7	2-3m into footwall	
U12487-8	Sp	Granular	+1.6	2-3m into footwall	
U12507-1	Py	Framboidal	-9.4	2-3m into footwall	
U12507-2	Py	Framboidal	-18.2	2-3m into footwall	
U12507-4	Py	Framboidal	-14.2	2-3m into footwall	
U12507-5	Ma	Bladed	+9.6	2-3m into footwall	
U12474-2	Sp	Granular	-2.62	1-2m into footwall	
U12474-3	Ga	Bladed	+15.8	1-2m into footwall	
U12474-5	Ga	Bladed	+9.3	1-2m into footwall	
U12474-6	Sp	Granular	+7.9	1-2m into footwall	
U12474-7	Py	Framboidal	-24.5	1-2m into footwall	
U12491-1	Sp	Granular	+9.9	<1m into footwall	
U12491-2	Ma	Bladed	+16.8	<1m into footwall	
U12494-1	Sp	Granular	+0.8	<1m into footwall	
U12498-1	Py	Framboidal	-32.3	<1m into footwall	} Figure 4-12
U12498-2	Py	Framboidal	-28.4	<1m into footwall	
U12498-3	Py	Framboidal	-34.3	<1m into footwall	
U12498-4	Py	Framboidal	-35.1	<1m into footwall	
U12498-5	Py	Framboidal	-35.4	<1m into footwall	
U12498-6	Py	Framboidal	-35.3	<1m into footwall	
U12505-1	Ma	Bladed	+14.8	<1m into footwall	
U12505-2	Sp	Granular	+4.5	<1m into footwall	
U12505-3	Ma	Bladed	+11.9	<1m into footwall	
U12504-1	Ga	Cubic	-6.3	1 to 2m into hanging wall	
U12504-2	Sp	Honeyblende	-16.3	1 to 2m into hanging wall	
U12510-1	Ga	Cubic	-26.4	1 to 2m into hanging wall	
U12510-2	Sp	Honeyblende	-21.3	1 to 2m into hanging wall	
U12496-1	Ga	Cubic	-9.2	3m into hanging wall	
U12496-2	Py	Framboidal	-20.2	3m into hanging wall	
U12496-3	Sp	Honeyblende	-9.7	3m into hanging wall	
U12499-2	Py	Framboidal	-32.0	10m into hanging wall	
U12499-3	Sp	Honeyblende	-19.5	10m into hanging wall	

¹ Sample taken from core of clast exhibited in Fig. 4-9

² Sample taken from Py overgrowth of clast as exhibited in Fig. 4-9.

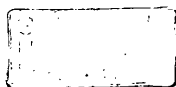
³ Sample taken from Ga overgrowth of Py as shown in Fig. 4-9.

⁴ Sample taken from coarse grained Sp shown in matrix in Fig. 4-9.

APPENDIX 3

Table of laboratory standard sulfur isotope data (see Chapter 4).

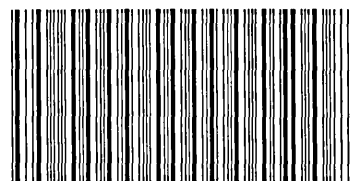
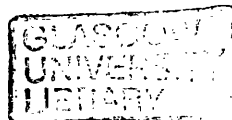
Sample	Mineral	Line No.	$\delta^{34}\text{S}_{\text{CDT}}(\text{‰})$	$\delta^{34}\text{S}_{\text{CDT}}(\text{‰})$	Disparity (Meas-Act)	Comment
			Actual	Measured		
CP-1	CuFeS ₂	SA5507	-4.6	-4.9	-0.3	
CP-1	CuFeS ₂	SA5518	-4.6	-4.4	0.2	
CP-1	CuFeS ₂	SA5635	-4.6	-4.4	0.2	
CP-1	CuFeS ₂	SA5653	-4.6	-4.7	-0.1	
CP-1	CuFeS ₂	SA5665	-4.6	-4.8	-0.2	
CP-1	CuFeS ₂	SA5667	-4.6	-4.7	-0.1	
CP-1	CuFeS ₂	SA5676	-4.6	-4.6	0.0	
CP-1	CuFeS ₂	SA6038	-4.6	-5.2	-0.6	Low Yield
CP-1 Mean ($\pm 1\sigma$) = $-4.7 \pm 0.3\text{‰}$, without Low Yield sample: $-4.6 \pm 0.2\text{‰}$						
IAEA-S-3	Ag ₂ S	SA5514	-31	-30.9	0.1	Outlier of group of 3
IAEA-S-3	Ag ₂ S	SA5662	-31	-30.4	0.6	
IAEA-S-3	Ag ₂ S	SA5663	-31	-30.9	0.1	
IAEA-S-3	Ag ₂ S	SA5664	-31	-31.1	-0.1	
IAEA-S-3	Ag ₂ S	SA5673	-31	-30.9	0.1	
IAEA-S-3	Ag ₂ S	SA5696	-31	-31.1	-0.1	
IAEA-S-3	Ag ₂ S	SA6024	-31	-31.7	-0.7	Extreme result
IAEA-S-3 Mean ($\pm 1\sigma$) = $-31 \pm 0.4\text{‰}$, without outlier and extreme result: $-31 \pm 0.1\text{‰}$						
NBS 123	ZnS	SA5499	17.1	17.2	0.1	
NBS 123	ZnS	SA5504	17.1	15.0	-2.1	Very low yield
NBS 123	ZnS	SA5645	17.1	17.2	0.1	
NBS 123	ZnS	SA5658	17.1	17.1	0.0	
NBS 123	ZnS	SA5666	17.1	17.1	0.0	
NBS 123	ZnS	SA6031	17.1	18.5	1.4	Preceding line extraction highly contaminated, therefore result suspect.
NBS 123 Mean ($\pm 1\sigma$) = $17.1 \pm 0.1\text{‰}$, without v. Low Yield and contaminated samples						



Please be aware that computer discs which are used in several machines run a high risk of corruption, especially as a result of infection by a virus. You are strongly recommended, if you intend to use the disc(s) enclosed, to ensure that your computer is protected with appropriate software for the detection of known viruses, and for the repair of damage they may cause.

Please refer any problems to the Library Enquiry Desk (ext 6704/5).

GUL 96.40



30114011410233